Department for Farm Animals and Veterinary Public Health

University of Veterinary Medicine Vienna

University Clinic for Swine

(Head: Univ.-Prof. Dr. med. vet. Andrea Ladinig, Dipl. ECPHM)

Investigation of local immune responses at the maternal-fetal interface during infection with Porcine Reproductive and Respiratory Syndrome Virus

PhD thesis submitted for the fulfilment of the requirements for the degree of

DOCTOR OF PHILOSOPHY (PhD)

University of Veterinary Medicine Vienna

Submitted by

Melissa R. Stas

Vienna, February 2023

First Supervisor:

Univ.-Prof. Dr. med. vet. Andrea Ladinig, Dipl. ECPHM

University Clinic for Swine

Department for Farm Animals and Public Health

University of Veterinary Medicine Vienna

Veterinärplatz 1 1210 Vienna, Austria

andrea.ladinig@vetmeduni.ac.at

Second Supervisor:

Dr. Wilhelm Gerner

Institute of Immunology

Department of Pathobiology

University of Veterinary Medicine Vienna

Veterinärplatz 1 1210 Vienna, Austria

Present address: The Pirbright Institute, Woking, United Kingdom.

Wilhelm.Gerner@pirbright.ac.uk

Declaration

I hereby declare that this PhD thesis was written and shaped autonomously. The rules of good scientific practice have been followed during the whole PhD journey. Citations where needed are in place and all the figures presented in this work were drawn by me unless indicated otherwise.

Melissa R. Stas

Vienna, February 2023

Table of contents

List of publications included in the PhD thesis

Publication 1:

Melissa R. Stas, Michaela Koch, Maria Stadler, Spencer Sawyer, Elena L. Sassu, Kerstin H. Mair, Armin Saalmüller, Wilhelm Gerner and Andrea Ladinig. NK and T Cell Differentiation at the Maternal-Fetal Interface in Sows During Late Gestation. Frontiers in Immunology 2020; https://doi.org/10.3389/fimmu.2020.582065

Journal Impact Factor 2020: 6.429

Author contributions:

MRS, KHM, AS, WG, and AL were in charge of the study design. ELS and SS were involved in tissue collection and the tissue separation procedure. MRS, MK, MS, SS, and ELS performed laboratory work and experiments. MRS carried out the phenotyping experiments and analyzed the data. MRS, KHM, ELS, AS, WG, and AL thoroughly discussed and interpreted the data. MRS, WG, and AL wrote the manuscript. All authors read and approved the final manuscript.

Publication 2:

Melissa R. Stas, Heinrich Kreutzmann, Julia Stadler, Elena L. Sassu, Kerstin H. Mair, Michaela Koch, Christian Knecht, Maria Stadler, Marlies Dolezal, Gyula Balka, Marianne Zaruba, Marlene Mötz, Armin Saalmüller, Till Rümenapf, Wilhelm Gerner and Andrea Ladinig. Influence of PRRSV-1 vaccination and infection on mononuclear cells at the maternal-fetal interface. Frontiers in Immunology 2022; https://doi.org/10.3389/fimmu.2022.1055048

Journal Impact Factor 2022: 7.561

Author contributions:

MRS, KM, JS, AS, TR, WG, and AL were in charge of the study design. HK, CK, JS, GB, and AL organized the animal experiment and were responsible for the sample collection. ES, KM, MK, MS, MZ, MM, and TR performed the laboratory work. MRS, WG, and AL analyzed the data and MD performed the statistical analysis. MRS, WG, and AL discussed and interpreted the data and prepared the manuscript. All authors read and approved the final manuscript.

List of publications not included in the PhD thesis

Selma Schmidt, Heinrich Kreutzmann, Maria Stadler, Kerstin H. Mair, Melissa R. Stas, Michaela Koch, Eleni Vatzia, Sophie Dürlinger, Christian Knecht, Joachim Spergser, Marlies Dolezal, Sven Springer, Tobias Theuß, Vicky Fachinger, Andrea Ladinig, Armin Saalmüller, and Wilhelm Gerner. T-cell Cytokine Response in Salmonella Typhimurium-Vaccinated versus Infected Pigs. Vaccines 2021, 9, 845; https://doi.org/10.3390/vaccines9080845

Journal Impact Factor 2021: 4.961

Christine Unterweger, Aleksandra Inic-Kanada, Sara Setudeh, Christian Knecht, Sophie Dürlinger, Melissa Stas, Daisy Vanrompay, Celien Kiekens, Romana Steinparzer, Wilhelm Gerner, Andrea Ladinig, and Talin Barisani-Asenbauer. Characteristics of Chamydia suis Ocular Infection in Pigs. Pathogens 2021, 10(9), 1103; https://doi.org/10.3390/pathogens10091103

Journal Impact Factor 2021: 3.492

Marlene Mötz, Melissa R. Stas, Sabine E Hammer, Tereza Duckova, Frederic Fontaine, Alexandra Kiesler, Kerstin Seitz, Andrea Ladinig, André C. Müller, Christiane Riedel, Armin Saalmüller, and Till Rümenapf. Identification of MHC-I-Presented Porcine Respiratory and Reproductive Syndrome Virus (PRRSV) Peptides Reveals Immunogenic Epitopes within Several Non-Structural Proteins Recognized by $CD8^+$ T Cells. Viruses 2022, 14(9), 1891; https://doi.org/10.3390/v14091891

Journal Impact Factor 2022: 4.911

Alix Pierron, Eleni Vatzia, Maria Stadler, Kerstin H. Mair, Selma Schmidt, Melissa R. Stas, Sophie Dürlinger, Heinrich Kreutzmann, Christian Knecht, Gyula Balka, Julia Lagler, Marianne Zaruba, Till Rümenapf, Armin Saalmüller, Elisabeth Mayer, Andrea Ladinig, and Wilhelm Gerner. Influence of deoxynivalenol-contaminated feed on the immune response of pigs after PRRSV vaccination and infection. Archives of Toxicology 2023, https://doi.org/10.1007/s00204-023-03449-9

Journal Impact Factor 2023: 5.153

Acknowledgements

I would like to express my gratitude to both my supervisors, Andrea Ladinig and Wilhelm Gerner, for providing me the opportunity to steer this PhD project in a professional and supportive environment. I would like to specially thank Andrea Ladinig for her guidance and support with regard to my career development, her encouragement, and expertise in the veterinary field. I have learned lot during the past years. I would like to thank Wilhelm Gerner for his guidance and support, his insights, and all our exciting scientific discussions. Furthermore, I have always enjoyed the extensive meetings the three of us have had.

I would also like to extent my gratitude to Kerstin Mair and Armin Saalmüller for their support and expertise on interpreting the obtained results. I would also like to take a moment to appreciate the support provided by Marlies Dolezal. I would never have been able to run this complex statistical analysis in a timely manner.

I would like to thank the members of the Clinic for Swine, both the old and the new, for their excellent support, expertise, and help with all the experiments done. Next, I would like to thank my colleagues at the Institute of Immunology for all their help and support to make this PhD project possible. It always comes down to great teamwork!

Special thanks should also be extended to our collaborator Boehringer Ingelheim for their assistance and financial support. As a member of the graduate school for pig and poultry (PaP), I would like to thank all members for the lively discussions at the PaP seminars, PaP retreats, and PaP symposia.

Finally, I would like to thank Katinka for her unwavering support and my aunt for believing in me.

Abstract (max 500 words)

In humans and mice, extensive research on the phenotype and function of immune cells that reside at the maternal-fetal interface has been performed with the goal to understand the complexity of reproductive immunology. In pigs, however, studies that addressed immune cell phenotypes at the maternal-fetal interface mainly focused on early gestation, whereas late gestation has not been investigated so far. In addition, the literature available so far only addressed the major lymphocyte subsets without going into much detail. Therefore, this PhD thesis aimed to establish a methodology tailored to porcine epitheliochorial placenta which would allow for the investigation of the immune cell composition in the maternal endometrium (ME) and fetal placenta (FP) separately. In the first study we performed in-depth phenotyping experiments for the characterization of natural killer cells (NK), non-conventional, and conventional T cells within maternal blood (mBld), ME, FP, and fetal spleen (fSpln). The results showed that between the investigated anatomic locations that observed NK and T cell phenotypes were considerably different. Lymphocyte subsets originating from the maternal compartments (mBld and ME) displayed highly differentiated phenotypes. Furthermore, even in the absence of any stimuli, lymphocytes isolated from the maternal compartments had a high capacity to spontaneously release interferon-gamma (IFN-γ) which reflected the high degree of NK and T cell differentiation within those anatomic sites. In the fetal compartments (FP and fSpln), mainly naive phenotypes were found. Nevertheless, also differentiated phenotypes e.g. $CD2^{+}CD8\alpha^{+}CD27^{dim/-}$perforin^{+} γδ T cells, $CD27^{-}$perforin^{+} cytolytic T cells (CTLs), and T-bet$^{+}CD4^{+}CD8\alpha^{+}CD27^{-}$ Tem cells were identified in the FP. Porcine reproductive and respiratory syndrome virus (PRRSV) causes reproductive failure during late gestation. As to date, the local immune response at the maternal-fetal interface remains poorly characterized and specific literature available is sparse. Therefore, our second study aimed to investigate the phenotypic changes at the maternal-fetal interface following PRRSV infection and/or vaccination in a reproductive gilt model. A total of twenty-four gilts were included, twelve gilts were vaccinated with a modified live virus (MLV) vaccine whilst the other twelve gilts were not. During late gestation (day 84) gilts were challenged with either one of the two selected PRRSV-1 field isolates or sham-inoculated with cell culture medium. Three weeks post-infection all gilts and their litters were euthanized and two fetuses per gilt were randomly selected in order to study the local immune response in the ME and FP. In non-vaccinated gilts, infection resulted in a strong expansion of effector lymphocytes which might contribute to pathology at the maternal-fetal interface rather than confer protection. A more contained immune response was observed in the vaccinated gilts and conferred protection. Taken together, these studies provide the groundwork to further explore local immunity *in utero* and provide insight into local events in response to PRRSV infection. Furthermore, the same methodology could be applied to other pathogens that cause reproductive failure.

Abbreviations

Bcl-6	B-cell lymphoma 6
CCR7	C-C chemokine receptor type 7
CD	Cluster of differentiation
CTL	Cytolytic T cell
dCD4	decidual CD4 T cell
dCD8	decidual CD8 T cell
dpi	days post infection
ELISpot	Enzyme-linked immunosorbant spot assay
EMA	European Medicines Agency
FP	Fetal placenta
fSpln	Fetal spleen
gd	gestation day
HCMV	Human cytomegalovirus
HLA	Human leukocyte antigen
HV	High virulent
ICOS	Inducible co-stimulatory molecule
IFN-γ	Interferon-gamma
IL	Interleukin
LAG-3	Lymphocyte-activation gene 3
LV	Low virulent
MA-104	African green monkey kidney cell line
mBld	Maternal blood
ME	Maternal endometrium
MHC	Major histocompatibility complex
MLV	Modified live virus
nAbs	Neutralizing antibodies
NK	Natural killer cell
ORF	Open reading frame
PAM	Pulmonary alveolar macrophage
PCV-2	Porcine Circovirus Type 2,
PD-1	Programmed cell death protein-1
PPV	Porcine Parvovirus

PRRS	Porcine Reproductive and Respiratory syndrome
PRRSV	Porcine Reproductive and Respiratory syndrome virus
SLA	Swine leukocyte antigen
TCR	T cell receptor
TIM-3	T cell immunoglobulin and mucin-domain containing 3
TNF-α	Tumor necrosis factor-alpha
Tfh	Follicular T helper T cell
Th	T helper cell
Tn	Naive T cell
Tcm	Central memory T cell
Tem	Effector memory T cell
TEMRA	Terminally differentiated CD8 T cell
Treg	Regulatory T cell
uNK	Uterine natural killer cell

1. Introduction

1.1. Porcine immune cells

The toolbox to study porcine immune cells has expanded substantially and can be used to investigate immune cells in health, following vaccination, and disease. Using multicolor flow cytometry, various lymphocyte subsets can be identified using various cluster of differentiation (CD) molecules **(Figure 1)**. Natural killer (NK) cells are part of the innate immune system and play an important role in the defense against a multitude of pathogens. As a porcine NK cell specific marker has not yet been identified, a combination of markers needs to be applied for their identification. Porcine NK cells can be identified using the phenotype perforin^{+}CD3^{-} CD8α$^{+/-}$CD16^{+}CD172a^{-}NKp46$^{+/-}$ (1-3). These cells lack the expression of CD4, CD5, CD6, and CD8β (1, 2). Furthermore, not all porcine NK cells express the activating receptor NKp46 (CD335, natural cytotoxicity receptor-1), as compared to other species (2, 3). In the pig NKp46^{-}, NKp46^{+}, and NKp46^{high} NK cells can be identified (2, 3). These NKp46-defined subsets differ in their expression pattern of CD8α, cytokine production capacity, and killing capacity (2, 3).

T cell receptors (TCRs) can either be formed by a γ and δ-chain or an α and β-chain, delineating γδ T cells and αβ T cells, respectively. Alongside with sheep, cattle, and chickens, pigs belong to the γδ-high species which means that a substantial proportion of the T cells in the blood and secondary lymphoid organs belong to this lineage (4, 5). Little is known about their role in the immune system as these cells may fulfill multiple actions (6, 7). The adhesion molecule CD2 separates porcine γδ T cells into a positive and negative subset, which are believed to represent two distinct lineages that are already established in the thymus (8). This notion can be substantiated by the expression of certain molecules, functionalities, and mode of antigen recognition (5, 9). The expression of the transcription factor T-bet and perforin, and capacity to produce interferon-gamma (IFN-γ) has mostly been associated with a CD2^{+} phenotype, whereas the expression of the transcription factor GATA-3 and production of interleukin-17A (IL-17A) seems to be associated with a CD2^{-} phenotype (4, 5). For CD2^{+} γδ T cells, the expression of CD8α and CD27 might delineate naive and differentiated phenotypes (5). Ageing also seems to drive phenotypic changes in the peripheral γδ T cell compartment (5). Over the course of life, the frequency of CD2^{-} drops which coincides with an increase in CD2^{+} γδ T cells which express T-bet, perforin, and CD8α (5). αβ T cells, including both CD4 and CD8 T cells, can be identified via the expression of T cell co-receptors. CD4 T cells are important regulators of immune responses, as they help other lymphocyte subsets and exhibit direct effector functions (10). Alongside the expression of CD3 and CD4, a wide variety of surface molecules, transcription factors, and the cytokine production profile can be used for their in-depth characterization (11-15). The differentiation and activation status can be assessed based on the CD8α/CD27-expression pattern which discriminates CD8α^{-}CD27^{+} naive (Tn), CD8α^{+}CD27^{+} central memory (Tcm), and CD8α^{+}CD27^{-} effector memory (Tem) CD4 T cells (12). In pigs, upregulation of CD8α is a sign of antigen-experience and is

associated with immunological memory (12, 16-19). These three CD8α/CD27-defined subsets differ in their functional capacity. Tem have an increased capacity to produce effector cytokines like IFN-γ and tumor necrosis factor-alpha (TNF-α) but a reduced proliferative capacity as compared to Tcm and Tn (12). In contrast, following stimulation, Tn mostly produce IL-2 and have a comparable proliferative capacity to the Tcm (12). Based on an overlapping expression pattern with CD27, also the lymph node homing receptor CCR7 (and CD62L) can be used to assess CD4 T cell differentiation (12, 18). Following activation and depending on the polarizing cytokine environment, CD4 T cells can differentiate into various T helper (Th) subsets. In men and mice, phenotypic plasticity of CD4 T cells has been observed (20), this might also apply to pigs (15). The characterization of these Th subsets in the pig, however, is not as evident as they have not been investigated in such detail (15). Porcine regulatory T cells have been identified based on a $CD4^{+}CD25^{high}Foxp3^{+}$phenotype (21). *In vitro* experiments have shown that in a Th2 and Th1 polarizing milieu porcine CD4 T cells upregulate the expression of the transcription factors GATA-3 and T-bet, respectively (13). This was further confirmed following a parasitic or viral infection and *in vitro* recall experiments (11, 13). Furthermore, the expression of T-bet in porcine CD4 T cells has been associated with the production of IFN-γ (11, 13), a Th1 hallmark cytokine. IL17A-producing CD4 T cells have also been characterized following infection with *Salmonella* Typhimurium (22). As CD8α is expressed on many porcine immune cell subsets, it is not an ideal marker for the unambiguous identification of porcine CD8 T cells (also designated as cytolytic T cells, CTLs). Therefore, a $CD3^{+}CD4^{-}CD8\alpha^{high}CD8\beta^{+}$ phenotype can be applied (19). Since the vast majority of peripheral CD8 T cells at birth exhibit a $CD27^{+}$SLA-$DR^{-}perforin^{-}$ phenotype they are considered to represent the naive subset (19). Over the course of life, the expression of CD27 gets downregulated whilst the expression of SLA-DR and perforin increases, and it has been suggested that $CD27^{dim}$SLA-$DR^{+}perforin^{+}$ represent early effector (or Tcm) and $CD27^{-}$ SLA-$DR^{+}perforin^{+}$ represent late effector (or Tem) CD8 T cells (15, 19). Recently, the transcriptomic profiles of $CD8\beta^{+}CD27^{+}CD11a^{low}$, $CD8\beta^{+}CD27^{dim}CD11a^{+}$, and $CD8\beta^{+}CD27^{-}$ $CD11a^{high}$ were evaluated and these cell subsets were designated as naive, intermediate, and terminally differentiated cells (23). The expression of CD11a and perforin is positively correlated, therefore, depending on the downstream applications staining of CD11a might be preferred as it is a cell surface molecule. In human immunology, CD8 T cell differentiation is tackled based on the expression pattern of CCR7 and CD45RA which also seems to be applicable to porcine CD8 T cells (24). Based on this expression pattern $CCR7^{+}CD45RA^{+}$, $CCR7^{+}CD45RA^{-}$, $CCR7^{-}CD45RA^{-}$, and $CCR7^{-}CD45RA^{+}$represent CD8 T cells with a Tn, Tcm, Tem, and terminally differentiated phenotype (known as TEMRAs) (24). Furthermore, following polyclonal stimulation it was shown that the Tem (and TEMRAs) were the greatest producers of IFN-γ and TNF-α (24). CD8 T cells, play an important role in the antimicrobial defense and fulfill major effector functions following viral infections (25, 26).

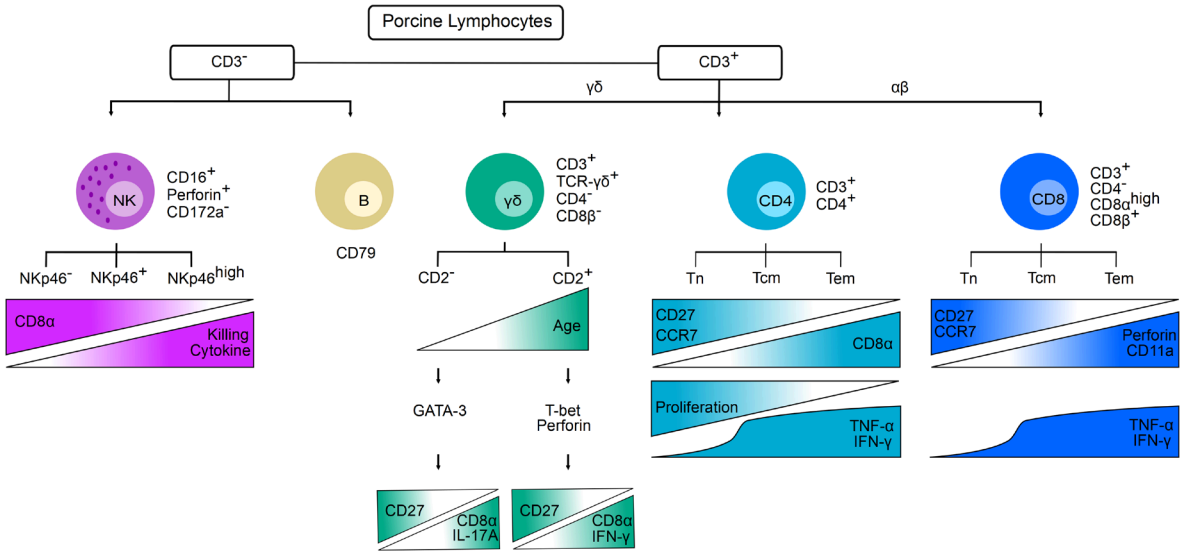

Figure 1 | Overview of porcine lymphocytes investigated in this PhD project. Multicolor flow cytometry panels have allowed the identification and characterization of various lymphocyte subsets. NK cells have a perforin^{+}CD3^{-}CD8α$^{+/-}$CD16^{+}CD172a^{-} phenotype which can further be delineated in three NKp46-defined subsets which exhibit distinct functional profiles. CD79, known as the pan-B cell marker, identifies all B cells. T cell subsets can be divided into αβ and γδ T cells, based on their composition of the T cell receptor. Two lineages of γδ T cells have been identified based on their surface expression of CD2. Ageing seems to increase the balance towards a higher frequency of CD2^{+}. Research indicates that a high GATA-3 expression is a feature of the CD2^{-} lineage whereas the expression of T-bet and perforin is restricted to the CD2^{+} lineage. Over the course of life, these cells start to express CD8α and downregulate CD27. These potentially differentiated CD2^{-} and CD2^{+} γδ T cells have been shown to produce IL-17A and IFN-γ, respectively. Co-expression of CD3 and CD4 identifies the T helper cells which can be monitored for CD8α/CD27-expression to follow their differentiation. Upon antigen encounter naive T cells (Tn) upregulate CD8α and progressively downregulate CD27 resulting in the generation of central memory (Tcm) and effector memory (Tem) cells. The effector functions, the proliferative response and cytokine producing capacity, of the Tn, Tcm, and Tem cells are distinct. CD8 T cells can be defined via a CD3^{+}CD8α^{high}CD8β^{+} phenotype. Further functional delineation can be based on the combination of perforin and CD27 (or alternatively CD27 and CD11a) which demarcates Tn, Tcm or early effector, and Tem or late effector phenotypes. This figure was made in Inkscape.

Porcine monocytes and macrophages are leukocytes that belong to the mononuclear phagocyte system. The first surface marker universally used for the identification of porcine myeloid cells is CD172a (SIRPα, signal regulatory protein α) (27). Porcine monocytes and macrophages can be further identified via the expression of CD16 and CD163 (27). Monocytes express CD14 and lack the expression of CD169 (sialoadhesin, Siglec-1) whereas macrophages express CD169 and exhibit a variable CD14 expression (27). CD14 and CD16 have been shown to mediate phagocytosis (27). CD169 is a lectin that that can bind sialic acid and therefore is involved in the uptake of sialylated pathogens (28). CD163 is a scavenger receptor that clears hemoglobulin/haptoglobulin complexes and seems to be a mediator of inflammatory processes (27, 28). However, the list of markers for their identification provided here is not complete.

1.2. The biology of the maternal-fetal interface (in the pig)

Depending on the breed, the gestation length in pigs is on average 115 days (29). The gestational period can be demarcated in three stages: early, mid, and late gestation representing the implantation and the initial establishment of the placenta, massive expansion of the placenta, and exponential growth of the fetus, respectively.

Following the fertilization of oocytes in the oviduct, zygotes undergo a series of cell divisions and reach the uterus after two to three days (29-31). As blastocysts, consisting of an inner cell mass surrounded by trophectoderm/trophoblast, they migrate into the uterine horns to become evenly distributed by gestation day (gd) 12 (29, 30). The blastocysts provide hormonal signals, e.g. estrogens and prostaglandin E2, necessary to maintain the corpus luteum, the progesterone source during gestation (29, 30). The blastocysts, undergo morphological changes, elongate, and attach to the uterine lining in order to reduce the distance between the maternal and fetal circulation, this process is called implantation and results in the establishment of the placenta (30, 32). During implantation, the conceptuses rapidly elongate by gd16 to increase the surface area for placental development (30, 32, 33). Besides estrogen and prostaglandin E2, conceptuses also secrete a range of cytokines including interleukin-1β2, IFN-γ, interferon-δ, and transforming growth factor β (30, 33). These chemical signals induce endometrial changes that promote the attachment and implantation to uterine epithelium (30, 33, 34). Following the rapid elongation, the trophectoderm and uterine epithelium develop adhesion competency resulting in their attachment (30, 32, 33). This initiates extensive remodeling of the trophoblast and uterine epithelium resulting in the formation of placental and endometrial folds which increases the surface area of the maternal-fetal interface and reduces the distance between the maternal and fetal blood circulation (30, 32, 33). Furthermore, interdigitating villi develop between the trophoblast and uterine epithelium which cover most of the placenta (30, 32, 33). Approximately between gd20 - gd30, areolae are formed at the openings of the uterine glands (29, 30, 32). At the end of early gestation (day 30 - 35), a functional epitheliochorial placenta is established. Over the course of gestation, more defined and longer folds (placental and endometrial) are formed and by day 70 of gestation the placenta reaches its maximum weight, maximal surface area, and maximal number of areolae (30, 32). Furthermore, a strong increase in vascularization at both sides of the maternal-fetal interface occurs during mid-gestation (35) in order to support the exponential growth of the fetus in late gestation.

The placenta is an essential organ that supports the growth and development of the semiallogeneic fetus as it enables the exchange of gases, micro and macronutrients, and waste products. In addition, the placenta is also a source of chemical mediators. Across placental mammals, differences in placenta types can be observed. Classification systems group the placenta types based on either the shape or histology (36). Based on the shape: diffuse, multicotyledonary, zonary, and discoid placenta types can be described (36). This classification is dependent on the extent of the exchange area of the maternal-fetal interface e.g. covering the entire surface of the uterine epithelium with formation of folds, as in diffuse types, to an interaction that is confined via a circular area in discoid types (36). Based on histology and thus the extent of invasiveness epitheliochorial, endotheliochorial, and hemochorial placenta types are recognized (36). Hemochorial placenta types (e.g. primates,

mice) are considered the most invasive type of placenta as the trophoblast actively invades the endometrial lining (36), following the apposition and attachment phase, to gain access to maternal blood (37-40). Furthermore, extensive remodeling, termed decidualization, occurs (37-40). Epitheliochorial placentation is considered superficial and non-invasive (30, 36, 40). The trophoblasts merely attach and interdigitate to the uterine epithelium without invading this layer and without endometrial decidualization (30, 31, 36, 40).

Pigs have a diffuse epitheliochorial placenta which is comprised of six layers that separate the maternal and fetal blood circulation (illustrated in **Figure 2**). The porcine maternal-fetal interface is composed of maternal blood vessels, endometrial connective tissue, an epithelial interdigitating bilayer formed by the uterine epithelium and trophoblasts, fetal connective tissue, and fetal blood vessels (30, 31). Thus, the maternal and fetal compartment remain completely separated and are further referred to as maternal endometrium (ME) and fetal placenta (FP). Having these additional layers has implications for the maternal-fetal exchange (histotrophic or hemotrophic exchange). For instance, it has been shown that maternal immunoglobulins cannot permeate the epithelial bilayer (41), which highlights the importance of colostrum uptake by newborn piglets. This implicates that immune cells also cannot migrate across this barrier. Furthermore, the uptake of certain nutrients, e.g. fatty acids, across the maternal-fetal interface is rather low in epitheliochorial placentation (36). Uterine glands secrete histotroph in the lumen of the areolae which are absorbed by the trophoblast via fluid-phase pinocytosis for fetal consumption (32, 42). Histotroph plays an important role in the transfer of iron to the fetus in order to support fetal hematopoiesis (32, 42). In addition, growth factors, enzymes, hormones, transport proteins, glucose, and amino acids are also provided via the uterine secretions (32, 42).

1.3. The immunology of the maternal-fetal interface

During the gestational period, the maternal immune system needs to be able to tolerate the presence of the fetus and if needed to launch an appropriate immune response to intruding pathogens. This balance is tightly regulated by mediators of the innate and adaptive immune system and the local microenvironment (43). Initially, it was thought that pregnancy was a state where constant immunosuppression was needed, but over the last decades this has been refuted. It is now clear that pregnancy is an immunologically dynamic process in which implantation, placentation and labor represent a pro-inflammatory state and mid-gestation is thought to be an anti-inflammatory stage with the goal to support fetal growth and development (37). This implicates that the local composition of decidual immune cells, their phenotype, and function also changes (37, 44). In the human decidua, the maternal uterine tissue in which the trophoblast invades, is composed of approximately 40% leukocytes. In early gestation, ~70% are uterine NK cells (uNK), ~20% macrophages, and ~5-20% T cells. Over the course of gestation, the frequency of uNK cells decreases whereas the T cell frequency increases (up

to 80%) (45-47). Overall, leukocytes that reside at the maternal-fetal interface are phenotypically and functionally different as compared to their peripheral counterparts.

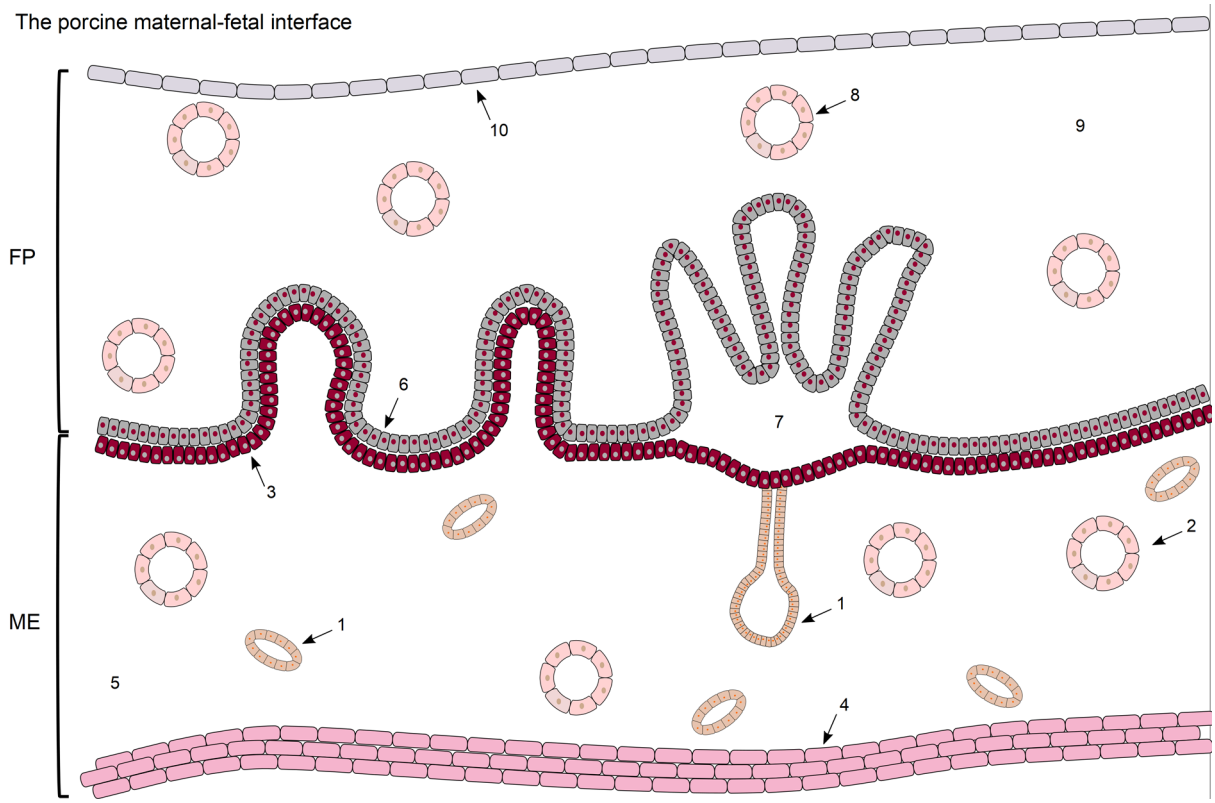

Figure 2 | Schematic overview of the porcine maternal-fetal interface. The following structures are indicated: 1) Uterine glands, 2) Maternal blood vessels, 3) Uterine epithelial layer, 4) Myometrium, 5) Maternal connective tissue, 6) Trophoblast or fetal epithelial layer, 7) Areolae, 8) Fetal blood vessel, 9) Fetal connective tissue, 10) Amnion. ME; Maternal endometrium, FP; Fetal placenta. This figure was made using Inkscape.

Post-ovulation and during the first trimester, human uNK cells become enriched and more granulated in a progesterone-dependent manner and can be characterized using a $CD56^{bright}CD16^{-}KIR^{+}CD9^{+}CD49a^{+}$ phenotype (46). During implantation, they coordinate the remodeling of the spiral arteries and regulate the invasion of the trophoblast in order to ensure a sufficient blood supply (46, 48). uNK cells can mediate these processes by secreting a variety of cytokines, angiogenic factors, growth factors, and proteases (48, 49). Although it has been shown that uNK cells contain cytolytic machinery comparable to their peripheral counterpart, they exhibit poor cytolytic activity. As NK cell function depends on the balance between activating and inhibitory receptors and the cytokine environment (e.g. IL-15), it is plausible that under certain conditions NK cell function is altered (50, 51). Research has shown that uNK cells can combat viral threats in the decidua in order to limit the spread to the fetus (50). uNK cells are able to kill human cytomegalovirus (HCMV)-infected endometrial cells (50), but not HCMV-infected trophoblasts (52). Recent work has shown that uNK cells can kill bacteria in trophoblasts via the transfer of gransulin, without affecting the integrity of the maternal-fetal interface (53). However, in context of infection with ZIKA-virus, it has been shown that uNK cells kill co-cultivated infected trophoblast-like cell lines or infected trophoblasts (54). Nevertheless, a mouse model has shown that depletion of NK cells and

subsequent infection with ZIKA-virus resulted in severe placental pathology which provided evidence that the uNK cells have a protective role by preventing viral spread although some trophoblast cells may get killed in the process (54). However, most studies that investigate the involvement of uNK cells to fight local infections were done with samples collected from the first trimester. Recently, Vieira and colleagues demonstrated that uNK cells at term exhibit a lower capacity to respond to HCMV infected cells as compared to early gestation (47).

Various T cell populations, both αβ and γδ T cells, have been identified in the human decidua (55, 56). Over the course of gestation, the local T cell population is composed of CD8 T cells (45-75%), CD4 T cells (30-45%), and γδ T cells (5-20%) (55-57). Literature demonstrates that based on the expression pattern of CD45RA/CD45RO or CD45RA/CCR7 antigen-experienced decidual CD4 (dCD4) and decidual CD8 (dCD8) T cells prevail (58-61). Depending on the cytokine microenvironment, CD4 T cells can differentiate into Th1, Th2, Th17, and Treg cells. In humans, these are identified based on the expression of certain chemokine receptors, transcription factors, and cytokine profiles. A $CCR6^{-}CCR4^{+}CXCR3^{+}$, $CCR6^{-}CCR4^{+}CXCR3^{-}$, and $CCR6^{+}CCR4^{+}CXCR3^{-}$ phenotype delineates Th1, Th2, and Th17 cells, respectively (62, 63). Using these marker combinations has allowed for the identification of these CD4 T cell subsets in the decidua. 5-45% of the CD4 T cells have a Th1 phenotype, 2-6% have a Th2 phenotype, and 2-5% have a Th17 phenotype (62, 63). Besides a physiological role during pregnancy, these cells can also surveil the local environment and provide a defense mechanism to intruding pathogens (63-65). Physiologically, Th1 cells secrete IFN-γ and TNF-α, and help to regulate the extent of trophoblast invasion and tissue repair. These effector cytokines, can alter cell adhesion and mobility of the trophoblasts and vascular remodeling (64, 65). IL-17 producing Th17 cells have been reported to support angiogenesis and during the first trimester to support trophoblast invasion and survival (64, 65). Thus, these cells are thought to play an important role during pregnancy. Th2 phenotypes and effector cytokines peak during mid-gestation and provide a supportive environment for fetal growth and development (37). Furthermore, CD4 T cells have been implicated to play a role during labor (66). During the first trimester, dCD8 T cells have been shown to secrete cytokines (e.g. IFN-γ, IL-8) and are able to kill target cells (67). The supernatant of these dCD8 T cells, enabled the isolated trophoblasts to invade Matrigel *in vitro*, which implicates a role for these cells in trophoblast invasion (67). dCD8 T cells, at term, have lower protein expression levels of the cytolytic molecules perforin and granzyme B, despite their differentiation state as compared to their peripheral counterpart (60, 68). Nevertheless, the mRNA levels of these cytolytic molecules was higher as compared to peripheral CD8 T cells (60). Upon activation, dCD8 T cells showed an increase in cytolytic protein expression, which indicates that posttranscriptional regulation mechanisms are involved which can be affected by pro-inflammatory events (e.g. like infections) (59). The phenotype and thus the level of antigen-experience is indicative of the presence of antigens. Research has shown that these

decidual T cells can recognize fetal antigens (61) and viral antigens (69). Cross reactivity of pathogen-specific dCD8 T cells against (human leukocyte antigen) HLA-C has also been reported (70). For instance, an HLA-B*08:01- restricted Epstein-Barr virus-specific T cell clone and HLA-C restricted HLA-C*06:02/TRA restricted HCMV-specific T cell clone showed cross reactivity to HLA-C*01:02 and HLA-C*03:02, respectively. Nonetheless, most pathogen-specific dCD8 T cells are HLA-A or B specific and have been shown to provide protection as the trophoblast does not express these HLA-types (69). However, trophoblasts express HLA-C (and non-classical HLA molecules), therefore, they may become a target when infected and lead to potential complications (70). Nevertheless, most pregnancies occur without major complications which indicate that regulatory mechanisms are involved. $CD25^{high}Foxp3^{+}$ Tregs have been shown to comprise 5-20% of the decidual CD4 T cell population (45, 61-63). Decidual Tregs can suppress fetal/paternal-specific and non-specific responses in order to maintain tolerance (71). This notion can be substantiated by experiments that have demonstrated an increase in proliferating T cells with fetal specificity following the depletion of Tregs (61, 72, 73). Furthermore, various regulatory Treg subsets (74) with differentiated Treg phenotypes reside at the maternal-fetal interface (63, 75). Some decidual T cells also express NK cell associated receptors which may provide additional means of tolerance (56). Furthermore, decidual T cells express checkpoint molecules of which their ligands are locally expressed (59, 61). Overall, it is clear that the immunology of pregnancy is very complex, every cell subsets serves its physiological purpose, and a tight balance is needed. A disturbance in the cellular balance or regulatory mechanisms might result in pregnancy complications (43, 64, 65, 75).

In the pig, research addressing reproductive immunology at the maternal-fetal interface is sparse and has predominantly focused on the earlier stages of gestation. Initial findings demonstrated that at the endometrium/conceptus attachment sites leukocytes (potentially NK and T cells) were enriched as compared to the endometrium between attachment sites (76, 77). Another study reported that classical $CD16^{+}$ NK cells relocated over the course of early gestation (78). Initially $CD16^{+}$ NK cells were found in the sub-epithelial stroma and following implantation NK cells were mostly found in the glandular stroma (78). The authors postulated that this relocation might be a way to protect the semiallogeneic fetus against its potential cytolytic activity (78). This hypothesis is based on the findings that endometrial cells isolated at gd 10 and 20 were able to lyse target cells (K562 cell line) (79). Based on the morphology and a positive perforin staining using cytospin, and the fact that CTLs do not kill K562 cells unless they are primed for their recognition, these cells were assumed to be NK cells (79). The lytic activity, however, was abrogated at gd 30 (79). Later, the same group showed that these NK cells were also able to kill trophoblasts between gd 17 and 20 (80). Further, $CD3^{-}$ $CD8\alpha^{+}$ and $CD56^{+}$ NK cell phenotypes were also described in the porcine endometrium during early gestation. $CD3^{-}CD8\alpha^{+}$ NK cells peaked at gd 10, reaching about 20% of total

lymphocytes, and declined by gd 30 (78). $CD56^+$ NK cells, potentially resembling the human uNK cells, represented about 12% of local lymphocytes in the pre-attachment phase, declined during the attachment phase and progressively increased following the attachment phase (78). Of note, the same antibody clone to detect CD56 was also tested at our university and did not work in our hands (data not published), therefore, these data should be interpreted with care. Furthermore, only processed results are shown in reference (78). Besides NK cells, T cells are recruited to the implantation site and might play an important role for the establishment of the porcine epitheliochorial placenta (81). CD4, CD8, and γδ T cells seem to play a role during early gestation, however, comprehensive details on their phenotype and functionality is lacking. Nevertheless, it is assumed that endometrial lymphocytes coordinate angiogenic processes and are an additional source of IFN-γ (82). Recent work using the CRISPR/Cas9 gene editing technology to generate $IFNG^{-/-}$ embryos has demonstrated the importance of conceptus derived IFN-γ for the recruitment of T cells to the site of implantation (83). However, lymphocytes when recruited are a superior source of IFN-γ as compared to the trophoblast (82). IFN-γ regulates the expression of angiogenic factors including vascular endothelial growth factor A and hypoxia-inducible factor-1-alpha (82). In addition, the expression of major histocompatibility complex (MHC) class II mRNA in the endometrium, in a gestation dependent manner, is induced by IFN-γ, and might implicate a role in regulating maternal immune response (84). Additional regulatory mechanisms might include the expression of chemokine decoy receptors (85) and the expression of tumor necrosis factor family (TNFSF10 and FasL) on uterine epithelium (86). Overall, a lot of questions regarding the phenotype and function of immune cells that reside at the maternal-fetal interface and how they are regulated, even during early gestation, remain largely unanswered. Furthermore, infection with certain pathogens, especially during late gestation, can cause reproductive complications. In order to fully understand the role of local immune cells in health and disease, in-depth characterization is needed.

1.4. Porcine Reproductive and Respiratory Syndrome Virus

Porcine reproductive and respiratory syndrome (PRRS) is one of the most important infectious swine diseases with a negative economic impact on global swine industry and is caused by the porcine reproductive and respiratory syndrome virus (PRRSV) (87-89). Historically, PRRS is in literature also referred to as ‘mystery swine disease’, ‘blue-eared pig disease’, ‘porcine epidemic abortion and respiratory syndrome’, and ‘swine infertility and respiratory syndrome’ (90). PRRSV is an enveloped, positive-stranded RNA virus belonging to the *Arteriviridae* family, which can be further classified within the order of Nidovirales (87). The virion is a spherical to elliptical shaped entity with a 55 nm diameter, which comprises a 15 kb long RNA genome that is packed by nucleocapsid proteins that are further surrounded by a lipid-bilayer containing surface glycoproteins and membrane proteins (87). The viral genome encodes multiple open reading frames (ORFs) yielding both non-structural (ORF1a and ORF1b) and

structural (ORF2-7) proteins (87). Two genetically distinct species have been identified: '*Betaarterivirus suid 1'* (PRRSV-1, formerly known as European genotype 1) and '*Betaarterivirus suid 2'* (PRRSV-2, formerly known as North American genotype 2) (91-93). There is a 30-45% nucleotide variation between the species (87), but also within one species several subtypes/lineages containing different viral strains exist (94-96). This high degree of genetic diversity, derived from a high mutation rate and genetic recombination events (94, 95), might explain differences observed in the field concerning virulence, severity in clinical outcome, and *in vitro* cultivation (97-99).

The last three decades have shown that PRRSV is a pig specific pathogen that has a strong tropism for cells of the monocytic lineage (87). *In vivo* fully differentiated pulmonary alveolar macrophages (PAMs) are considered as primary target for infection (100). Also other tissue-specific macrophages e.g. in the nose, lymph node, tonsils, spleen, thymus, intravascular, and at the maternal-fetal interface are targets for infection (31, 87, 101-104). Initially, it was shown that blood derived monocytes are not that susceptible to the virus, however, more recently it has been shown that they can be infected (104). In addition, monocyte derived dendritic cells have also been reported to support viral replication (105, 106). Certain cell lines, including the African green monkey kidney cell line (MA-104 cells) and derivatives (MARC-145 cells), are permissive for the virus (87, 107) and are often used for viral propagation and *in vitro* investigations. Furthermore, a porcine trophoblast cell line, derived from a day 12 porcine conceptus, has been shown to support viral replication following exposure to PRRSV-2 (108). Moreover, PRRSV non-permissive cells have been used for the recombinant expression of specific receptors (107). Therefore, it is thought that this tropism is driven by the expression of certain cellular molecules associated with viral entry (109). Various molecules have been identified including: CD163, non-muscle myosin heavy chain 9 (MYH9), heparan sulphate, vimentin, CD151, and DC-SIGN (CD209) (28, 109). CD163 is one of the most studied molecules in PRRSV biology and is considered as the main receptor for infection as complete CD163 knock-out pigs are impervious to the virus (28, 110). Research shows that CD163 interacts with the GP2a/GP3/GP4 heterotrimeric complex and thereby is involved in viral internalization and uncoating (28, 87, 109). CD169 interacts with the GP5/M heterodimer and thereby might facilitate viral attachment and initiate clathrin-mediated endocytosis (28, 87, 109). However, a complete knock-out of CD169 does not protect pigs from infection (28, 87). MYH9, a motor protein, might also be a viral entry mediator via its interaction with GP5 (28). Heparan sulphate binds the GP5/M heterodimer and concentrates the virus on the surface of the target cell and thereby promotes the binding to subsequent receptor(s) for internalization (28, 109). Expression of vimentin, CD151, and DC-SIGN in PRRSV non-permissive cells renders them susceptible to infection but, the exact role of these molecules need to be further characterized (28, 109). Furthermore, other viral entry mediators may still be identified and validated (104, 111).

Viral transmission can occur both horizontally and vertically and can affect pigs at all ages (112). As to date, various routes of viral exposure (e.g. intranasal, intramuscular, oral, intra-uterine, and vaginal) have been described (112). In the field, clinical signs can vary from farm to farm, ranging from no signs to severe, and are dependent on several factors including: virulence of the virus strain, the immune status and susceptibility of the host, environmental factors, and concurrent (opportunistic) infections (112). Respiratory disease and impeded growth performance rates are often reported in nursery and grower-finisher pigs (112). In pregnant females infection during late gestation causes reproductive failure which includes: abortions, early farrowings, fetal death, and the birth of weak, congenitally infected piglets that have an increased pre-weaning mortality (113-115). All post-implanted embryos and fetuses throughout the course of gestation are susceptible to PRRSV upon direct intra-fetal or intra-amniotic exposure (31, 112). Transplacental transmission, from the dam to fetus, and the occurrence of reproductive disease is mostly associated with late gestation (gd > 70) whilst the occurrence is very uncommon during early and mid-gestation (31, 112). This restriction to late gestation might be related to the presence of PRRSV-permissive cells, e.g. $CD163^{+}CD169^{+}$ macrophages, at the maternal-fetal interface (102). However, the underlying mechanisms/events that facilitate viral transmission *in utero* still remain to be elucidated.

Over the last decades, research indicates that fetal deterioration and demise are the result of the events at the maternal-fetal interface in response to the pathogen as opposed to the viral replication within the fetus (87, 112, 116-120). Altogether, the local events at the maternal-fetal interface and potential modes of vertical transmission have been proposed (e.g. direct cell-to-cell contact, paracellular or transcellular spread of free virions, migration of PRRSV-infected macrophages from the ME to the FP also known as the trojan horse hypothesis, and the uterine glands-areolae system (31, 121-123)) and will be further explored and are summarized in **Figures 3 + 4**. Following intranasal exposure, PRRSV breaches the respiratory mucosa, replicates in its target cells located in the nose, respiratory tract, and tonsils, and inevitably viremia occurs (31, 87). In the blood circulation, the virus most likely attaches to a susceptible monocyte that adheres to the endometrial vessels and extravasates into the endometrial connective tissue (31, 87). Subsequently, the virus replicates in endometrial $CD163^{+}CD169^{+}$ macrophages and induces apoptosis of infected cells and bystander apoptosis (31, 87, 117, 118). The virus crosses the epithelial bilayer, comprised of the uterine epithelium and trophoblasts, and efficiently replicates in placental macrophages also resulting in apoptosis (31, 117, 118). A study has shown that PRRSV-infected macrophages in the FP are closely localised to the blood vessels in the FP, after which the virus reaches the fetus (31, 117).

One of the current hypotheses of congenital transmission includes the viral spread from an infected endometrial macrophage to the uterine epithelium and through the epithelial bilayer to the in the FP located fetal macrophages (31) (**Figure 3**, H1). This, however, is considered

the least likely scenario due to the strict tropism of the virus and the fact that the epithelial bilayer lacks the expression of viral entry associated molecules (31, 117). A recent study showed that the PTr2 porcine trophoblast cell line is susceptible to PRRSV-2 and even supports the release of virions (108). As the PTr2 cell line is derived from a d12 conceptus, which is not yet attached to the endometrial lining of the uterine horn and the epithelial bilayer is not yet formed, it is very different to a late gestation epithelial bilayer. Alternatively, PRRSV might cross the maternal-fetal interface in a cell-associated manner, where the maternal infected macrophage serves as a trojan horse, or as free virions via paracellular or transcellular transport (31) (**Figure 3**, H2+H3). Using immunofluorescence microscopy it recently has been shown that PRRSV-2 as free virions or in association with $CD163^{+}$ macrophages can be detected in the areolar region (123) (**Figure 3**, H4).

As an intact epitheliochorial placenta is impervious to maternal antibodies it seems unlikely that immune cells or even free PRRSV virions, which both are larger as compared to the size of an antibody, can migrate across. Several local events might impact the integrity of the epithelial bilayer and thereby might facilitate transplacental transmission (**Figure 4**). Bystander apoptosis, as a result of localised viral replication, was shown to affect other surrounding macrophages, lymphocytes, and even the uterine epithelial cells and trophoblast cells (117, 118). In addition, recent research has shown that PRRSV affects the expression of tight junction proteins, important for epithelial integrity and its barrier function, at the maternal-fetal interface thereby facilitating paracellular transport (119, 120). An increased number of putative NK cells, with a $CD3^{-}CD8\alpha^{+}$ phenotype, have been found in the ME of infected animals (116). Furthermore, it was shown that these putative NK cells were located in close proximity to the uterine epithelium, which in its efforts to combat the virus, might impair the integrity of the epithelial bilayer (31, 116). Altogether, these events can affect the integrity of the maternal-fetal interface, and allow the transit of free virus or infected cells from the ME to FP, impairing the placental functions, and thereby result in reproductive failure. However, knowledge on the phenotype and the contribution of other lymphocyte subsets are currently lacking and are necessary to fully comprehend the full extent of reproductive disease.

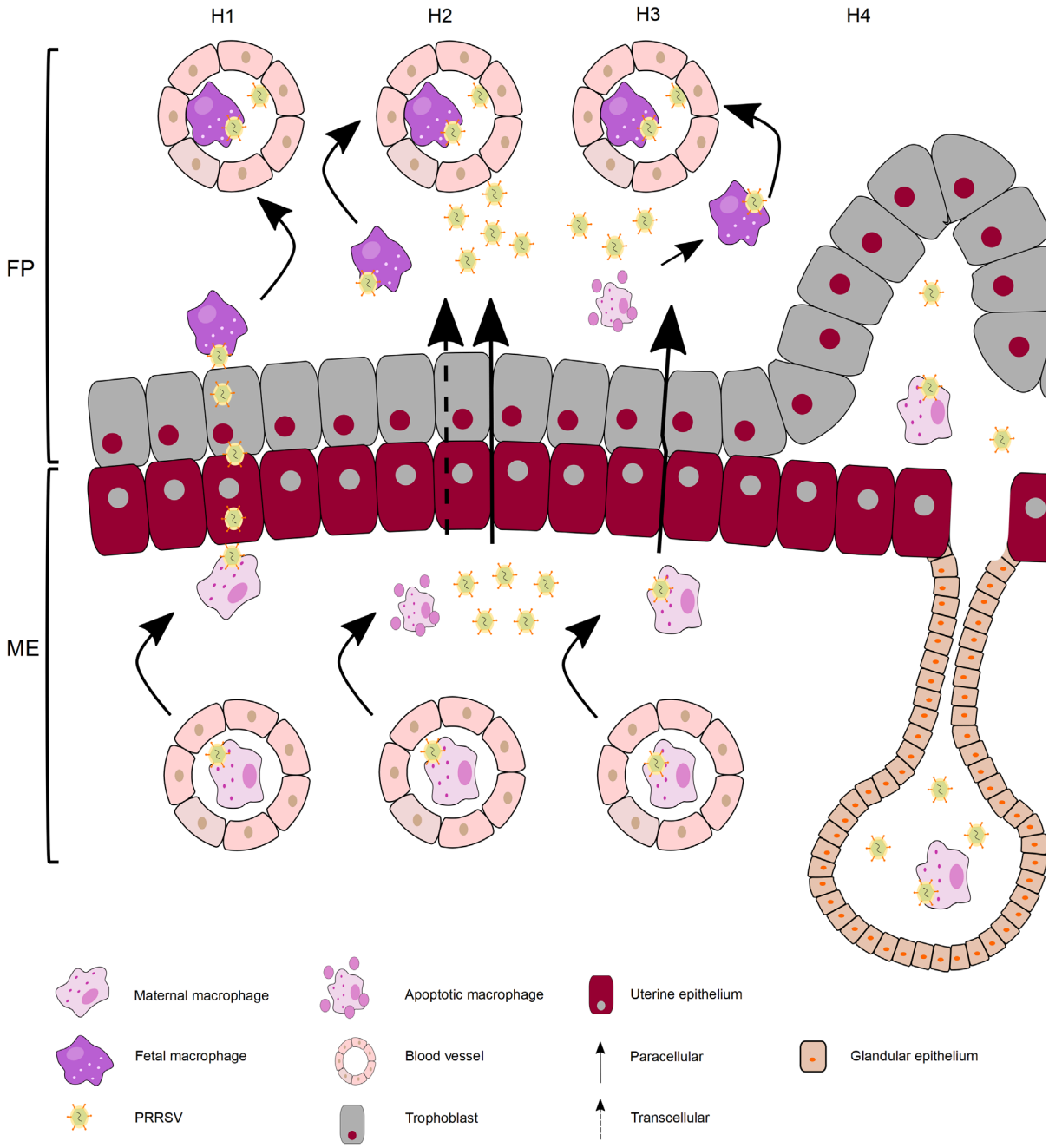

Figure 3 | Transplacental routes of transmission: current hypotheses. After reaching the maternal endometrium (ME) H1) the infected macrophage infects the uterine epithelium which infects the trophoblast layer and subsequently a fetal macrophage in the FP is infected. H2) Free virions can either be transmitted in a transcellular or paracellular fashion. H3) An infected maternal macrophage crosses the epithelial bilayer, the maternal macrophage dies via apoptosis which releases new virions that in turn can infect fetal macrophages. H4) Free virions or virus-infected cells are transmitted via the uterine gland/areolae system. Once the virus breaches this epithelial bilayer, it enters the fetal circulation which will result in the replication in fetal organs. ME, Maternal endometrium; FP, Fetal placenta. This figure was made using Inkscape.

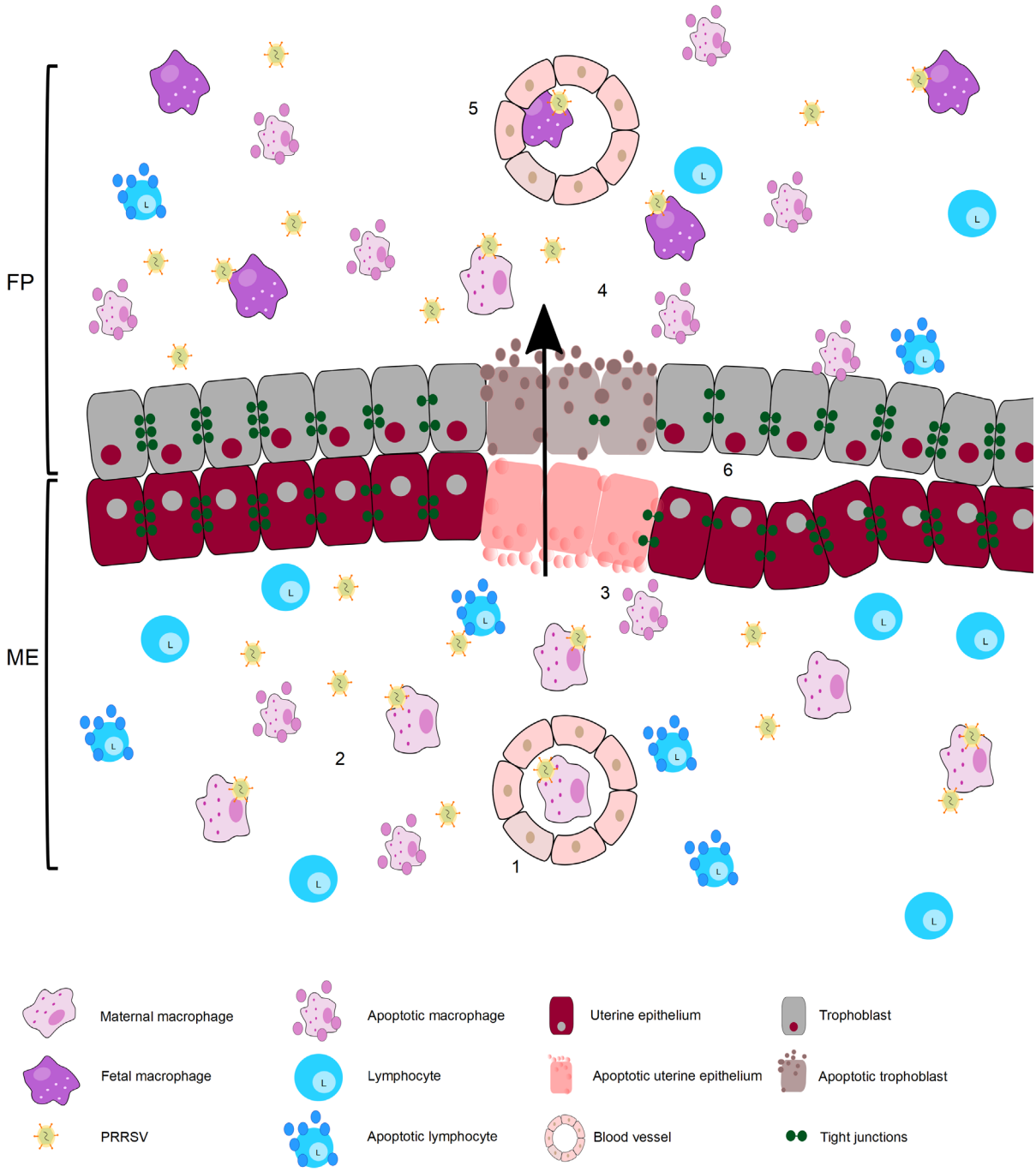

Figure 4 | Events at the maternal-fetal interface following infection with PRRSV. 1) A virus infected cell extravasates into the maternal endometrium (ME). 2) The virus replicates locally in the maternal macrophages. The virus induces apoptosis of infected cells and bystander apoptosis of surrounding lymphocytes. In proximity of the epithelial bilayer, bystander apoptosis can also affect the uterine epithelium and the trophoblast layer. Furthermore, the local microenvironment following viral replication can impact the integrity of the epithelial bilayer by affecting the tight junctions. 3-4) The virus breaches the maternal-fetal interface and efficiently replicates in fetal macrophages. Also here viral replication results in apoptosis and bystander apoptosis. 5) The viruses reach the fetal circulation and viral replication proceeds in fetal target organs. 6) All these events affect the integrity of the epithelial bilayer and result in the focal detachment. ME, Maternal endometrium; FP, Fetal placenta. This figure was made using Inkscape.

2. Aims and Hypotheses of the PhD project

The porcine placenta is impermeable, however, certain pathogens like for example PRRSV can breach this barrier and impact fetuses. Infection during late gestation consequently results in reproductive failure. Research addressing the phenotype and function of immune cells that reside at the porcine maternal-fetal interface, either in health or disease, is sparse. So far, investigations addressing the immune cell composition locally have mainly focused on early gestation and only major immune cell subsets have been characterized. Therefore, this PhD project aims to investigate the phenotype of various immune cell subsets at the maternal-fetal interface during late gestation in health and disease. This work will provide more insight into phenotypic changes of immune cells that occur following PRRSV infection and or vaccination.

This PhD project first aims to extensively characterize the immune cell subsets that reside at the maternal-fetal interface during late gestation.

- For this project a unique methodology tailored to the porcine epitheliochorial placenta was established and allowed us to study the immune cell phenotypes and function separately in the maternal endometrium (ME) and fetal placenta (FP) from healthy sows. We hypothesized that:
    - The ME and FP differ in immune cell composition e.g. antigen-experienced *vs.* naive phenotypes that dominate the two anatomic locations.
    - Functionality of immune cells obtained from the ME *vs.* FP is different.

The second aim of this PhD thesis is to investigate the phenotypic changes that occur following PRRSV infection and or vaccination.

- An animal trial, including six groups of pregnant gilts, was designed and performed in order to study potential changes in immune cell phenotypes in response to PRRSV infection and or vaccination. We hypothesized that:
    - Infection induces phenotypic changes in ME and FP located immune cells, indicative of local responses to the virus
    - Vaccination induces quantitative and qualitative differences in immune cell phenotypes that contribute to protection.

Overall, this work will provide the groundwork for further research to study the phenotype and function of immune cells in response to PRRSV but also other pathogens that can be transmitted *in utero.*

3. Publications

3.1. Publication 1

Melissa R. Stas, Michaela Koch, Maria Stadler, Spencer Sawyer, Elena L. Sassu, Kerstin H. Mair, Armin Saalmüller, Wilhelm Gerner and Andrea Ladinig. NK and T Cell Differentiation at the Maternal-Fetal Interface in Sows During Late Gestation. Frontiers in Immunology 2020; https://doi.org/10.3389/fimmu.2020.582065

Journal Impact Factor 2020: 6.429

Author contributions:

MRS, KHM, AS, WG, and AL were in charge of the study design. ELS and SS were involved in tissue collection and the tissue separation procedure. MRS, MK, MS, SS, and ELS performed laboratory work and experiments. MRS carried out the phenotyping experiments and analyzed the data. MRS, KHM, ELS, AS, WG, and AL thoroughly discussed and interpreted the data. MRS, WG, and AL wrote the manuscript. All authors read and approved the final manuscript.

frontiers in Immunology

ORIGINAL RESEARCH
published: 11 September 2020
doi: 10.3389/fimmu.2020.582065

NK and T Cell Differentiation at the Maternal-Fetal Interface in Sows During Late Gestation

Melissa R. Stas[1], Michaela Koch[1], Maria Stadler[2], Spencer Sawyer[1], Elena L. Sassu[1], Kerstin H. Mair[2], Armin Saalmüller[2], Wilhelm Gerner[2,3†] and Andrea Ladinig[1†]*

[1] University Clinic for Swine, Department for Farm Animals and Veterinary Public Health, University of Veterinary Medicine Vienna, Vienna, Austria, [2] Institute of Immunology, Department of Pathobiology, University of Veterinary Medicine Vienna, Vienna, Austria, [3] Christian Doppler Laboratory for Optimized Prediction of Vaccination Success in Pigs, Institute of Immunology, Department of Pathobiology, University of Veterinary Medicine Vienna, Vienna, Austria

OPEN ACCESS

Edited by:
Javier Dominguez, National Institute for Agricultural and Food Research and Technology (INIA), Spain

Reviewed by:
François J. M. A. Meurens, UMR INRAE-Oniris 1300 Oniris – Nantes Atlantic National College of Veterinary Medicine, France
Martin Faldyna, Veterinary Research Institute (VRI), Czechia

***Correspondence:**
Andrea Ladinig
Andrea.ladinig@vetmeduni.ac.at

† These authors have contributed equally to this work

Specialty section:
This article was submitted to Comparative Immunology, a section of the journal Frontiers in Immunology

Received: 10 July 2020
Accepted: 21 August 2020
Published: 11 September 2020

Citation:
Stas MR, Koch M, Stadler M, Sawyer S, Sassu EL, Mair KH, Saalmüller A, Gerner W and Ladinig A (2020) NK and T Cell Differentiation at the Maternal-Fetal Interface in Sows During Late Gestation. Front. Immunol. 11:582065. doi: 10.3389/fimmu.2020.582065

The phenotype and function of immune cells that reside at the maternal-fetal interface in humans and mice have been, and still are, extensively studied with the aim to fully comprehend the complex immunology of pregnancy. In pigs, information regarding immune cell phenotypes is limited and mainly focused on early gestation whereas late gestation has not yet been investigated. We designed a unique methodology tailored to the porcine epitheliochorial placenta, which allowed us to address immune phenotypes separately in the maternal endometrium (ME) and fetal placenta (FP) by flow cytometry. In-depth phenotyping of NK cells, non-conventional and conventional T cells within maternal blood (mBld), ME, FP, and fetal spleen (fSpln) revealed major differences between these anatomic sites. In both maternal compartments, all NK cells were perforin$^+$ and had NKp46-defined phenotypes indicative of late-stage differentiation. Likewise, T cells with a highly differentiated phenotype including CD2$^+$CD8α$^+$CD27$^{dim/-}$perforin$^+$ γδ T cells, CD27$^-$perforin$^+$ cytolytic T cells (CTLs), and T-bet$^+$ CD4$^+$CD8α$^+$CD27$^-$ effector memory T (Tem) cells prevailed within these compartments. The presence of highly differentiated T cells was also reflected in the number of cells that had the capacity to produce IFN-γ. In the FP, we found NK cells and T cell populations with a naive phenotype including CD2$^+$CD8α$^-$CD27$^+$perforin$^-$ γδ T cells, T-bet$^-$CD4$^+$CD8α$^-$CD27$^+$ T cells, and CD27$^+$perforin$^-$ CTLs. However, also non-naive T cell phenotypes including CD2$^+$CD8α$^+$CD27$^+$perforin$^-$ γδ T cells, T-bet$^+$CD4$^+$CD8α$^+$CD27$^-$ Tem cells, and a substantial proportion of CD27$^-$perforin$^+$ CTLs resided within this anatomic site. Currently, the origin or the cues that steer the differentiation of these putative effector cells are unclear. In the fSpln, NKp46^{high} NK cells and T cells with a naive phenotype prevailed. This study demonstrated that antigen-experienced immune cell phenotypes reside at the maternal-fetal interface, including the FP. Our methodology and our findings open avenues to study NK and T cell function over the course of gestation. In addition, this study lays a foundation to explore the interplay between immune cells and pathogens affecting swine reproduction.

Keywords: porcine placenta, CD4 T cells, CD8 T cells, natural killer cells, late gestation, flow cytometry

INTRODUCTION

A successful pregnancy builds upon two aspects of the maternal immune system that need to be balanced. On the one hand, the maternal immune system needs to tolerate the semi-allogeneic fetus, but at the same time it should also be able to detect and respond to local pathogens in order to protect the fetus. This is coordinated by cells of the innate and adaptive immune systems but also the decidual microenvironment (1). Immune cells in the decidua vary in composition, phenotype and function and change with the stage of gestation (2, 3). During human pregnancy, ∼40% of the decidual stromal cells can be characterized as $CD45^+$ leukocytes (4, 5). Blastocyst implantation is characterized by the upregulation of inflammatory genes (6), production of pro-inflammatory cytokines, and immune cell recruitment (2). The following immune cells populate the first trimester human decidua: uterine natural killer (uNK) cells (∼70%), macrophages (∼20%), and T cells (∼5–20%) (7–9). In addition, dendritic cells, mast cells, and B cells are present, but in low frequencies (10, 11). Toward term, the frequency of uNK cells in human decidua diminishes whereas the T cell frequency increases (5, 9). Dynamic changes in immune cell composition also occur over the course of murine gestation (12). Altogether, cooperation of various immune cells and dynamic changes are a prerequisite of successful pregnancy.

The prominent population of uNK cells, found in humans, can be identified by a $CD56^{bright}CD16^-KIR^+CD9^+CD49a^+$ phenotype (13). These uNK cells have a poor cytolytic activity despite the fact that they contain ample granules filled with cytolytic machinery (13). Their main task during pregnancy is to produce a wide range of cytokines, proangiogenic factors, and proteases by which they are involved in vascular remodeling, neovascularization, and fetal tolerance (10, 14, 15). Apart from their essential role in maintaining fetal tolerance, it has recently been shown that uNK cells can also effectively combat potential viral threats in the decidua (16, 17).

Moreover, conventional TCR-$\alpha\beta^+$ and a sparse population of non-conventional TCR-$\gamma\delta^+$ T cells populate the decidua during gestation (18, 19). In humans, decidual $CD8^+$ T cells account for ∼45–75% whereas decidual $CD4^+$ T cells only account for ∼30–45% (4, 8, 18, 19). These frequencies seem to remain constant over time, however, one study showed an increase of $CD4^+$ T cells at term which seems to play a role in parturition (20). Furthermore, many studies have shown that for both T cell subsets an antigen-experienced phenotype, based on CD45RA/CD45RO or CD45RA/CCR7 phenotypes, prevails (21–23). Decidual $CD8^+$ (dCD8) T cells are competent producers of cytokines and show cytolytic activity (24). At term, $dCD8^+$ T cells seem to be activated but have reduced protein expression of perforin and granzyme B (22, 25). Recently, it has been shown that the translation of cytolytic molecules is blocked (17), and that this blockage might be lifted by pro-inflammatory events (26). $CD4^+$ T cell subsets, or T helper cells (Th), can be categorized based on their cell surface expression of chemokine receptors (CCR6, CCR4, and CXCR3) and intracellular expression of specific transcription factors. In the human decidua Th1, Th2, and Th17 cells constitute about ∼30, ∼5, and 2–5%, respectively (8, 27). It has been shown that decidual T cells with viral specificity might provide fetal protection (28). Specificity for fetal/paternal antigens has also been demonstrated (29–31), so in this context it is crucial that potential aberrant responses are contained. One of the mechanisms suppressing T cell effector functions is mediated by regulatory T (Treg) cells with/without fetal/paternal specificity (29, 30, 32, 33). Indeed, in humans and mice, $CD4^+CD25^{high}Foxp3^+$ cells comprise about 5–20% of the decidual $CD4^+$ T cells (8, 9, 30, 34).

Pigs have an epitheliochorial type of placenta as defined by the presence of two epithelial layers that compartmentalize the maternal and fetal component. Due to this special anatomy, the porcine placenta is considered as a tight barrier through which the transfer of maternal antibodies is impossible (35). Hence, it is assumed that the porcine placenta is also impermeable to cells. Nevertheless, some pathogens like the porcine reproductive and respiratory syndrome virus (PRRSV) can breach this barrier and infect the porcine fetuses. If these infections occur during late gestation, abortions are a frequent outcome. The immune cells populating the porcine placenta during health and disease have not been studied in detail so far. It has been reported that NK cells and T cells can be identified in the endometrium of pregnant pigs during early gestation, however, only major immune cell subsets were characterized (36–38).

In this study, we aimed to investigate immune cell subsets in the porcine placenta and their phenotypes related to functional traits in detail. We exploited the feature of an epitheliochorial placenta and established a separation and leukocyte isolation procedure in order to study immune cells from the maternal endometrium (ME) and fetal placenta (FP). We focused on NK and T cell phenotypes due to their abundance in the human and murine placenta but also to lay foundation for future studies addressing the functionality and role of these cells during viral infections in the porcine reproductive tract.

MATERIALS AND METHODS

Animals and Sample Collection

Three healthy multiparous crossbred (Landrace × Large White) pregnant sows were obtained from a commercial Austrian piglet producing farm, unsuspicious for PRRSV, confirmed by regular serological monitoring. Sows are routinely vaccinated against porcine parvovirus in combination with *Erysipelothrix rhusiopathiae* and swine influenza virus. The age of the sows (sow No. 2, 3.3 years; and sow No. 3, 2.7 years) were determined based on the date of birth and date of scheduled euthanasia. Unfortunately, we were unable to determine the age of sow No. 1. The sows and their litters (gestation days >100) were anesthetized by intravenous injection of Ketamine (Narketan® 100 mg/mL, Vetoquinol Österreich GmbH, Vienna, Austria, 10 mg/kg body weight) and Azaperone (Stresnil® 40 mg/mL, Elanco GmbH, Cuxhaven, Germany, 1.5 mg/kg body weight) during late gestation. Maternal blood (mBld) was taken by cardiac puncture and transferred into collection cups containing heparin. Afterward, animals were euthanized via intracardial injection of T61® (Intervet GesmbH, Vienna,

Austria, 1 mL/10 kg body weight). The abdomen of the sows was incised and the complete uterus was removed and placed in a trough. Uteri were opened at the anti-mesometrial side. Per sow, three average sized fetuses were randomly selected and removed with their umbilical cord, placenta and a portion of uterus adjacent to the umbilical stump. The abdomen of each fetus was opened in order to collect the intact fetal spleen (fSpln) in collection cups containing phosphate-buffered saline (PBS, PAN-Biotech, Aidenbach, Germany). For collection of the maternal-fetal interface of each fetus, the myometrium was trimmed off and the ME and FP were mechanically separated by the use of forceps. Approximately 80 g of ME and 90 g of FP were collected and transferred into RPMI-1640 with stable L-glutamine supplemented with 100 IU/mL penicillin and 0.1 mg/mL streptomycin (all from PAN-Biotech). During pathological examination of the sows, no pathologic lesions were found and their litters were normal. Since all procedures were done on dead animals, no federal animal ethics approval was required according to Austrian law. The project plan has been discussed and approved by the institutional ethics and animal welfare committee in accordance with GSP guidelines and national legislation (approval number ETK-32/02/2016).

Cell Isolation

Peripheral blood mononuclear cells (PBMCs) were procured from heparinized maternal blood via density gradient centrifugation (Pancoll human, density 1.077 g/mL, PAN-Biotech, 30 min at 920 × *g*). fSplns were kept on ice and cut into small pieces. The tissue was further dissociated by sieving it through a coarse-meshed sieve, which was regularly rinsed with cold PBS (PAN-Biotech). Collected cells were washed by centrifugation and after resuspension in PBS filtered through a Corning® 70 μm cell strainer (Falcon, BD Biosciences, San Jose, CA, United States). The obtained cell suspension was subjected to density gradient centrifugation under the conditions described above. Tissues from ME and FP were cut into small pieces and digested in RPMI-1640 supplemented with 2% (v/v) heat-inactivated fetal calf serum (FCS, Sigma-Aldrich, Schnelldorf, Germany), 25 U/mL DNase type I (Thermo Fisher Scientific, Carlsbad, CA, United States), 300 U/mL Collagenase Type I (Thermo Fisher Scientific), 100 IU/mL penicillin (PAN-Biotech) and 0.1 mg/mL P/S streptomycin (PAN-Biotech) for 1 h at 37°C during constant shaking. Obtained cell suspensions were drained through a coarse-meshed sieve and the flow-through was filtered through cotton wool to eliminate dead cells. Cells were resuspended in 40% Percoll (13 mL, Thermo Fisher Scientific), underlaid with 70% Percoll (13 mL) and subjected to density gradient centrifugation under the same conditions as described before. Isolated cells from mBld, fSpln, ME, and FP were subjected to three consecutive washing steps (350 × *g*, 10 min, 4°C): first with PBS, followed by two washes with RPMI-1640 (first wash 5% FCS, second wash 10% FCS, all other supplements as described above). Thereafter, cells were immediately used for immune phenotyping or subjected to IFN-γ enzyme-linked immune absorbent spot (ELISpot) assays.

Flow Cytometry Staining

A detailed overview of the mAbs and secondary reagents used for flow cytometry (FCM) staining is given in **Table 1**. A total of 2 × 10^6 cells were plated out in a round-bottom 96-well microtiter plate (Greiner Bio-One, Frickenhausen, Germany) and were stained in a six or seven step-procedure. After each incubation step (20 min, 4°C) the cells were washed twice with 200 μl PBS + 10% (v/v) porcine plasma (in-house preparation) or as indicated. Surface markers were stained with biotinylated or non-conjugated primary mAbs followed by isotype-specific secondary antibodies or streptavidin conjugates. This was followed by incubation with whole mouse IgG molecules (2 μg/sample, ChromPure, Jackson ImmunoResearch, West Grove, PA, United States) in order to block free binding sites of mouse-isotype specific secondary antibodies. In a further incubation step, the Fixable Viability Dye eFluor 780 (Thermo Fisher Scientific) was applied according to the instructions of the manufacturer. During this incubation, samples were also labeled with directly conjugated mAbs or biotinylated antibodies. For the CD4 and CD8β T cell samples (**Table 1**) this was followed by incubation with the streptavidin conjugate BV510 (BioLegend, San Diego, CA, United States). Samples were fixed and subsequently permeabilized with the Foxp3/Transcription Factor Staining Buffer Set (Thermo Fisher Scientific) according to the manufacturer's instructions. Finally, an intracellular staining for transcription factors or perforin was performed. For NK cells, γδ T cells, and CD8 T cells fluorescence minus one (FMO) control samples without perforin, GATA-3, and CD8β were prepared, respectively.

FCM Analysis

Flow cytometry samples were measured on a CytoFLEX LX (Beckman Coulter GmbH, Krefeld, Germany) flow cytometer equipped with six lasers (375, 405, 488, 561, 638, and 808 nm). For all samples, at least 1 × 10^5 lymphocytes were recorded. Single stains were performed using the VersaComp antibody capture kit (Beckman Coulter GmbH, Krefeld, Germany), according to the manufacturer's instructions, and compensation values were calculated by CytExpert software version 2.3.1.22 (Beckman Coulter). Further data processing was completed by FlowJo software version 10.5.3 (BD Biosciences). A consecutive gating strategy was applied for the phenotypic characterization of the isolated cells (**Supplementary Figure 1**). First, a time gate was applied and lymphocytes were selected according to their light scatter properties (FSC-A vs. SSC-A) and were subjected to doublet discrimination (FSC-H vs. FSC-A and SSC-H vs. SSC-A). Hereafter, viable cells were gated using the fixable viability dye eFluor780® and cells with a high auto fluorescent signal were excluded by using a bandpass filter 610/20 in the excitation line of the blue laser.

IFN-γ ELISpot Assay

Cells isolated from mBld, ME, FP, and fSpln were subjected to IFN-γ ELISpot assays. Coating and development of ELISpot plates was performed as described (39), with the only

TABLE 1 | Antibodies and streptavidin-conjugates used for FCM staining.

Marker	Clone	Isotype	Source	Labeling	Fluorophore
Leukocyte characterization					
CD45	K252.1E4	IgG1	Bio-Rad	Direct	Alexa647
NK cells and CD16$^+$ T cells					
CD3	PPT3	IgG1	In-house	Indirect[A]	PerCP-eFluor710
CD8α	11/295/33	IgG2a	In-house	Indirect[B]	BV510
CD172a	74-22-15A	IgG2b	In-house	Indirect[C]	BV421
NKp46	VIV-KM1	IgG1	In-house	Direct	Alexa647
CD16	G7	IgG1	Bio-Rad	Direct	FITC
Perforin	δ-G9	IgG2b	eBioscience	Direct	PE
γδ T cells					
TCR-γδ	PPT16	IgG2b	In-house	Indirect[C]	BV421
CD8α	11/295/33	IgG2a	In-house	Indirect[B]	BV510
CD2	MSA4	IgG2a	In-house	Direct	Alexa488
CD27	b30c7	IgG1	In-house	Direct	Alexa647
GATA-3	TWAJ	IgG2b	eBioscience	Direct	PerCP-eFluor710
Perforin	δ-G9	IgG2b	eBioscience	Direct	PE
CD4$^+$ T cells					
CD4	74-12-4	IgG2b	In-house	Indirect[D]	Alexa488
CD8α	11/295/33	IgG2a	In-house	Indirect[E]	PerCP-eFluor710
CD25	3B2	IgG1	In-house	Indirect[F]	BV421
CD27	b30c7	IgG1	In-house	Direct	Alexa647
CD3	PPT3	IgG1	SBA	Indirect[B]	BV510
Foxp3	FJK-16s	IgG2a	eBioscience	Direct	PE
T-bet	4B10	IgG1	eBioscience	Direct	PE
CD8$^+$ T cells					
CD8β	PPT23	IgG1	In-house	Indirect[G]	Alexa488
CD8α	11/295/33	IgG2a	In-house	Indirect[B]	BV510
CD3	BB23-8E6	IgG2b	SBA	Indirect[C]	BV421
CD27	b30c7	IgG1	In-house	Direct	Alexa647
Perforin	δ-G9	IgG2b	eBioscience	Direct	PE

[A]Rat-anti-mouse anti-IgG1-PerCPefluor710, eBioscience, [B]Streptavidin-BV510, BioLegend, [C]Goat-anti-mouse anti-IgG2b-BV421, Jackson Immuno Research, [D]Goat-anti-mouse anti-IgG2b-Alexa488, Jackson Immuno Research, [E]Rat-anti-mouse anti-IgG2a-PerCPefluor710, [F]Rat-anti-mouse anti-IgG1-BV42, BioLegend, [G]Goat-anti-mouse anti-IgG1-Alexa488, Thermo Fisher Scientific.

difference that for detection the biotinylated mouse anti-porcine IFN-γ clone P2C11 (Mabtech, Nacka Strand, Sweden) was used at a concentration of 0.125 μg/mL. Per well, 3×10^5 cells were plated in cell culture medium (RPMI1640 with 10% FCS, other ingredients as above). To induce IFN-γ production, cells were stimulated with Staphylococcal enterotoxin B (SEB, 500 ng/mL, Sigma-Aldrich). Cells from each location were plated in duplicates for 24 h at 37°C and 5% CO_2. Spots were counted with an AID ELISpot reader (AID, Straßberg, Germany).

Statistical Analysis and Data Representation

The frequencies of cell lineages, expressed within viable lymphocytes, were exported to Microsoft Excel (Office 2016, Microsoft, Redmond, WA, United States) and were corrected for CD45 expression by multiplying the percentage with the CD45 correction factor. The CD45 correction factor was calculated, for each individual sample, by dividing 100% by the percentage of CD45$^+$ cells. Data processed in FlowJo and Microsoft Excel were imported into Graphpad Prism version 8.1.0 (GraphPad Software Inc., San Diego, CA, United States) for descriptive analysis and graphical representation. For each anatomic location and for each cell population the mean and individual values are given. For the IFN-γ producing cells in the ELISpot assay results of each duplicate are shown as the mean ± standard error of the mean (SEM).

RESULTS

Identification and Frequency of CD45$^+$ Lymphocytes

Leukocyte isolation procedures for ME and FP based on enzymatic tissue digestion and subsequent gradient centrifugation were established for this study. To evaluate the performance of this procedure, we initially investigated the presence of total lymphocytes in the obtained cell preparations by studying the cell surface expression of CD45 (leukocyte common antigen) in a two-parameter FCM staining (**Figure 1**).

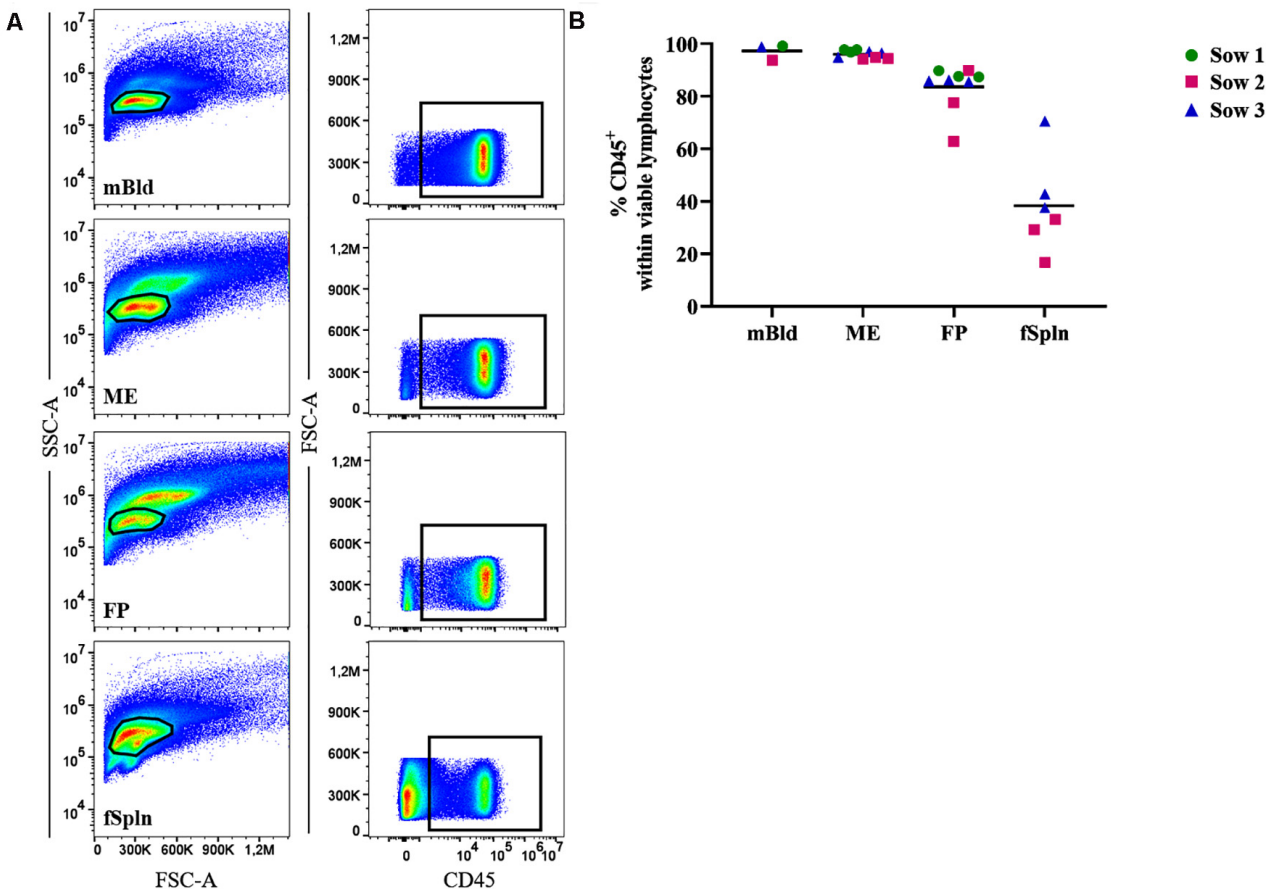

FIGURE 1 | Frequency of CD45$^+$ lymphocytes in mBld, ME, FP and fSpln. **(A)** Lymphocytes were gated based on their SSC-A vs. FSC-A properties and after consecutive gating to exclude doublets, dead cells and cells with high autofluorescence (see **Supplementary Figure 1**), CD45$^+$ cells were gated. Representative pseudocolor plots for maternal blood (mBld), maternal endometrium (ME), fetal placenta (FP), and fetal spleen (fSpln) are shown. **(B)** Frequency of CD45$^+$ cells within viable lymphocytes. Each colored symbol represents data from one sow for mBld (n = 3) or fetuses coming from that sow for ME (n = 9), FP (n = 9), and fSpln (n = 6). The black bars display the mean within the respective anatomic location.

We investigated the frequency of CD45$^+$ cells in our predefined lymphocyte gate, as shown by a basic gating overview, for mBld, ME, FP, and fSpln (**Figure 1A**). An overview of the complete consecutive gating strategy for all investigated locations is provided in **Supplementary Figure 1**. Collective data of CD45$^+$ cells for the investigated anatomic locations are displayed in **Figure 1B**. In mBld and ME, over 95% of cells within our population of viable cells expressed CD45. In FP, with the exception of two individual fetuses (62.8% and 77.5%), on average 84.1% of the viable lymphocytes expressed CD45. For cells isolated from the fSpln the frequency of CD45$^+$ cells within the population of viable lymphocytes varied with a range of 16.3–70.8%. Hence, the vast majority of cells in our predefined lymphocytes gate were CD45$^+$ cells for the investigated locations, with the exception of fSpln. In embryos, fetuses, and neonates, the spleen is also capable of hematopoiesis; therefore, it is conceivable that the CD45$^-$ cells represent immature stem cells that will acquire CD45 during their maturation process (40). Accordingly, with the obtained CD45 frequencies a CD45-correction factor was calculated and used to determine the distribution of the major NK and T cell frequencies thereafter (see also section "Statistical Analysis and Data Representation").

Characterization of NK Cells

Porcine NK cells can be defined by their perforin$^+$CD3$^-$CD8α$^{+/dim}$CD16$^+$CD172a$^-$NKp46$^{+/-}$ phenotype (41–43). Following FCM staining, we used a CD3$^-$CD8α$^+$CD16$^+$CD172a$^-$ phenotype to identify the total NK cell population in the investigated anatomic sites during late gestation (**Figure 2A**). An enrichment of total NK cells in the ME (mean: 23%) and the FP (mean: 22.8%) as opposed to their frequency in mBld and fSpln (mean: 3.2 and 4.2%) was found (**Figure 2B**). CD3$^-$CD8α$^+$CD16$^+$CD172a$^-$ NK cells were further analyzed for their expression of NKp46 (CD335; NCR1). This enabled us to identify NKp46$^-$, NKp46$^+$, and NKp46^{high} expressing NK cells in mBld, ME, FP, and fSpln (**Figure 2C**). Collective data with regard to the distribution of the NKp46-defined populations are summarized in **Figures 2D–F**. Both NKp46$^-$ and NKp46$^+$ NK cells could be identified in mBld, ME, and FP. Overall, in mBld NKp46$^-$ and NKp46$^+$

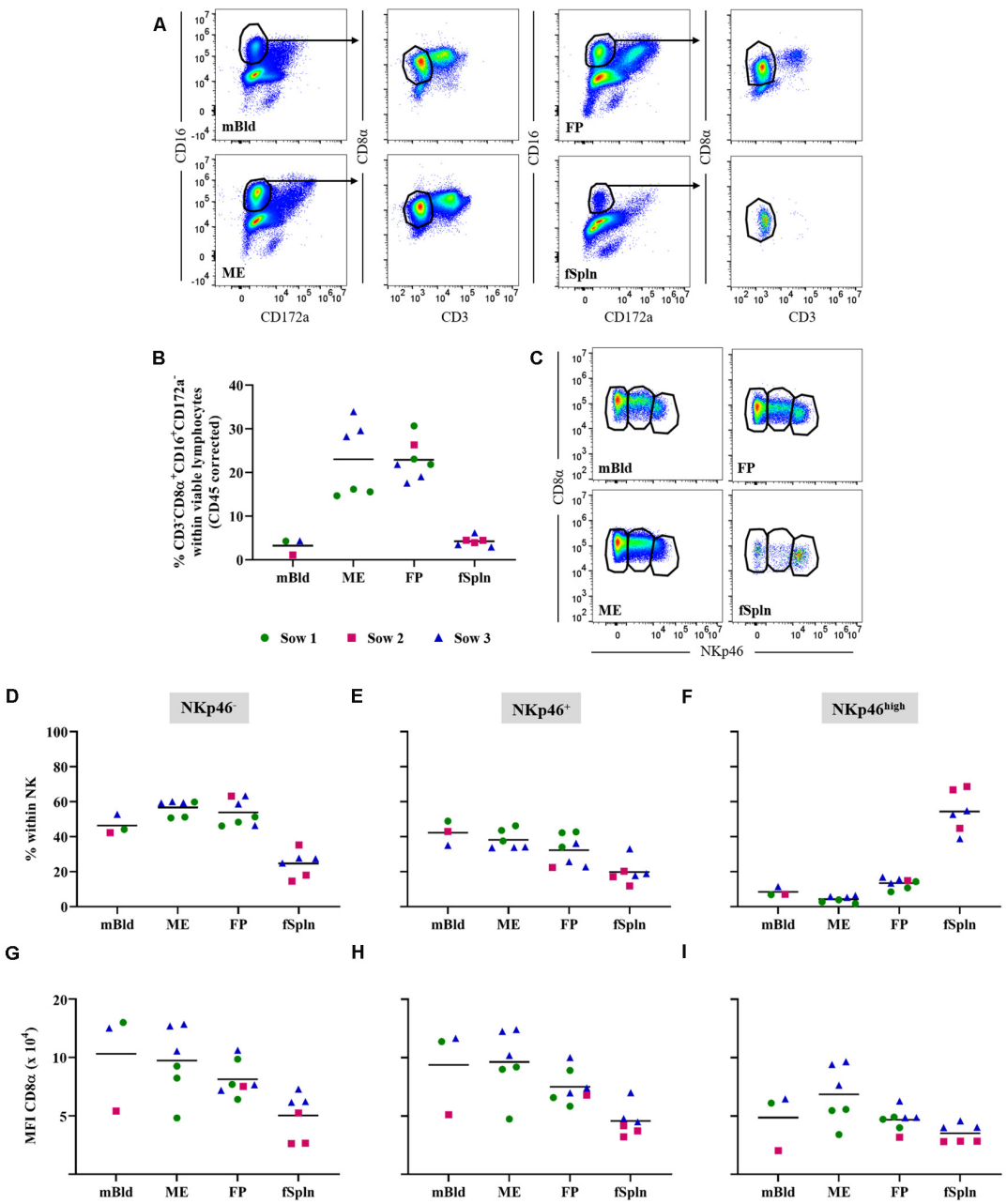

FIGURE 2 | Characterization of NK cells. **(A)** Following exclusion of doublets, dead cells, and cells with high autofluorescence (see **Supplementary Figure 1**), total NK cells were identified by gating on $CD16^+CD172a^-$ cells and further subgated for $CD3^-CD8\alpha^+$ cells. Representative pseudocolor plots for maternal (left) and fetal compartments (right) are shown. **(B)** Frequencies of $CD3^-CD8\alpha^+CD16^+CD172a^-$ cells (total NK cells) within viable lymphocytes corrected for CD45 expression. **(C)** Total NK cells in the different anatomic locations were gated to identify three NK cell subsets: $CD8\alpha^+NKp46^-$, $CD8\alpha^+NKp46^+$, and $CD8\alpha^{dim}NKp46^{high}$ (from left to right). **(D–F)** Distribution of CD8α/NKp46-defined NK cell subsets within the respective anatomic locations. **(G–I)** CD8α/NKp46-defined NK cells subsets were further analyzed for their CD8α expression levels. The median fluorescence intensity (MFI) for CD8α within the respective NK cell subsets is shown. **(B,D–I)** For all graphs, each colored symbol represents data from one sow for mBld (n = 3) or fetuses coming from that sow for ME (n = 6), FP (n = 7), and fSpln (n = 6). The black bars display the mean within the respective anatomic location.

NK cells were represented in equal numbers (46.4 and 42.3%) whereas in ME and FP their distribution was on average 56.7 and 53.9% vs. 38.1 and 32.3%. Within fSpln all three NK cell populations were found to be present, however, the $NKp46^{high}$ subset predominated (mean: 54.4%). In addition, CD8α expression levels in the three NKp46-defined NK cell subsets were investigated (**Figures 2G–I**) and highlighted similarities and dissimilarities between the three NK cell subsets. NK cells with a $NKp46^-$ and $NKp46^+$ phenotype consistently showed comparable CD8α expression levels (**Figures 2F,G**) whereas

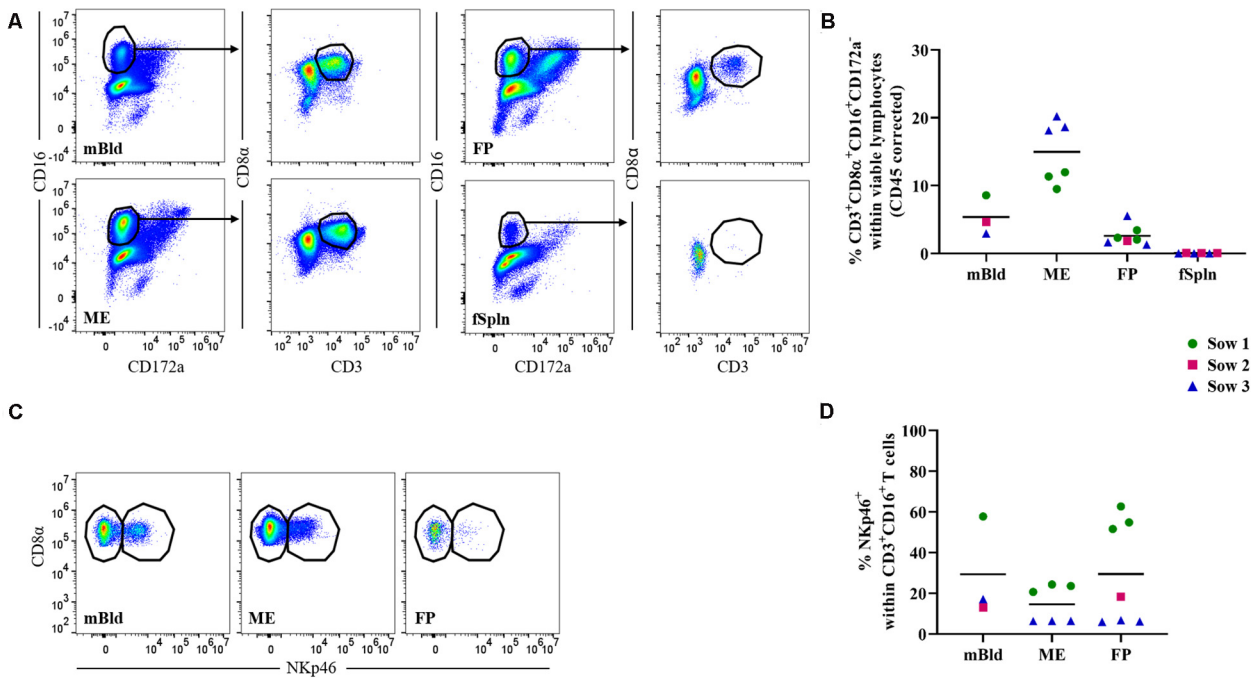

FIGURE 3 | Characterization of lymphocytes with phenotypic features of NK and T cells. **(A)** Following exclusion of doublets, dead cells, and cells with high autofluorescence (see **Supplementary Figure 1**), $CD16^+$ T cells were identified by gating on $CD16^+CD172a^-$ cells and further subgated on $CD3^+CD8\alpha^+$ cells. Representative pseudocolor plots for maternal (left) and fetal compartments (right) are shown. **(B)** Frequencies of non-conventional $CD3^+CD8\alpha^+CD16^+CD172a^-$ cells within viable lymphocytes corrected for CD45 expression. **(C)** $CD16^+$ T cells in mBld, ME, and FP were analyzed for their NKp46 surface expression and separated in $CD8\alpha^+NKp46^-$ and $CD8\alpha^+NKp46^+$ $CD16^+$ T cells. **(D)** Frequency of $CD8\alpha^+NKp46^+$ within $CD16^+$ T cells in mBld, ME, and FP. **(B,D)** For all graphs, each colored symbol represents data from one sow for mBld (n = 3) or fetuses coming from that sow for ME (n = 6), FP (n = 7), and fSpln (n = 6). The black bars display the mean within the respective anatomic location.

$NKp46^{high}$ NK cells showed the lowest expression of CD8α as reflected by the MFI levels (**Figure 2I**). In order to complete the NK cell phenotype, we addressed the intracellular expression of the cytolytic molecule perforin (**Supplementary Figure 2**). It was found that all NK cells expressed perforin within all investigated anatomic locations.

Characterization of Lymphocytes With Phenotypic Features of NK and T Cells

Within our NK cell sample, a $CD3^+CD8\alpha^+CD16^+CD172a^-$ lymphocyte population could be identified in all anatomic sites with the exception of the fSpln (**Figure 3A**). Interestingly, this phenotype constituted between 9.5 and 20.2% of total viable lymphocytes in the ME while the abundance of this phenotype in mBld (<5.4%) and FP (<2.6%) was lower (**Figure 3B**). We further analyzed the $CD3^+CD8\alpha^+CD16^+CD172a^-$ lymphocytes for their surface expression of NKp46 and intracellular expression of perforin in a similar manner to the NK cells. Due to the absence of this phenotype in the fSpln, no data on NKp46 or perforin expression is shown for this anatomic location. In mBld and at the maternal-fetal interface, a substantial proportion of $CD3^+NKp46^+$ lymphocytes could be observed (**Figures 3C,D**). However, we did observe a high degree of sow-to-sow variation which was most pronounced in the FP where the average frequency of $NKp46^+$ cells within $CD3^+$ T cells for fetuses from one sow (No. 1) was 56.3% and for those from sow No. 3 was 6.3% (**Figure 3D**). Furthermore, all $CD3^+CD8\alpha^+CD16^+CD172a^-$lymphocytes were positive for perforin (**Supplementary Figure 3**), and therefore might be capable of cytolytic activity.

Characterization of γδ T Cells

Porcine γδ T cells can be characterized by a set of surface molecules including CD2, CD8α, and CD27, as well as intracellular molecules including transcription factors and cytolytic molecules (44). We aimed to identify the total γδ T cell population by targeting a γδ-specific CD3 molecule by using monoclonal antibody clone PPT16 (45), as depicted in **Figure 4A** (black gate). The mean frequencies of total γδ T cells varied slightly between the investigated anatomic locations (**Figure 4B**; black box), with the highest abundance in mBld (mean: 13.9%) followed by 12.8% in ME, 10.2% in FP, and the lowest frequency was found in the fSpln (mean: 7.8%). Following the characterization of total γδ T cells we analyzed their expression of CD2, intending to determine the $CD2^+/CD2^-$ γδ T cell ratio within the investigated locations (**Figure 4A**; orange gate). Both γδ T cell subsets were found and revealed striking differences between the four investigated anatomic locations. Results procured from all investigated locations are visualized in **Figure 4C**. The ratio of $CD2^+$ to $CD2^-$ γδ T cells in

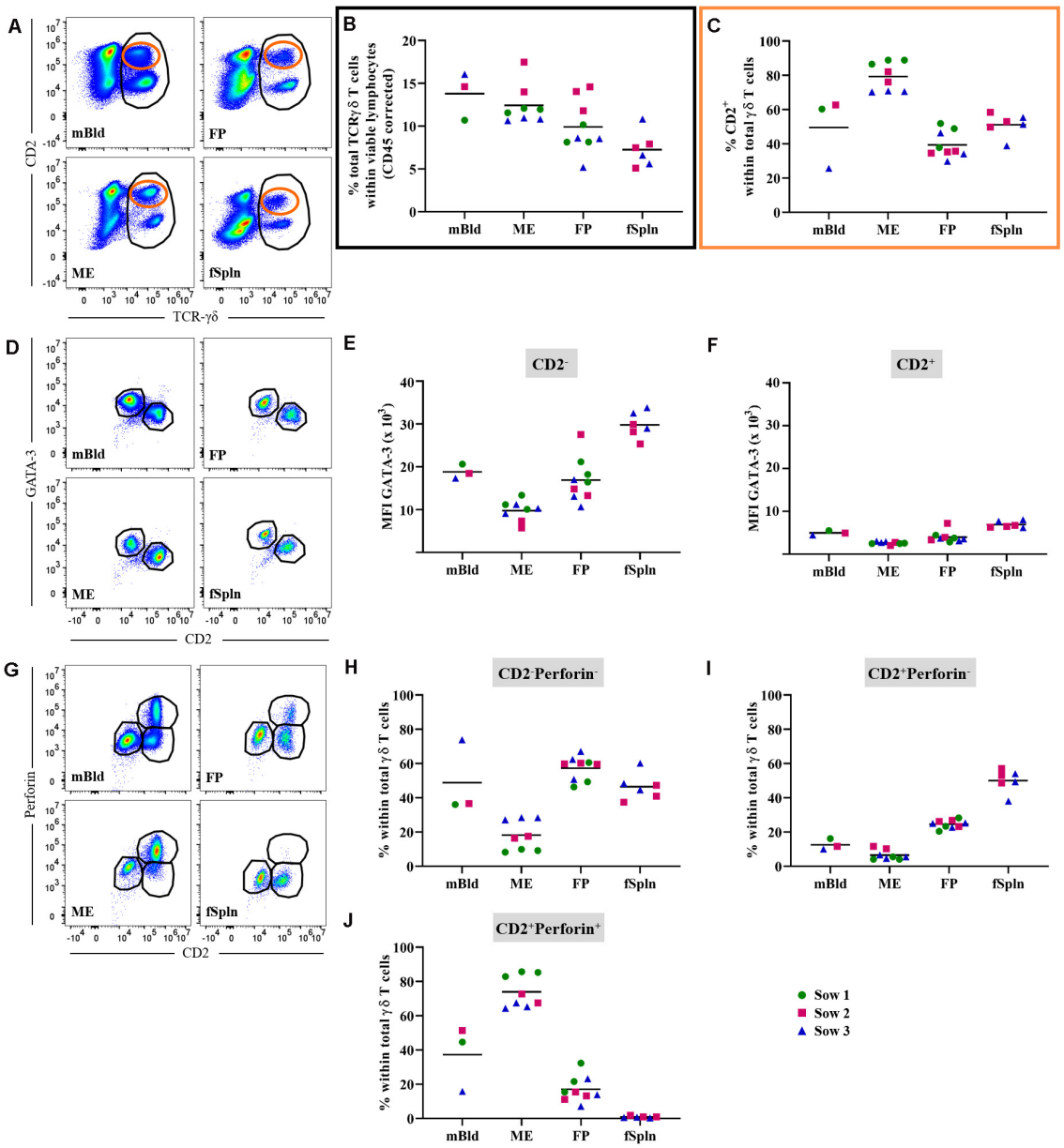

FIGURE 4 | Characterization of γδ T cells. **(A)** Following exclusion of doublets, dead cells, and cells with high autofluorescence (see **Supplementary Figure 1**), total γδ T cells at all four anatomic locations were gated (black gate) based on their TCR-γδ expression. The γδ T cells were further subgated based on their $CD2^+$ phenotype (orange gate). Representative pseudocolor plots for maternal (left) and fetal compartments (right) are shown [applies also for **(D,G)**]. **(B)** Frequencies of total TCR-γδ T cells within viable lymphocytes corrected for CD45 expression. **(C)** Frequency of $CD2^+$ TCR-γδ T cells within total γδ T cells. **(D)** Analysis of total γδ T cells for their expression of CD2 and GATA-3. $CD2^-GATA3^+$ subsets and $CD2^+GATA\text{-}3^{-/low}$ subsets were gated. **(E,F)** Median fluorescence intensity (MFI) of GATA-3 in $CD2^-$ **(E)** and $CD2^+$ **(F)** γδ T cells at the four anatomic locations. **(G)** Analysis of total γδ T cells for their expression of CD2 and perforin. $CD2^-perforin^-$, $CD2^+perforin^-$, and $CD2^+perforin^+$ population were gated. $CD2^+perforin^+$ γδ T cells could not be identified in fetal spleen (fSpln). **(H–J)** Distribution of the three CD2/perforin-defined γδ T cell subsets within the respective anatomic locations. **(B,C,E,F,H–J)** For all graphs, each colored symbol represents data from one sow for mBld (n = 3) or fetuses coming from that sow for ME (n = 8), FP (n = 9), and fSpln (n = 6). The black bars display the mean within the respective anatomic location.

mBld and fSpln was on average 1:1. The ME was particularly enriched for $CD2^+$ γδ T cells (79.3%) whilst the FP was predominantly colonized by $CD2^-$ γδ T cells (39.3% $CD2^+$, 60.7% $CD2^-$) (**Figure 4C**).

Additionally, we explored the expression of CD2 in association with GATA-3 or perforin within all investigated anatomic sites. We were able to detect a subset of $CD2^-GATA\text{-}3^+$ and $CD2^+GATA\text{-}3^{low/-}$ γδ T cells within all four locations (**Figure 4D**). To demonstrate the differences in GATA-3 expression levels between the two γδ subsets, we calculated the MFI for both subsets within the investigated locations. The results for the MFI for all samples analyzed for both γδ subsets are

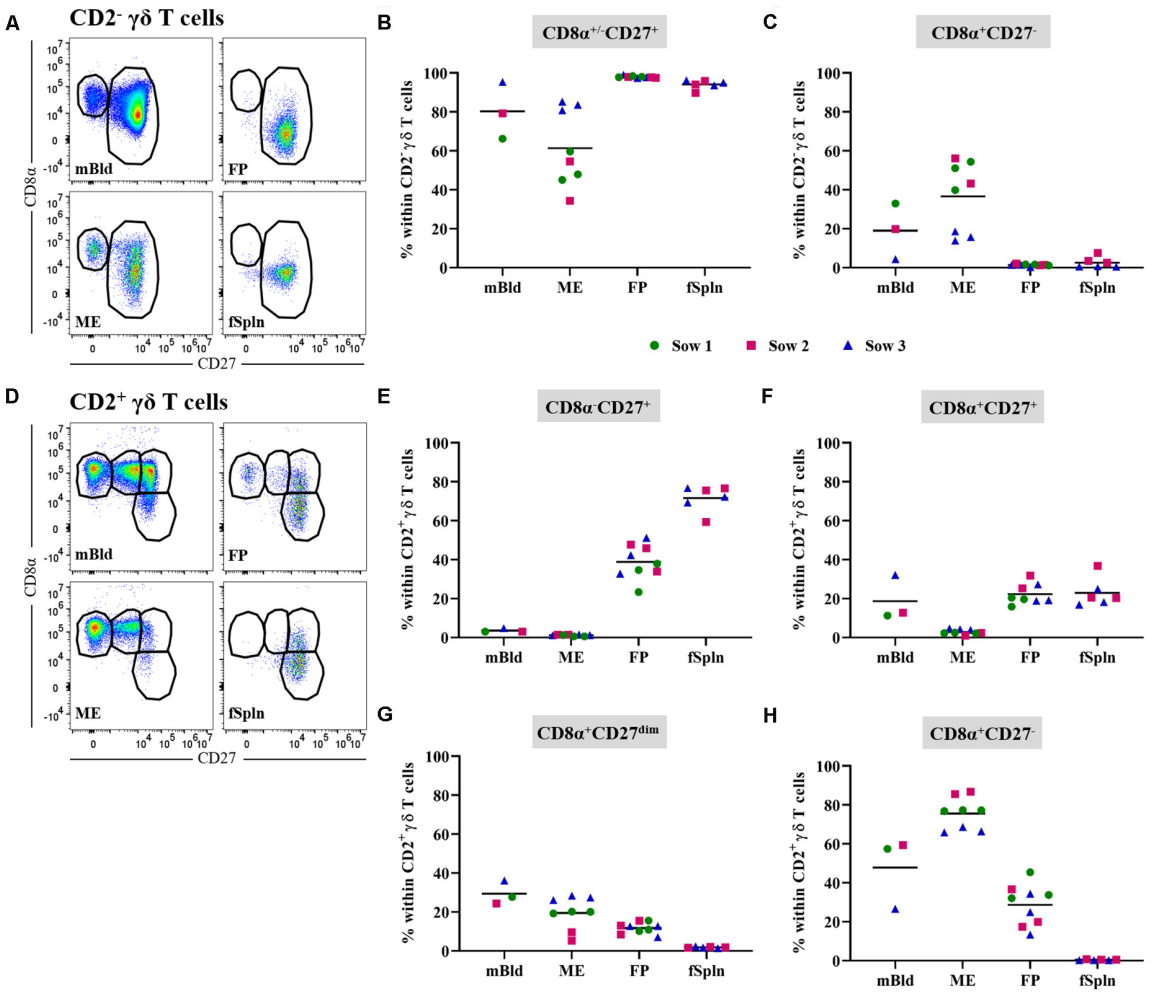

FIGURE 5 | CD8α/CD27 expression on CD2$^-$ and CD2$^+$ γδ T cells. CD2$^-$ and CD2$^+$ γδ T cells were analyzed for their expression of CD8α and CD27. **(A)** Within CD2$^-$ γδ T cells CD8α$^{+/-}$CD27$^+$ and CD8α$^+$CD27$^-$ cells were gated. Representative pseudocolor plots for maternal (left) and fetal compartments (right) are shown [applies also for **(D)**]. **(B,C)** Frequencies of CD8α$^{+/-}$CD27$^+$ CD2$^-$ γδ T cells **(B)** and CD8α$^+$CD27$^-$ CD2$^-$ γδ T cells **(C)** within all investigated anatomic locations. **(D)** CD2$^+$ γδ T cells were gated for CD8α$^-$CD27$^+$, CD8α$^+$CD27$^+$, CD8α$^+$CD27^{dim}, and CD8α$^+$CD27$^-$ cells. **(E–H)** Frequencies of the four CD8α/CD27-defined CD2$^+$ γδ T cell subsets within the investigated anatomic locations. **(B,C,E–H)** Each colored symbol represents data from one sow for mBld (n = 3) or fetuses coming from that sow for ME (n = 8), FP (n = 9), and fSpln (n = 6). The black bars display the mean within the respective anatomic location.

summarized in **Figures 4E,F**. For all investigated locations, CD2$^-$ γδ T cells showed consistently a higher expression of GATA-3 (**Figure 4E**) as compared to their CD2$^+$ counterpart (**Figure 4F**). However, CD2$^-$ γδ T cells isolated from the ME displayed the lowest expression of GATA-3 (MFI ranging from 5681 to 13,338) while the highest expression was observed in fSpln (MFI varied from 25,330 to 33,773) (**Figure 4E**). The expression pattern of CD2 in association with perforin allowed us to identify CD2$^-$perforin$^-$, CD2$^+$perforin$^-$, and CD2$^+$perforin$^+$ γδ T cells within all investigated locations except the fSpln (**Figure 4G**). The composition of the CD2/perforin-defined γδ T cell subsets diverged between the anatomic locations (**Figures 4H–J**). The frequency of CD2$^-$perforin$^-$ γδ T cells was the lowest in the ME (mean: 18.1%) and highest in FP (mean: 57.3%). In mBld and fSpln this phenotype constituted on average 48.8 and 46.4% of the γδ T cells, respectively. γδ T cells with a CD2$^+$perforin$^-$ phenotype were highest in fSpln (mean: 50%) whereas lower frequencies were found in FP, mBld, and ME (24.5, 12.5, and 6.5%, respectively). Furthermore, phenotyping revealed that the ME was enriched with CD2$^+$perforin$^+$, putative cytolytic effector γδ T cells, which constituted about 74% of total γδ T cells. In the fSpln this phenotype could not be observed. Interestingly, this phenotype of putative effector cells was also found in the FP (mean: 17%) and mBld (mean: 37.3%).

In this study, we also investigated the two CD2-defined γδ T cell subsets for their CD8α/CD27 expression pattern within mBld, ME, FP, and fSpln (**Figure 5**). Across all anatomic sites, CD2$^-$ γδ T cells mainly had a CD8α$^{+/-}$CD27$^+$ phenotype (≥60%) whereas a CD8α$^+$CD27$^-$ phenotype was only found in mBld and ME (mean: 19 and 36.6%, respectively) (**Figures 5A–C**). However, it should be noted that for the CD8α$^{+/-}$CD27$^+$ phenotype identified within the ME we observed again variations

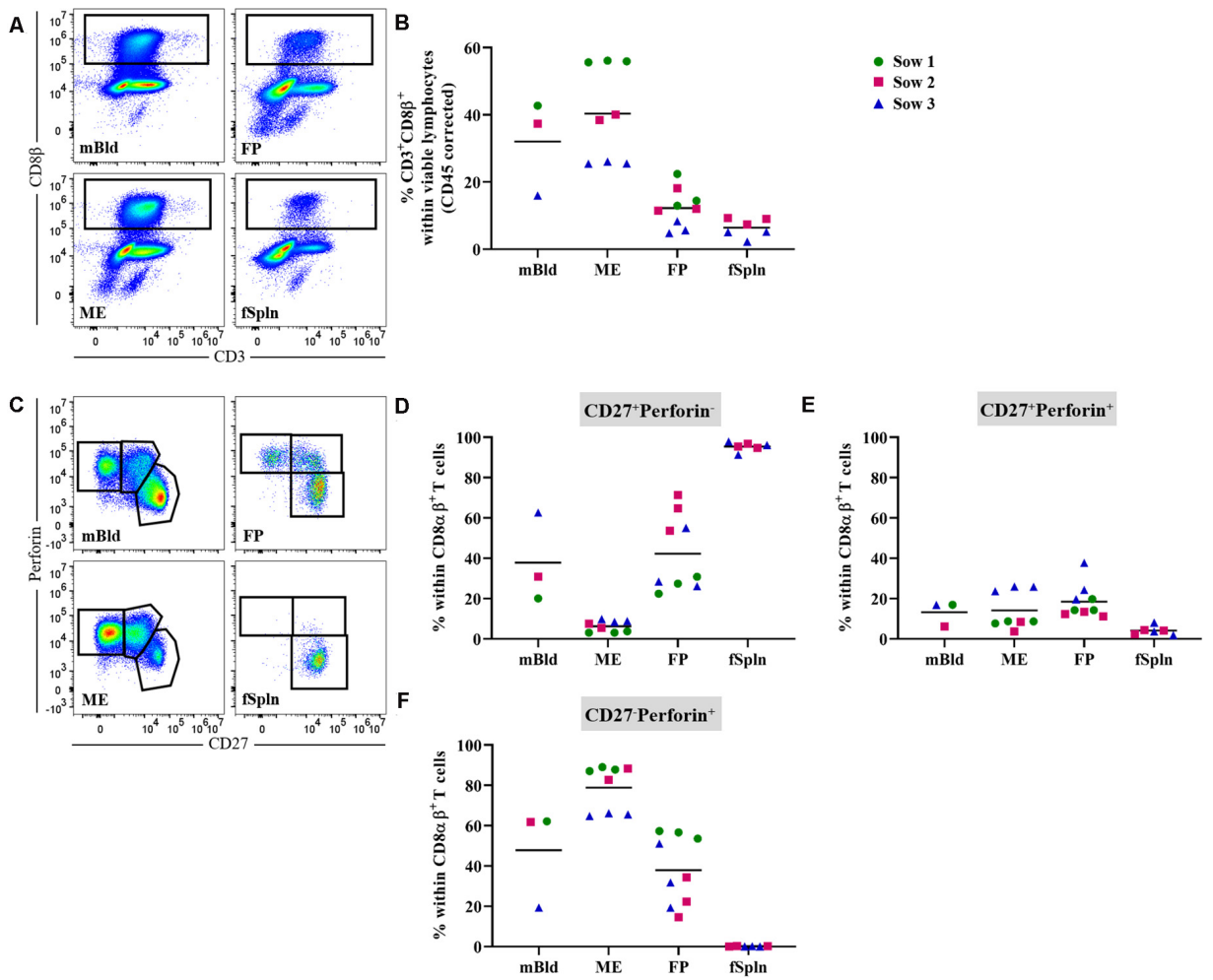

FIGURE 6 | Characterization of porcine CD8 T cells. **(A)** Following exclusion of doublets, dead cells, and cells with high autofluorescence (see **Supplementary Figure 1**), total CD8 T cells, in the four investigated anatomic locations were identified by gating on CD8β$^+$ cells. Representative pseudocolor plots for maternal (left) and fetal compartments (right) are shown [applies also for **(C)**]. **(B)** Frequencies of total CD8β$^+$ T cells within viable lymphocytes corrected for CD45 expression. **(C)** Within CD8αβ$^+$ T cells (see **Supplementary Figure 4**) perforin$^-$CD27$^+$, perforin$^+$CD27$^+$, and perforin$^+$CD27$^-$ cells were gated. **(D–F)** Distribution of the three perforin/CD27-defined CD8 T cell populations within the investigated anatomic locations. **(B,D–F)** For all graphs, each colored symbol represents data from one sow for mBld (n = 3) or fetuses coming from that sow for ME (n = 8), FP (n = 9), and fSpln (n = 6). The black bars display the mean within the respective anatomic location.

among fetuses influenced by the sow, where for sow No. 3 the mean frequency was 83.2% and for the other two sows this was lower than 60%. This difference might be attributed to a combination of animal-to-animal variation and the age (44). In addition, it should be noted that in the fetal compartments, including FP and fSpln, most CD2$^-$ γδ T cells did not express CD8α (**Figure 5C**). Among the CD2$^+$ γδ T cells, four distinct CD8α/CD27-defined phenotypes were characterized (CD8α$^-$CD27$^+$, CD8α$^+$CD27$^+$, CD8α$^+$CD27^{dim}, and CD8α$^+$CD27$^-$) and highlighted distinct differences between the maternal and fetal sites (**Figures 5D–H**). The maternal compartments were mainly populated by CD2$^+$ γδ T cells with a CD8α$^+$CD27$^-$ phenotype (mean: 47.8 and 75.5% for cells isolated from mBld and ME) while the fetal compartments were mainly populated by a CD8α$^-$CD27$^+$ phenotype (mean: 38.8 and 71.6% for cells isolated from FP and fSpln) (**Figures 5E,H**). CD2$^+$ γδ T cells with a CD8α$^+$CD27$^+$ phenotype were nearly undetectable within the ME but accounted for approximately 20% in the other investigated locations (**Figure 5F**). In addition, CD2$^+$CD8α$^+$CD27$^-$ γδ T cells were also found in the FP although a degree of variation between individual fetuses could be observed (13.3–45.4%). Lastly, γδ T cells with a CD2$^+$CD8α$^+$CD27^{dim} phenotype were more prominent in the maternal compartments (**Figure 5G**).

Characterization of CD8β T Cells

Presently, porcine CD8 T cells can be defined by a CD3$^+$CD4$^-$CD8α^{high}CD8β$^+$ phenotype and the expression of perforin in combination with CD27 might be applied to assess differentiation stages (46). Here total CD8 T cells in the anatomic sites from the maternal and fetal compartments were identified by gating on CD3$^+$CD8β$^+$ cells (**Figure 6A**). Mean frequencies of

$CD3^+CD8\beta^+$ T cells were higher in the maternal compartments (32 and 40.4% for cells isolated from mBld and ME) as compared to the fetal compartments (12.2 and 6.4% for cells isolated from the FP and fSpln) (**Figure 6B**). Of note, $CD3^+CD8\beta^+$ T cell frequencies for sow No. 3 and its fetus-associated tissues (depicted by blue triangle) were consistently lower as opposed to samples from the other sows. Further analysis demonstrated that across all investigated anatomic sites the $CD8\beta^+$ cells co-expressed CD8α and therefore can be regarded as CTLs (**Supplementary Figures 4A,B**). We assessed the co-expression of perforin and CD27 to gain information about the putative differentiation stages of porcine CTLs. $CD27^+perforin^-$, $CD27^+perforin^+$, and $CD27^-perforin^+$ phenotypes were present within almost all investigated anatomic sites except fSpln (**Figure 6C**). The frequencies of these CTL subsets for the three sows and fetus-associated tissues are presented in **Figures 6D–F**. CTLs with a $CD27^+perforin^-$ phenotype were the sole representatives within the fSpln (>95%) and were hardly detected in the ME (mean: 6.2%) (**Figure 6D**). In mBld and FP the frequency of this phenotype ranged from 20 to 62.6% and 22.4 to 71.3%, respectively. Across all anatomic sites, the abundance of CTLs with a $CD27^+perforin^+$ phenotype was rather low ranging from 4% in the fSpln to 18.5% in FP (**Figure 6E**). The highest frequency of CTLs with a $CD27^-perforin^+$ phenotype, potentially representing late effectors or memory cells, was found in the ME (mean: 78.9%) followed by mBld (mean: 47.8%) and FP (mean: 37.8%) (**Figure 6F**).

Characterization of CD4 T Cells

The differentiation and activation state of porcine $CD3^+CD4^+$ Th cells can be described based on the CD8α/CD27-expression pattern, and transcription factors can be used to address the functionality of these T cells (47–49). In this study we started by investigating frequencies of total Th cells based on a $CD3^+CD4^+$ phenotype (**Figure 7A**) and the data for total $CD4^+$ T cells in the four anatomic sites are displayed in **Figure 7**. A higher abundance within the maternal compartments (mean: 35.7 and 24.6% for cells isolated from mBld and ME) was found as opposed to less than 20.9% in fetal compartments (mean: 15% in FP and 20.9% in fSpln). Moreover, $CD3^+CD4^+$ T cells were further analyzed for their expression of activation markers, differentiation markers, and transcription factors as outlined below.

Regulatory CD4 T Cells

First, we investigated all anatomic sites for the presence and abundance of Tregs based on the expression of Foxp3 and CD25 within $CD3^+CD4^+$ T cells (**Figure 7C**). Mean Treg frequencies within total $CD4^+$ T cells were highest in fSpln and FP with 18.2 and 15.4%, respectively (**Figure 7D**). The mean Treg frequency in blood-derived $CD4^+$ T cells ranged from 4.3 to 8.5% (**Figure 7D**). More intriguingly, even fewer Tregs could be identified in the ME (2.2%) (**Figure 7D**). Across all anatomic sites, we further analyzed the $CD3^+CD4^+Foxp3^+CD25^{high}$ Tregs for the expression of CD8α and CD27 which revealed the existence of $CD8\alpha^-CD27^+$, $CD8\alpha^+CD27^+$, and $CD8\alpha^+CD27^-$ Treg phenotypes. However, the latter phenotype was completely absent within the fetal compartments (mean: 0.3% in FP and 0.04% fSpln) and only a few $CD8\alpha^+CD27^-$ Tregs could be observed in mBld and ME (mean: 4.5 and 3.7%, respectively) (**Figure 7E**). The mean frequencies of the three CD8α/CD27-defined Treg populations are summarized in **Figures 7F–H** and show that most Tregs in mBld and ME had a $CD8\alpha^+CD27^+$ phenotype (61.3–76.3%) whilst in the FP and fSpln this frequency ranged from 20.6 to 38.2%. Tregs in FP and fSpln mainly displayed a $CD8\alpha^-CD27^+$ phenotype (between 61.3 and 79.1%).

Non-regulatory CD4 T Cells

$CD3^+CD4^+$ T cells (**Figure 7A**) were also investigated in detail for the abundance of non-Treg $CD4^+$ T cells within the different anatomic sites. Therefore, we excluded $CD4^+CD25^{high}$ expressing T cells, the prospective Tregs [**Figure 7C** and (48)]. Subsequently, $CD4^+CD25^{-/dim}$ cells were analyzed for the expression of CD8α and CD27 (**Figure 8A**) delineating a $CD8\alpha^-CD27^+$ naive, $CD8\alpha^+CD27^+$ central memory (Tcm), and $CD8\alpha^+CD27^-$ effector memory (Tem) population. The mean and individual frequencies of these phenotypes for all investigated locations are shown in **Figures 8B–D**. Again, $CD8\alpha^-CD27^+$ naive $CD4^+$ T cells constituted the major fraction in FP and fSpln and only a few antigen-experienced $CD4^+$ T cells, with a $CD8\alpha^+CD27^+$ Tcm or $CD8\alpha^+CD27^-$ Tem phenotype, could be identified in the FP. As expected, most non-Treg $CD4^+$ T cells isolated from mBld and ME had an antigen-experienced phenotype, hence the high prevalence of $CD8\alpha^+CD27^+$ Tcm in the mBld (mean: 42.8%; **Figure 8C**) and $CD8\alpha^+CD27^-$ Tem in the ME (mean: 67.8%; **Figure 8D**). Next, we assessed the Th1 polarization of the three CD8α/CD27-defined $CD4^+$ T cells subsets. For each investigated anatomic location, the T-bet expression for $CD8\alpha^-CD27^+$ naive, $CD8\alpha^+CD27^+$ Tcm, and $CD8\alpha^+CD27^-$ Tem populations are depicted in the histograms (**Figure 8E**). Across all anatomic sites, $CD8\alpha^-CD27^+$ naive $CD4^+$ T cells did not express T-bet (**Figure 8F**), and only a minor portion (∼20%) in mBld and fSpln of the $CD8\alpha^+CD27^+$ Tcm could be identified as $T\text{-}bet^+$ (**Figure 8G**). At the maternal-fetal interface, up to 46.6 and 41.9% of the Tcm expressed T-bet (**Figure 8G**). In mBld, on average 61.7% of the circulating $CD8\alpha^+CD27^-$ Tem cells had a Th1 phenotype whereas in ME and FP most cells expressed T-bet (mean: 86.2 and 90.2%, accordingly) (**Figure 8H**).

IFN-γ Production of Lymphocytes at the Maternal-Fetal Interface

In addition to the phenotyping data, we addressed the capacity for IFN-γ production for the isolated lymphocytes by means of an ELISpot. Following overnight cultivation in the presence of SEB or medium, IFN-γ-producing cells were visualized and quantified. Representative data of IFN-γ-producing cells for one sow and tissues from one associated fetus for medium control or SEB stimulation are presented in **Figure 9A** (medium, left column; SEB, right column). Results for all sows and all investigated anatomic sites are given in **Figure 9B**. Maternal lymphocytes, originating from mBld and ME, showed a high but animal-dependent spontaneous IFN-γ secretion following incubation with cell culture medium (**Figure 9A**, left column and **Figure 9B**, middle and bottom panel). Spontaneous secretion of

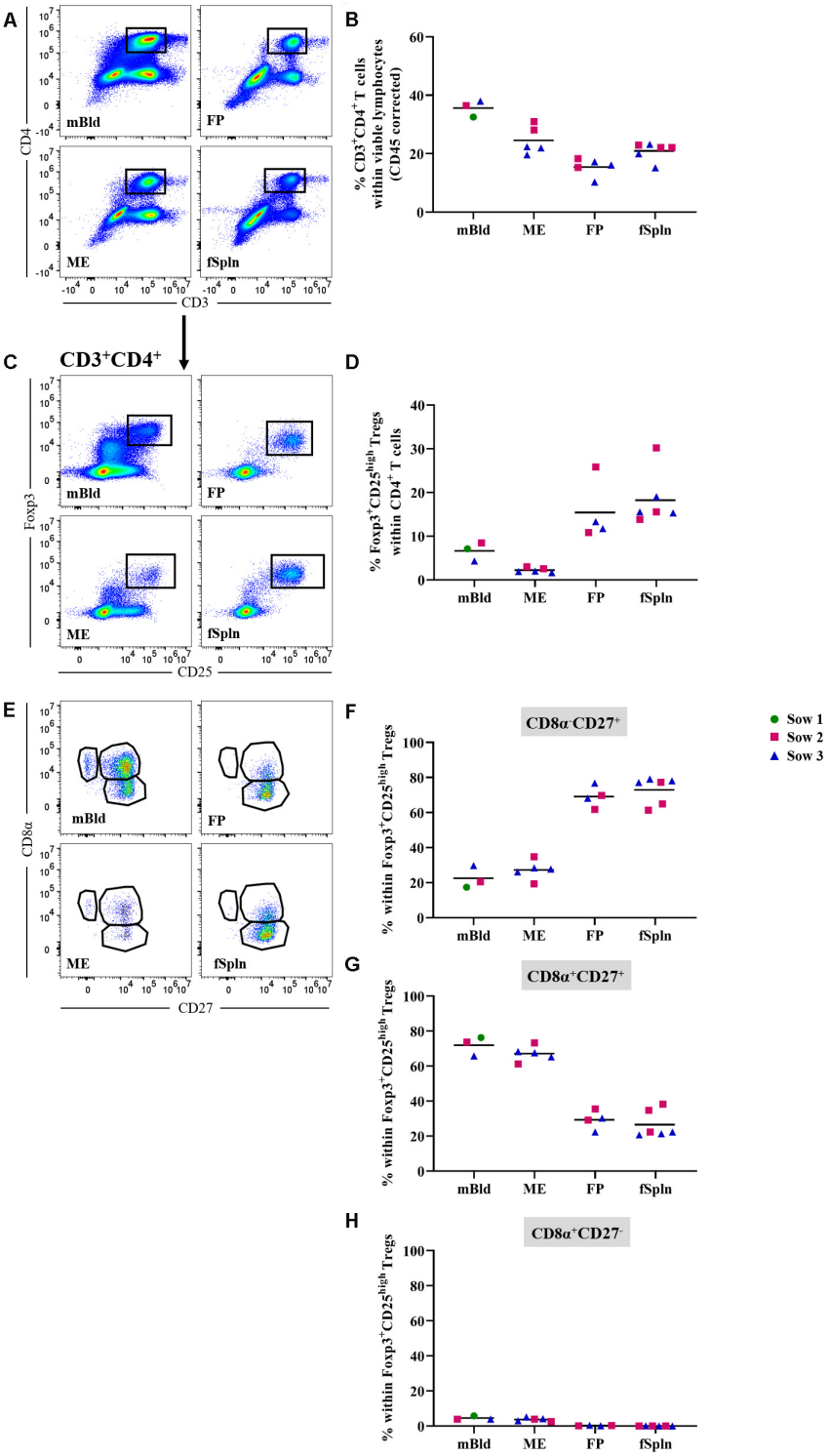

FIGURE 7 | Frequency of total CD4 T cells and characterization of CD4 regulatory T cells. **(A)** Following exclusion of doublets, dead cells, and cells with high autofluorescence (see **Supplementary Figure 1**), total CD4$^+$ T cells were identified by gating on CD3$^+$CD4$^+$ T cells. Representative pseudocolor plots for maternal (left) and fetal compartments (right) are shown [applies also for **(C,E)**]. **(B)** Frequency of total CD4 T cells within viable lymphocytes corrected for CD45 expression. **(C)** Within total CD4 T cells, Foxp3$^+$CD25^{high} cells were gated. **(D)** Frequency of Foxp3$^+$CD25^{high} Tregs within total CD4 T cells. **(E)** Foxp3$^+$CD25^{high} Tregs were further gated for CD8α$^-$CD27$^+$, CD8α$^-$CD27$^+$, and CD8α$^-$CD27$^+$ cells. **(F–H)** Distribution of the three CD8α/CD27-defined Treg populations. **(B,D,F–H)** For all graphs, each colored symbol represents data from one sow for mBld (n = 3) or fetuses coming from that sow for ME (n = 5), FP (n = 4), and fSpln (n = 6). The black bars display the mean within the respective anatomic location.

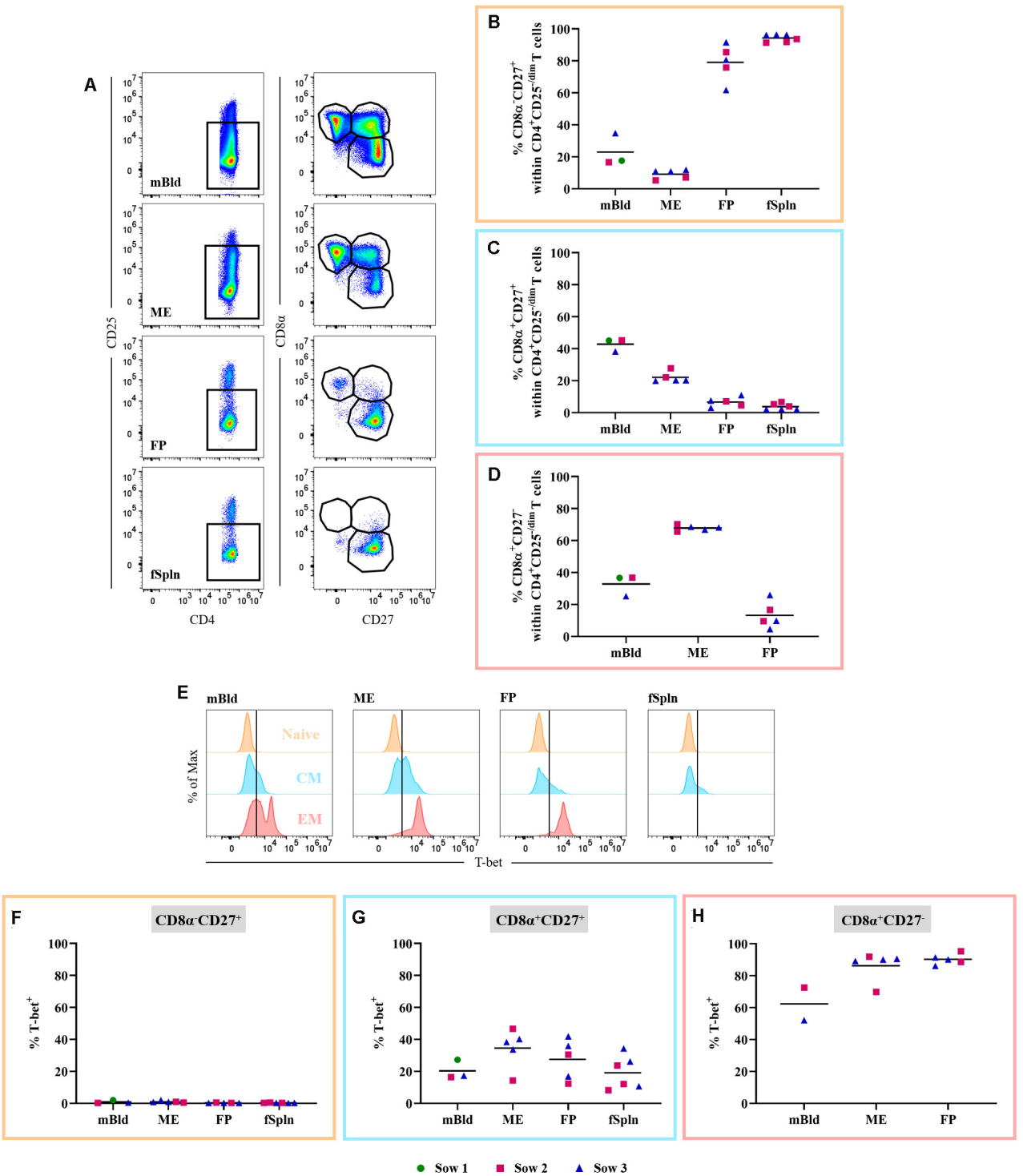

FIGURE 8 | Phenotype and T-bet expression of non-regulatory CD4 T cells. **(A)** Within $CD3^+CD4^+$ T cells $CD25^{high}$ expressing cells were excluded. These cells were gated for $CD8\alpha^-CD27^+$ (representing naive), $CD8\alpha^+CD27^+$ (central memory; Tcm), and $CD8\alpha^-CD27^+$ (effector memory; Tem) cells. Representative pseudocolor plots for maternal and fetal compartments are shown (top to bottom). **(B–D)** Frequency of CD8α/CD27-defined populations within the investigated anatomic locations. **(E)** Non-Treg CD4 T cell populations defined in **A** (naive, Tcm, and Tem) were further analyzed for their expression of the transcription factor T-bet. Representative histograms show the expression of T-bet within the different investigated anatomic locations. **(F,G)** Frequencies of $T\text{-bet}^+$ cells in naive, Tcm, and Tem within the investigated locations. **(B–D,F–H)** For all graphs, each colored symbol represents data from one sow for mBld (n = 3) or fetuses coming from that sow for ME (n = 5), FP (n = 5), and fSpln (n = 6). The black bars display the mean within the respective anatomic locations.

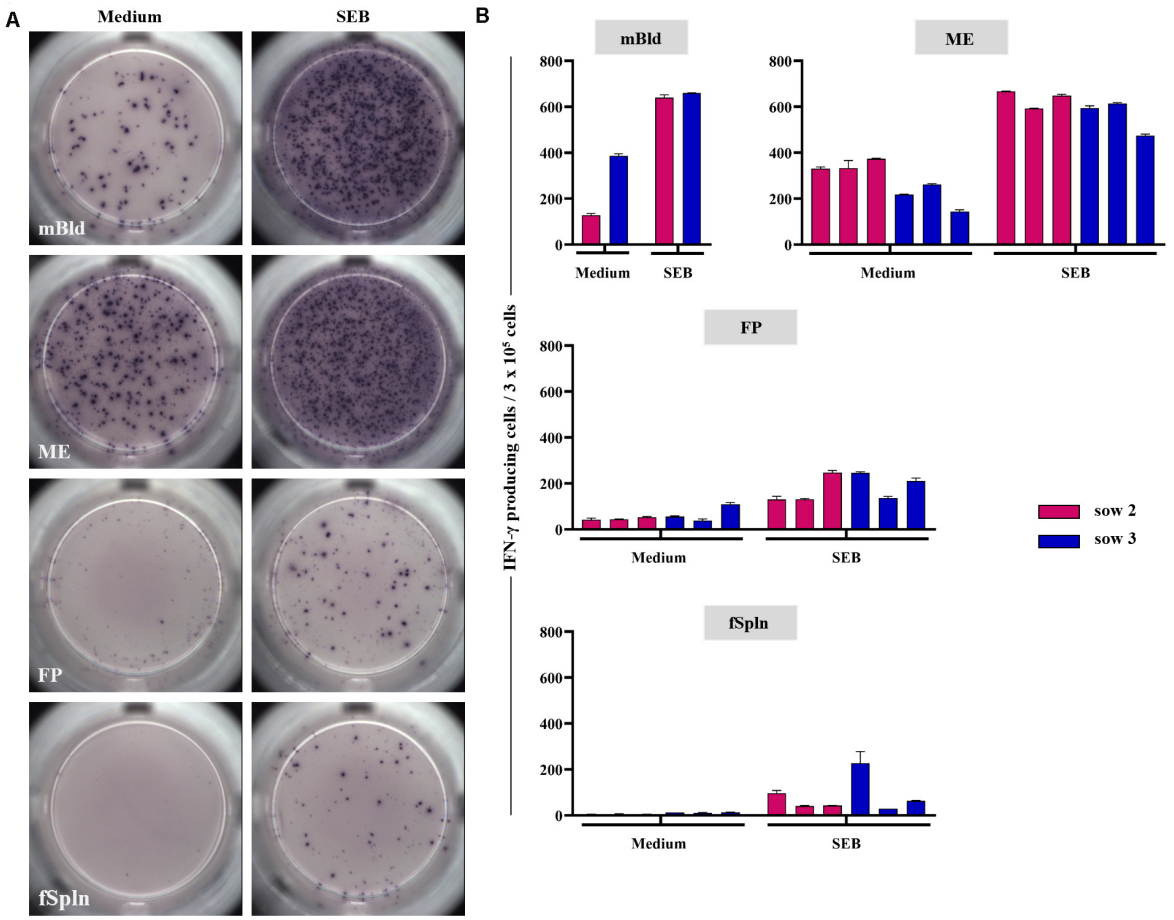

FIGURE 9 | IFN-γ production in ELISpot assays. Lymphocytes isolated from the different anatomic locations were stimulated overnight with staphylococcal enterotoxin B (SEB; 500 ng/mL) or were left untreated. **(A)** Representative raw data for one sow and associated fetal samples. Left: IFN-γ producing cells in unstimulated samples, right: IFN-γ producing cells after SEB stimulation. **(B)** Average IFN-γ producing cells within 3 × 10^5 cells of two technical replicates for medium control and SEB stimulated cells within each investigated anatomic location. The error bars show the standard error of the mean.

IFN-γ for lymphocytes isolated from the FP and fSpln was rather low to non-existent (**Figure 9A**, left column and **Figure 9B**, two graphs below) as compared to the maternal lymphocytes. Following stimulation with SEB, IFN-γ-producing cells were observed within all anatomic sites. However, the response was more vigorous for lymphocytes of maternal origin (mBld and ME) in comparison to lymphocytes from FP and fSpln which is in agreement with the increased frequency of memory T cells in the maternal compartments.

DISCUSSION

So far, research addressing reproductive immunity in the pig is extremely limited. The unique anatomic structure of the porcine placenta prompted us to establish a method that allowed us to elucidate immune cell phenotypes in the maternal and fetal compartment separately. To our knowledge, this has not been attempted before and our methodology will help to investigate immune cell phenotypes present at the maternal-fetal interface. Indeed, in-depth immune phenotyping of NK and T cells highlighted strong differences between ME and FP cell preparations which indicates that the separation contributes to a better understanding of the interplay between the maternal and fetal immune system. Obtaining these unique samples is not that easy, hence, the small sample size, which is one of the limitations in this study. Since this was a first attempt, further research is needed to validate our findings. Furthermore, we were the first to perform these detailed phenotyping experiments and we believe that the groundwork of this study will help to explore lymphocyte function as well as the interplay between pathogens and the immune system *in utero*.

Previous studies showed that porcine NK cells are present in different anatomic locations (e.g., blood, lymphatic, and non-lymphatic organs) (41, 42). Two studies reported an enrichment of $CD16^+$ cells in the porcine endometrium during early gestation as opposed to in peripheral blood (37, 38). In our study a more extended NK cell phenotype was used. We showed that total NK cells, with a $CD3^-CD8\alpha^+CD16^+CD172a^-$ phenotype, were enriched at the maternal-fetal interface as opposed to the

low frequency in the mBld and fSpln. Human and murine NK cells, including uNK cells, express the activating receptor NKp46 (13). In swine, NKp46 delineates three distinct NK cell subsets, namely NKp46^{-}, NKp46^{+}, and NKp46^{high} (42, 43), which were identified across all investigated anatomic locations in this study. The NKp46^{high} NK cell subset was substantially enriched in the fSpln while being a rarity in the mBld. Our results showed that the maternal-fetal interface is mainly populated by NKp46^{-} and NKp46^{+} NK cells. Recent data suggests that in porcine NK cells the expression of NKp46 gets downregulated during the differentiation process and coincides with a shift in transcription factor expression from Eomes to T-bet (Schmuckenschlager et al., in preparation). On the other hand, NKp46^{high} NK cells have been shown to be the superior source with regard to cytokine production and cytolytic activity (43). Similar to human uNK cells (13), we demonstrated that all identified NK cells contained perforin and, therefore, might possess cytolytic potential. However, the lytic activity of human uNK cells is actively regulated by the expression of human leukocyte antigen (HLA) ligands on the trophoblasts (13), and similar mechanisms might be employed by the porcine placenta. We also showed that prior to birth, fetal NK cells readily express perforin, potentially providing a first line of defense. In conclusion, our data indicates that the porcine maternal-fetal interface is rich in cells with a typical NK cell phenotype but, what this means in terms of local NK cell function remains to be elucidated.

NK cell-associated receptors have been shown to be expressed on a fraction of human decidual T cells at term and might serve as a way to regulate T cell function (19). Furthermore, natural killer T (NKT) cells (50, 51) and mucosal-associated invariant T (MAIT) cells (52) have been shown to populate the human decidua. NKT cells have been linked with pregnancy loss and preterm labor whereas MAIT cells seem to play a role in the anti-bacterial defense (50–52). In our study we identified a population of CD3^{+}CD8α^{+}CD16^{+}CD172a^{-} cells which was enriched in the ME but completely absent in the fSpln. In addition, we also showed that a fraction of these cells expressed NKp46 and all cells were positive for perforin, indicative of cytolytic potential. Within this fraction of CD3^{+}CD8α^{+}CD16^{+} T cell subsets of CD8β^{+} T cells, NKT cells, MAIT cells, and γδ T cells might be present (41, 53, 54). Nevertheless, our results show that lymphocytes with a mixed NK-/T cell phenotype are localized at the maternal-fetal interface, which suggests that they might play a role in modulating the immune response locally. Additional studies, however, are needed to specifically address which T cell populations are involved.

Pigs are one of the species, including cattle, sheep, and chicken, where γδ T cells represent a substantial proportion of the total T cell population in the blood circulation and secondary lymphoid organs (44, 55). When considering the expression of CD2, a positive and negative γδ T cell subset can be identified and it was suggested that these are two different lineages that are already established in the thymus (44, 56). Based on the role of transcription factors involved in T cell polarization, a recent study addressing the expression of GATA-3 and T-bet in porcine γδ T cells revealed striking differences between the two lineages (44, 49). A mutually exclusive relationship between the expression of GATA-3 and perforin was described and this related to the CD2^{-} and CD2^{+} γδ T cell phenotypes, respectively (44). In agreement to this, we consistently demonstrated that a CD2^{-} phenotype coincided with a GATA-3^{+}perforin^{-} co-expression while a CD2^{+} phenotype was associated with a GATA-3$^{-/low}$perforin^{+} phenotype. In swine, the ratio of CD2^{-} to CD2^{+} γδ T cells changes over time in an age-dependent manner and corresponds with a decrease of the GATA-3 expression (44). This is in line with our findings regarding GATA-3 in the CD2^{-} γδ T cells, where the MFI was highest in the fSpln and lowest in the ME. In the mBld and ME, putative effector cells with a CD2^{-}perforin^{-}CD8α^{+}CD27^{-} phenotype were observed and might be a local source of IL-17A (55). Similar observations were found for the CD2^{+} γδ T cells. CD2^{+}perforin^{+}CD8α^{+}CD27^{-} γδ T cells prevailed in the maternal compartments and this phenotype suggests a late stage of differentiation. Surprisingly, this phenotype of putative cytolytic effector cells could also be observed in the FP. Nevertheless, CD2^{+}perforin^{-}CD8α$^{dim/-}$CD27^{+} γδ T cells dominated the fetal tissues, which appears to correspond to a more naive phenotype. Overall, the γδ T cell composition differed greatly between the maternal and fetal tissues and needs to be investigated further in order to determine the role of γδ T cell subsets at the maternal-fetal interface.

Since CD8α in pigs is abundantly expressed on different immune cell types, a CD3^{+}CD8α^{high}CD8β^{+} phenotype was investigated to identify the abundance of CTLs within all investigated locations. The phenotypic differentiation of these cells in the pig is not yet completely elucidated; however, studies suggest that the combination of perforin and CD27 expression can be applied to assess CTL differentiation (46, 57, 58). Our results showed that in the fSpln all CTLs have a perforin^{-}CD27^{+} phenotype. This validates the findings that porcine neonates were born with naive CTLs (46). Over time these cells acquired the expression of perforin which coincides with a down regulation of CD27 (46). Perforin^{+}CD27^{+} might represent an early effector or Tcm phenotype while the complete loss of CD27 (perforin^{+}CD27^{-}) might indicate a terminally differentiated phenotype and, therefore, might contain late effectors or Tem cells (46, 57). Similar to human dCD8^{+} T cells (22, 23, 26, 30), we found that CTLs with a putative Tcm and Tem phenotype were enriched in the maternal compartments. To our surprise, we also detected a substantial proportion of CTLs with a Tcm and Tem phenotype in the FP. Currently, we do not know if the enrichment of antigen-experienced cells in the FP might be explained by a migration of maternal cells to the FP or if they represent antigen-experienced T cells of fetal origin.

Considering that CD4^{+} T cells can be identified in the human decidua (8, 27), we also characterized CD3^{+}CD4^{+} T cells at the porcine maternal-fetal interface, the mBld, and fSpln. Surprisingly, our in-depth analysis revealed that the Treg frequency in the ME was extremely low whereas an enrichment was observed in both fetal tissues. Although the abundance of Tregs was low in the maternal compartments, the majority was CD8α^{+}. Upregulation of CD8α on porcine CD4^{+} T cells coincides with antigen-experience and is associated with immunological memory [reviewed in (57)], hence, this might indicate that ME Tregs are activated or in a memory-like state.

Differently, in the fetal compartments most Tregs did not express CD8α, indicating a more naive state. Furthermore, analysis of non-Tregs showed that differentiated phenotypes, including Tcm and Tem, prevailed in mBld and ME, which is in agreement with results from the human field (27). As expected, the non-Treg $CD4^+$ T cells from the fetal tissues were predominantly naive, aside from the small Tem population in the FP. In pigs, the characterization of polarized $CD4^+$ T cell subsets is not as straightforward because not all subsets have been identified so far (57). However, it has been shown that following an infection with PRRSV an increase in T-bet^+ $CD4^+$ T cells can be observed (59). Evidently, a recent study demonstrated that also T-bet expression of porcine αβ T cells is associated with IFN-γ production (49). In the current study, the vast majority of Tem cells at the maternal-fetal interface, regardless of the anatomic site, expressed T-bet. In context of human pregnancy, a recent study demonstrated that PBMCs gradually acquire a more activated phenotype following the transition from the second to third trimester, but are still regulated (3). This transition is necessary for parturition (2). In our study the low abundance of Tregs in the ME might be an indicator of a gradual lift of the local immunosuppressive regulation in order to prepare for parturition. In line with this, it has been shown that the suppressive activity of Tregs decreases at term and thereby is implicated in the induction of parturition (20). However, investigating Treg frequencies and function at different gestational stages is necessary to address these speculations. Initially, pregnancy has been defined as being a Th2 phenomenon; however, first and last trimester decidua are enriched with Th1 cells (8, 27). In line with this, our data indicates that most terminally differentiated $CD4^+$ T cells have a Th1 phenotype at the porcine maternal-fetal interface. Prior to parturition, these cells might create a type-1 cytokine environment. Moreover, human $CD4^+$ T cells at the maternal-fetal interface have been shown to produce a variety of pro-inflammatory cytokines and matrix metalloproteinase-9 by which they play a role in the onset and perpetuation of parturition (20). Hence, the T-bet^+ Tem cells identified at the maternal-fetal interface in our study might have a similar function.

Overall, we identified several T cell populations, e.g., $CD2^+perforin^+CD8\alpha^+CD27^-$ γδ T cells, $perforin^+CD27^-$ CTLs, and T-bet^+ $CD4^+$ Tem cells, with putative effector functions in the FP. In humans and mice, microchimerism is a well-established fact. Therefore, these putative effector cells might be maternal cells that have migrated to the FP. However, the porcine placenta is considered as a tight impermeable barrier and contrasting findings regarding microchimerism in pregnant pigs have been reported (60, 61). Female DNA was found in the serum of male fetuses and female cells were detected in the male fetal liver, but the origin of the DNA and cells, either maternal or female siblings, could not be tracked (60). Furthermore, male DNA was detected in the maternal circulation (60). Data from another group, contradicts the previous findings and showed that there was no exchange of cells (61). It is also plausible that the effector cells in the FP are of fetal origin; however, the cues that drive their differentiation remain to be elucidated. Different pathogens, e.g., porcine parvovirus, manage to breach the placenta or reside in the uterus. Thus, the presence of local pathogens during late gestation might be implicated in the differentiation of effector cells.

The functional capacity of our isolated cells was assessed by means of an IFN-γ ELISpot assay. In the human field, SEB stimulation is often used as a positive control to induce cytokine production in T cells (62–64) and therefore was applied in our study. Our results demonstrated a substantial spontaneous IFN-γ release by cells isolated from the mBld and ME, which reflects the presence of highly differentiated cells within these anatomic sites. Lymphocytes isolated from all anatomic sites were able to produce IFN-γ, but the response for the fetal compartments was limited, further demonstrating that the fetal compartments reflect a naive immune phenotype in general.

In conclusion, with our uniquely designed methodology and the available porcine toolbox we were able to reveal immune phenotypes that reside at the maternal-fetal interface. Overall, a naive immune phenotype predominated the fetal compartments as opposed to the antigen-experienced immune phenotype of the maternal system. The physiological role of these cells during gestation and how they are coordinated open a broad array of questions that need to be answered. The groundwork of this study will help to explore lymphocyte function as well as the interplay between pathogens and the immune system *in utero* at different stages of gestation. Such findings might also instruct vaccine development and optimization.

DATA AVAILABILITY STATEMENT

The raw data supporting the conclusions of this article will be made available by the authors, without undue reservation.

ETHICS STATEMENT

Ethical review and approval was not required for the animal study because no live animals were included. Samples were collected from dead animals which does not require governmental animal ethics approval in Austria. The project plan has been discussed and approved by the institutional ethics and animal welfare committee in accordance with GSP guidelines and national legislation (approval number ETK-32/02/2016).

AUTHOR CONTRIBUTIONS

MRS, KM, AS, WG, and AL were in charge of the study design. ES and SS were involved in tissue collection and the tissue separation procedure. MRS, MK, MS, SS, and ES performed laboratory work and experiments. MRS carried out the phenotyping experiments and analyzed the data. MRS, KM, ES, AS, WG, and AL thoroughly discussed and interpreted the data. MRS, WG, and AL wrote the manuscript. All authors read and approved the final manuscript.

FUNDING

This work was financially supported by intramural funds of the University of Veterinary Medicine Vienna.

ACKNOWLEDGMENTS

We are grateful to Christian Knecht, Sophie Dürlinger, Heinrich Kreutzmann, Moritz Bünger, Rene Renzhammer, and Selma Schmidt for their support with the sample collection.

SUPPLEMENTARY MATERIAL

The Supplementary Material for this article can be found online at: https://www.frontiersin.org/articles/10.3389/fimmu.2020.582065/full#supplementary-material

REFERENCES

1. Schumacher A, Costa SD, Zenclussen AC. Endocrine factors modulating immune responses in pregnancy. *Front Immunol*. (2014) 5:196. doi: 10.3389/fimmu.2014.00196
2. Mor G, Aldo P, Alvero AB. The unique immunological and microbial aspects of pregnancy. *Nat Rev Immunol*. (2017) 17:469–82. doi: 10.1038/nri.2017.64
3. Shah NM, Herasimtschuk AA, Boasso A, Benlahrech A, Fuchs D, Imami N, et al. Changes in T cell and dendritic cell phenotype from mid to late pregnancy are indicative of a shift from immune tolerance to immune activation. *Front Immunol*. (2017) 8:1138. doi: 10.3389/fimmu.2017.01138
4. Bulmer JN, Morrison L, Longfellow M, Ritson A, Pace D. Granulated lymphocytes in human endometrium: histochemical and immunohistochemical studies. *Hum Reprod*. (1991) 6:791–8. doi: 10.1093/oxfordjournals.humrep.a137430
5. Vargas ML, Sántos JL, Ruiz C, Montes MJ, Alemán P, García-Tortosa C, et al. Comparison of the proportions of leukocytes in early and term human decidua. *Am J Reprod Immunol*. (1993) 29:135–40. doi: 10.1111/j.1600-0897.1993.tb00578.x
6. Hess AP, Hamilton AE, Talbi S, Dosiou C, Nyegaard M, Nayak N, et al. Decidual stromal cell response to paracrine signals from the trophoblast: amplification of immune and angiogenic modulators. *Biol Reprod*. (2007) 76:102–17. doi: 10.1095/biolreprod.106.054791
7. Bulmer JN, Williams PJ, Lash GE. Immune cells in the placental bed. *Int J Dev Biol*. (2010) 54:281–94. doi: 10.1387/ijdb.082763jb
8. Mjösberg J, Berg G, Jenmalm MC, Ernerudh J. FOXP3+ regulatory T cells and T helper 1, T helper 2, and T helper 17 cells in human early pregnancy decidua. *Biol Reprod*. (2010) 82:698–705. doi: 10.1095/biolreprod.109.081208
9. Tilburgs T, Claas FH, Scherjon SA. Elsevier trophoblast research award lecture: unique properties of decidual T cells and their role in immune regulation during human pregnancy. *Placenta*. (2010) 31:S82–6. doi: 10.1016/j.placenta.2010.01.007
10. Faas MM, de Vos P. Uterine NK cells and macrophages in pregnancy. *Placenta*. (2017) 56:44–52. doi: 10.1016/j.placenta.2017.03.001
11. Zenclussen AC, Hämmerling GJ. Cellular regulation of the uterine microenvironment that enables embryo implantation. *Front Immunol*. (2015) 6:321. doi: 10.3389/fimmu.2015.00321
12. Croy BA, Chen Z, Hofmann AP, Lord EM, Sedlacek AL, Gerber SA. Imaging of vascular development in early mouse decidua and its association with leukocytes and trophoblasts. *Biol Reprod*. (2012) 87:125. doi: 10.1095/biolreprod.112.102830
13. Gaynor LM, Colucci F. Uterine Natural Killer cells: functional distinctions and influence on pregnancy in humans and mice. *Front Immunol*. (2017) 8:467. doi: 10.3389/fimmu.2017.00467
14. Hanna J, Goldman-Wohl D, Hamani Y, Avraham I, Greenfield C, Natanson-Yaron S, et al. Decidual NK cells regulate key developmental processes at the human fetal-maternal interface. *Nat Med*. (2006) 12:1065–74. doi: 10.1038/nm1452
15. Vigano P, Gaffuri B, Somigliana E, Infantino M, Vignali M, Di Blasio AM. Interleukin-10 is produced by human uterine natural killer cells but does not affect their production of interferon-gamma. *Mol Hum Reprod*. (2001) 7:971–7. doi: 10.1093/molehr/7.10.971
16. Siewiera J, El Costa H, Tabiasco J, Berrebi A, Cartron G, Le Bouteiller P, et al. Human cytomegalovirus infection elicits new decidual natural killer cell effector functions. *PLoS Pathog*. (2013) 9:e1003257. doi: 10.1371/journal.ppat.1003257
17. Crespo AC, van der Zwan A, Ramalho-Santos J, Strominger JL, Tilburgs T. Cytotoxic potential of decidual NK cells and CD8+ T cells awakened by infections. *J Reprod Immunol*. (2017) 119:85–90. doi: 10.1016/j.jri.2016.08.001
18. Vassiliadou N, Bulmer JN. Quantitative analysis of T lymphocyte subsets in pregnant and nonpregnant human endometrium. *Biol Reprod*. (1996) 55:1017–22. doi: 10.1095/biolreprod55.5.1017
19. Tilburgs T, van der Mast BJ, Nagtzaam NM, Roelen DL, Scherjon SA, Claas FH. Expression of NK cell receptors on decidual T cells in human pregnancy. *J Reprod Immunol*. (2009) 80:22–32. doi: 10.1016/j.jri.2009.02.004
20. Gomez-Lopez N, Vega-Sanchez R, Castillo-Castrejon M, Romero R, Cubeiro-Arreola K, Vadillo-Ortega F. Evidence for a role for the adaptive immune response in human term parturition. *Am J Reprod Immunol*. (2013) 69:212–30. doi: 10.1111/aji.12074
21. Saito S, Nishikawa K, Morii T, Narita N, Enomoto M, Ito A, et al. A study of CD45RO, CD45RA and CD29 antigen expression on human decidual T cells in an early stage of pregnancy. *Immunol Lett*. (1994) 40:193–7. doi: 10.1016/0165-2478(93)00019-A
22. Tilburgs T, Schonkeren D, Eikmans M, Nagtzaam NM, Datema G, Swings GM, et al. Human decidual tissue contains differentiated CD8+ effector-memory T cells with unique properties. *J Immunol*. (2010) 185:4470–7. doi: 10.4049/jimmunol.0903597
23. Kieffer TEC, Laskewitz A, Scherjon SA, Faas MM, Prins JR. Memory T cells in pregnancy. *Front Immunol*. (2019) 10:625. doi: 10.3389/fimmu.2019.00625
24. Scaife PJ, Bulmer JN, Robson SC, Innes BA, Searle RF. Effector activity of decidual CD8+ T lymphocytes in early human pregnancy. *Biol Reprod*. (2006) 75:562–7. doi: 10.1095/biolreprod.106.052654
25. Tilburgs T, Scherjon SA, Roelen DL, Claas FH. Decidual CD8+CD28- T cells express CD103 but not perforin. *Hum Immunol*. (2009) 70:96–100. doi: 10.1016/j.humimm.2008.12.006
26. van der Zwan A, Bi K, Norwitz ER, Crespo AC, Claas FHJ, Strominger JL, et al. Mixed signature of activation and dysfunction allows human decidual $CD8^+$ T cells to provide both tolerance and immunity. *Proc Natl Acad Sci USA*. (2018) 115:385–90. doi: 10.1073/pnas.1713957115
27. Feyaerts D, Benner M, van Cranenbroek B, van der Heijden OWH, Joosten I, van der Molen RG. Human uterine lymphocytes acquire a more experienced and tolerogenic phenotype during pregnancy. *Sci Rep*. (2017) 7:2884. doi: 10.1038/s41598-017-03191-0
28. van Egmond A, van der Keur C, Swings GM, Scherjon SA, Claas FH. The possible role of virus-specific CD8(+) memory T cells in decidual tissue. *J Reprod Immunol*. (2016) 113:1–8. doi: 10.1016/j.jri.2015.09.073
29. Tilburgs T, Scherjon SA, van der Mast BJ, Haasnoot GW, Versteeg VDV-MM, Roelen DL, et al. Fetal-maternal HLA-C mismatch is associated with decidual T cell activation and induction of functional T regulatory cells. *J Reprod Immunol*. (2009) 82:148–57. doi: 10.1016/j.jri.2009.05.003
30. Powell RM, Lissauer D, Tamblyn J, Beggs A, Cox P, Moss P, et al. Decidual T cells exhibit a highly differentiated phenotype and demonstrate potential fetal specificity and a strong transcriptional response to interferon. *J Immunol*. (2017) 199:3406–17. doi: 10.4049/jimmunol.1700114
31. Lissauer D, Piper K, Goodyear O, Kilby MD, Moss PA. Fetal-specific CD8+ cytotoxic T cell responses develop during normal human pregnancy and exhibit broad functional capacity. *J Immunol*. (2012) 189:1072–80. doi: 10.4049/jimmunol.1200544
32. Tilburgs T, Roelen DL, van der Mast BJ, de Groot-Swings GM, Kleijburg C, Scherjon SA, et al. Evidence for a selective migration of fetus-specific CD4+CD25bright regulatory T cells from the peripheral blood to the decidua in human pregnancy. *J Immunol*. (2008) 180:5737–45. doi: 10.4049/jimmunol.180.8.5737
33. Shima T, Inada K, Nakashima A, Ushijima A, Ito M, Yoshino O, et al. Paternal antigen-specific proliferating regulatory T cells are increased in uterine-draining lymph nodes just before implantation and in pregnant uterus just after implantation by seminal plasma-priming in allogeneic mouse pregnancy. *J Reprod Immunol*. (2015) 108:72–82. doi: 10.1016/j.jri.2015.02.005

34. Samstein RM, Josefowicz SZ, Arvey A, Treuting PM, Rudensky AY. Extrathymic generation of regulatory T cells in placental mammals mitigates maternal-fetal conflict. *Cell*. (2012) 150:29–38. doi: 10.1016/j.cell.2012.05.031
35. Kim YB. Developmental immunity in the piglet. *Birth Defects Orig Artic Ser*. (1975) 11:549–57.
36. Dimova T, Mihaylova A, Spassova P, Georgieva R. Establishment of the porcine epitheliochorial placenta is associated with endometrial T-cell recruitment. *Am J Reprod Immunol*. (2007) 57:250–61. doi: 10.1111/j.1600-0897.2007.00472.x
37. Dimova T, Mihaylova A, Spassova P, Georgieva R. Superficial implantation in pigs is associated with decreased numbers and redistribution of endometrial NK-cell populations. *Am J Reprod Immunol*. (2008) 59:359–69. doi: 10.1111/j.1600-0897.2007.00579.x
38. Engelhardt H, Croy BA, King GJ. Evaluation of natural killer cell recruitment to embryonic attachment sites during early porcine pregnancy. *Biol Reprod*. (2002) 66:1185–92. doi: 10.1095/biolreprod66.4.1185
39. Talker SC, Koinig HC, Stadler M, Graage R, Klingler E, Ladinig A, et al. Magnitude and kinetics of multifunctional $CD4^+$ and $CD8\beta^+$ T cells in pigs infected with swine influenza A virus. *Vet Res*. (2015) 46:52. doi: 10.1186/s13567-015-0182-3
40. Golub R, Cumano A. Embryonic hematopoiesis. *Blood Cells Mol Dis*. (2013) 51:226–31. doi: 10.1016/j.bcmd.2013.08.004
41. Denyer MS, Wileman TE, Stirling CM, Zuber B, Takamatsu HH. Perforin expression can define CD8 positive lymphocyte subsets in pigs allowing phenotypic and functional analysis of natural killer, cytotoxic T, natural killer T and MHC un-restricted cytotoxic T-cells. *Vet Immunol Immunopathol*. (2006) 110:279–92. doi: 10.1016/j.vetimm.2005.10.005
42. Mair KH, Essler SE, Patzl M, Storset AK, Saalmüller A, Gerner W. NKp46 expression discriminates porcine NK cells with different functional properties. *Eur J Immunol*. (2012) 42:1261–71. doi: 10.1002/eji.201141989
43. Mair KH, Müllebner A, Essler SE, Duvigneau JC, Storset AK, Saalmüller A, et al. Porcine CD8αdim/-NKp46high NK cells are in a highly activated state. *Vet Res*. (2013) 44:13. doi: 10.1186/1297-9716-44-13
44. Rodríguez-Gómez IM, Talker SC, Käser T, Stadler M, Reiter L, Ladinig A, et al. Expression of T-Bet, Eomesodermin, and GATA-3 Correlates with distinct phenotypes and functional properties in porcine γδ T Cells. *Front Immunol*. (2019) 10:396. doi: 10.3389/fimmu.2019.00396
45. Yang H, Parkhouse RM, Wileman T. Monoclonal antibodies that identify the CD3 molecules expressed specifically at the surface of porcine gammadelta-T cells. *Immunology*. (2005) 115:189–96. doi: 10.1111/j.1365-2567.2005.02137.x
46. Talker SC, Käser T, Reutner K, Sedlak C, Mair KH, Koinig H, et al. Phenotypic maturation of porcine NK- and T-cell subsets. *Dev Comp Immunol*. (2013) 40:51–68. doi: 10.1016/j.dci.2013.01.003
47. Reutner K, Leitner J, Müllebner A, Ladinig A, Essler SE, Duvigneau JC, et al. CD27 expression discriminates porcine T helper cells with functionally distinct properties. *Vet Res*. (2013) 44:18. doi: 10.1186/1297-9716-44-18
48. Käser T, Gerner W, Hammer SE, Patzl M, Saalmüller A. Detection of Foxp3 protein expression in porcine T lymphocytes. *Vet Immunol Immunopathol*. (2008) 125:92–101. doi: 10.1016/j.vetimm.2008.05.007
49. Rodríguez-Gómez IM, Talker SC, Käser T, Stadler M, Hammer SE, Saalmüller A, et al. Expression of T-bet, Eomesodermin and GATA-3 in porcine αβ T cells. *Dev Comp Immunol*. (2016) 60:115–26. doi: 10.1016/j.dci.2016.02.022
50. Boyson JE, Aktan I, Barkhuff DA, Chant A. NKT cells at the maternal-fetal interface. *Immunol Invest*. (2008) 37:565–82. doi: 10.1080/08820130802191409
51. Gomez-Lopez N, StLouis D, Lehr MA, Sanchez-Rodriguez EN, Arenas-Hernandez M. Immune cells in term and preterm labor. *Cell Mol Immunol*. (2014) 11:571–81. doi: 10.1038/cmi.2014.46
52. Solders M, Gorchs L, Erkers T, Lundell AC, Nava S, Gidlöf S, et al. MAIT cells accumulate in placental intervillous space and display a highly cytotoxic phenotype upon bacterial stimulation. *Sci Rep*. (2017) 7:6123. doi: 10.1038/s41598-017-06430-6
53. Mair KH, Stadler M, Talker SC, Forberg H, Storset AK, Müllebner A, et al. Porcine CD3(+)NKp46(+) lymphocytes have NK-cell characteristics and are present in increased frequencies in the lungs of influenza-infected animals. *Front Immunol*. (2016) 7:263. doi: 10.3389/fimmu.2016.00263
54. Xiao X, Li K, Ma X, Liu B, He X, Yang S, et al. Mucosal-associated invariant T cells expressing the TRAV1-TRAJ33 chain are present in pigs. *Front Immunol*. (2019) 10:2070. doi: 10.3389/fimmu.2019.02070
55. Sedlak C, Patzl M, Saalmüller A, Gerner W. CD2 and CD8α define porcine γδ T cells with distinct cytokine production profiles. *Dev Comp Immunol*. (2014) 45:97–106. doi: 10.1016/j.dci.2014.02.008
56. Stepanova K, Sinkora M. Porcine gammadelta T lymphocytes can be categorized into two functionally and developmentally distinct subsets according to expression of CD2 and level of TCR. *J Immunol*. (2013) 190:2111–20. doi: 10.4049/jimmunol.1202890
57. Gerner W, Talker SC, Koinig HC, Sedlak C, Mair KH, Saalmüller A. Phenotypic and functional differentiation of porcine αβ T cells: current knowledge and available tools. *Mol Immunol*. (2015) 66:3–13. doi: 10.1016/j.molimm.2014.10.025
58. Gerner W, Käser T, Saalmüller A. Porcine T lymphocytes and NK cells–an update. *Dev Comp Immunol*. (2009) 33:310–20. doi: 10.1016/j.dci.2008.06.003
59. Ebner F, Rausch S, Scharek-Tedin L, Pieper R, Burwinkel M, Zentek J, et al. A novel lineage transcription factor based analysis reveals differences in T helper cell subpopulation development in infected and intrauterine growth restricted (IUGR) piglets. *Dev Comp Immunol*. (2014) 46:333–40. doi: 10.1016/j.dci.2014.05.005
60. Karniychuk UU, Van Breedam W, Van Roy N, Rogel-Gaillard C, Nauwynck HJ. Demonstration of microchimerism in pregnant sows and effects of congenital PRRSV infection. *Vet Res*. (2012) 43:19. doi: 10.1186/1297-9716-43-19
61. Garrels W, Holler S, Taylor U, Herrmann D, Niemann H, Ivics Z, et al. Assessment of fetal cell chimerism in transgenic pig lines generated by Sleeping Beauty transposition. *PLoS One*. (2014) 9:e96673. doi: 10.1371/journal.pone.0096673
62. Guerreiro M, Na IK, Letsch A, Haase D, Bauer S, Meisel C, et al. Human peripheral blood and bone marrow Epstein-Barr virus-specific T-cell repertoire in latent infection reveals distinct memory T-cell subsets. *Eur J Immunol*. (2010) 40:1566–76. doi: 10.1002/eji.200940000
63. Hanitsch LG, Lobel M, Mieves JF, Bauer S, Babel N, Schweiger B, et al. Cellular and humoral influenza-specific immune response upon vaccination in patients with common variable immunodeficiency and unclassified antibody deficiency. *Vaccine*. (2016) 34:2417–23. doi: 10.1016/j.vaccine.2016.03.091
64. Cossarizza A, Chang HD, Radbruch A, Acs A, Adam D, Adam-Klages S, et al. Guidelines for the use of flow cytometry and cell sorting in immunological studies (second edition). *Eur J Immunol*. (2019) 49:1457–973.

Conflict of Interest: The authors declare that the research was conducted in the absence of any commercial or financial relationships that could be construed as a potential conflict of interest.

frontiers

Supplementary Material

NK and T cell differentiation at the maternal-fetal interface in sows during late gestation

Melissa R. Stas, Michaela Koch, Maria Stadler, Spencer Sawyer, Elena L. Sassu, Kerstin H. Mair, Armin Saalmüller, Wilhelm Gerner† and Andrea Ladinig†*

†These authors have contributed equally to this work.

* Correspondence: Andrea Ladinig: Andrea.ladinig@vetmeduni.ac.at

1 Supplementary Figures

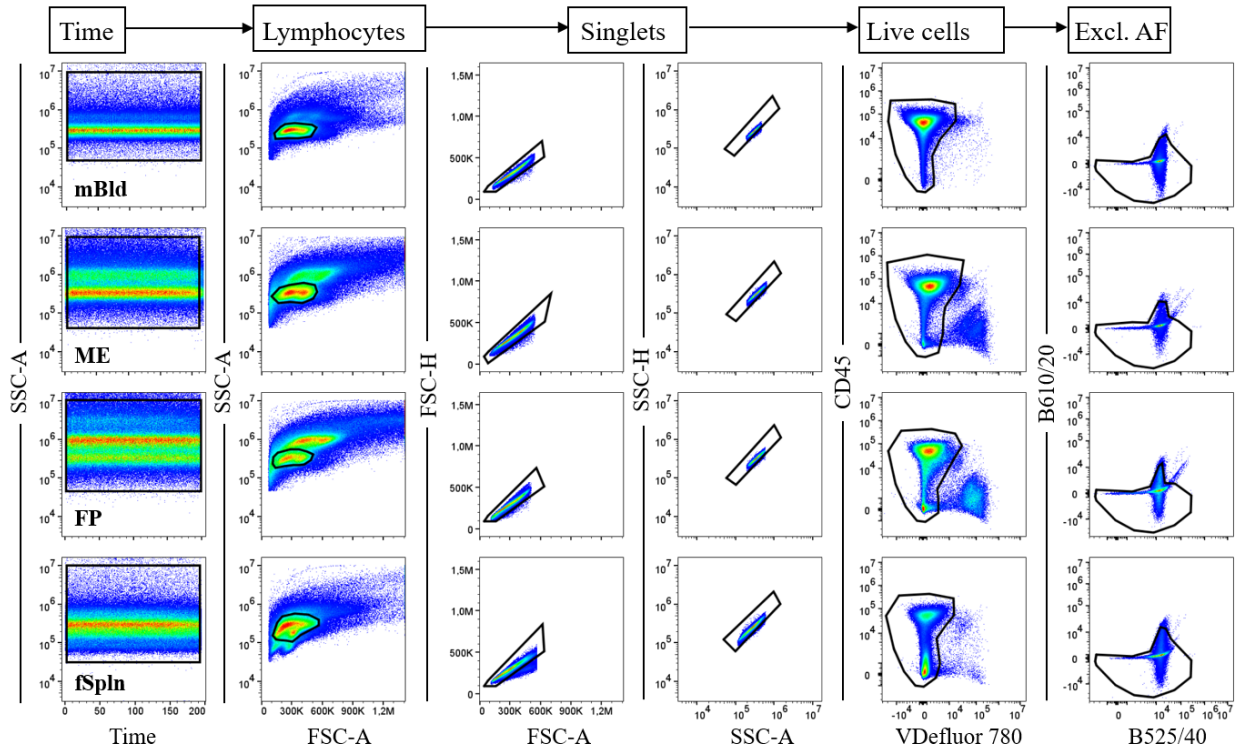

Supplementary Figure 1 | Consecutive gating strategy for lymphocytes isolated from the investigated anatomic locations. For each flow cytometry staining panel (see Table 1) the following gating hierarchy was applied: after a time gate, lymphocytes were selected according to their light scatter properties (FSC-A vs. SSC-A). Thereafter, a two-step doublet discrimination (FSC-H vs. FSC-A and SSC-H vs. SSC-A) was applied, which was followed by the exclusion of dead cells, based on a staining with the fixable viability dye eFluor780®. Hereafter, cells with a high auto fluorescent signal were excluded by using the bandpass filter 610/20 in the excitation line of the blue laser. Representative pseudocolor plots are shown (top to bottom): mBld, maternal blood; ME, maternal endometrium; FP, fetal placenta; fSpln, fetal spleen.

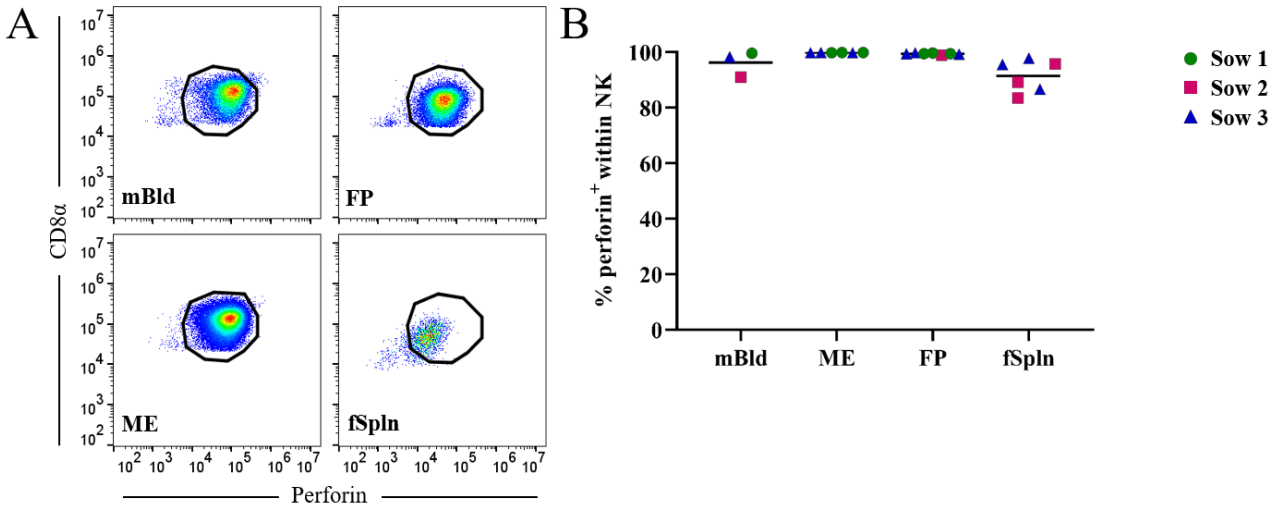

Supplementary Figure 2 | Expression of perforin in cells with an NK cell phenotype. (A) $CD3^-$ $CD8\alpha^+CD16^+CD172a^-$ cells (see Figure 2A) were further analyzed for their expression of perforin within all investigated anatomic locations. Representative pseudocolor plots for maternal (left) and fetal compartments (right) are shown. **(B)** Frequency of $perforin^+$ NK cells ($CD3^-$ $CD8\alpha^+CD16^+CD172a^-$) within the respective anatomic locations. Each colored symbol represents data from one sow for mBld (n = 3) or fetuses coming from that sow ME (n = 6), FP (n = 7), and fSpln (n = 6). The black bars display the mean within the respective anatomic location.

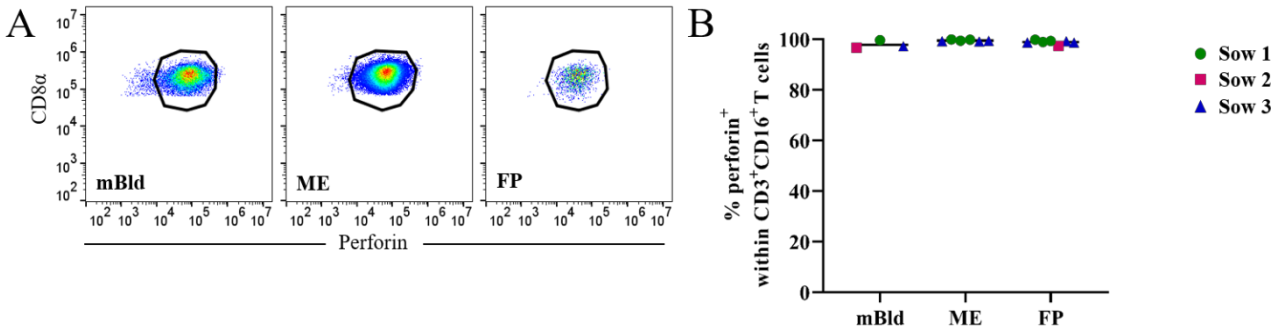

Supplementary Figure 3 | Expression of perforin in CD3$^+$CD16$^+$ T cells. (A) CD16$^+$ T cells (CD3$^+$CD8α$^+$CD16$^+$CD172a$^-$, see Figure 3A) were further analyzed for their expression of perforin. No CD16$^+$ T cells were found in fetal spleens (see Figure 3A) hence this location was not investigated further. Representative pseudocolor plots for maternal (left) and fetal compartments (right) are shown. **(B)** Frequency of perforin$^+$ cells within CD3$^+$CD16$^+$ T cells in mBld, ME and FP. Each colored symbol represents data from one sow for mBld (n = 3) or fetuses coming from that sow ME (n = 6), FP (n = 7), and fSpln (n = 6). The black bars display the mean within the respective anatomic location.

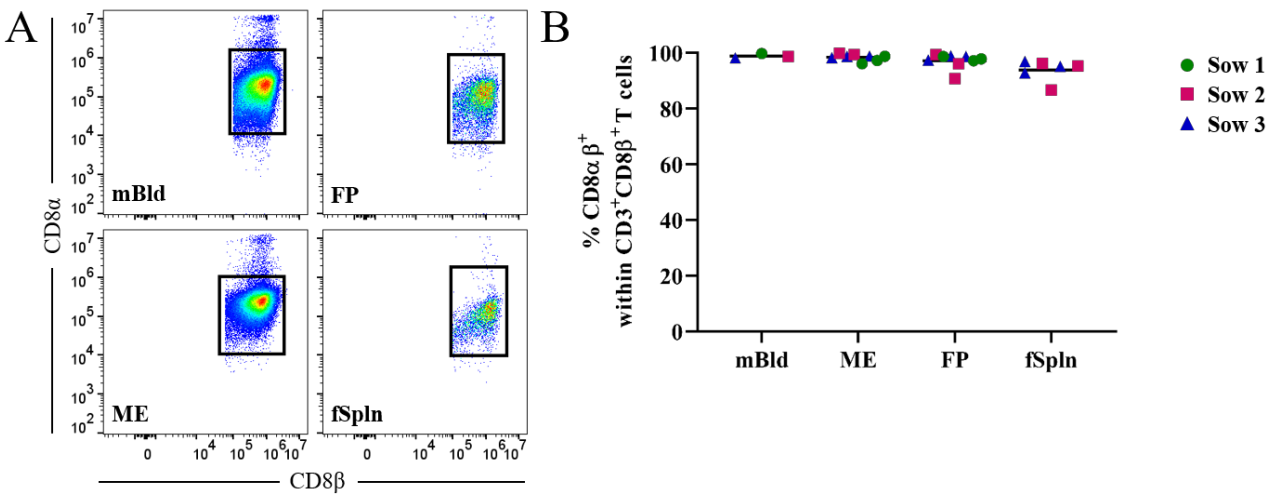

Supplementary Figure 4 | Expression of CD8αβ heterodimers on CD8 T cells. (A), CD8β$^+$ T cells (see Figure 6A) were further gated for their co-expression of CD8α and CD8β. Representative pseudocolor plots for maternal (left) and fetal compartments (right) are shown. **(B)** Frequency of CD8αβ heterodimer expressing cells within total CD8β$^+$ cells. Each colored symbol represents data from one sow for mBld (n = 3) or fetuses coming from that sow ME (n = 8), FP (n = 9), and fSpln (n = 6). The black bars display the mean within the respective anatomic location.

3.2. Publication 2

Melissa R. Stas, Heinrich Kreutzmann, Julia Stadler, Elena L. Sassu, Kerstin H. Mair, Michaela Koch, Christian Knecht, Maria Stadler, Marlies Dolezal, Gyula Balka, Marianne Zaruba, Marlene Mötz, Armin Saalmüller, Till Rümenapf, Wilhelm Gerner and Andrea Ladinig. Influence of PRRSV-1 vaccination and infection on mononuclear cells at the maternal-fetal interface. Frontiers in Immunology 2022; https://doi.org/10.3389/fimmu.2022.1055048

Journal Impact Factor 2022: 7.561

Author contributions:

MRS, KM, JS, AS, TR, WG, and AL were in charge of the study design. HK, CK, JS, GB, and AL organized the animal experiment and were responsible for the sample collection. ES, KM, MK, MS, MZ, MM, and TR performed the laboratory work. MRS, WG, and AL analysed the data and MD performed the statistical analysis. MRS, WG, and AL discussed and interpreted the data and prepared the manuscript. All authors read and approved the final manuscript.

frontiers | Frontiers in Immunology

TYPE Original Research
PUBLISHED 08 November 2022
DOI 10.3389/fimmu.2022.1055048

OPEN ACCESS

EDITED BY
Uladzimir Karniychuk,
University of Saskatchewan,
Canada

REVIEWED BY
Chang Huang,
National Institute of Allergy and Infectious Diseases (NIH),
United States
François JMA Meurens,
INRA Ecole Nationale Vétérinaire, Agroalimentaire et de l'alimentation de Nantes-Atlantique (Oniris), France

*CORRESPONDENCE
Andrea Ladinig
Andrea.ladinig@vetmeduni.ac.at

†PRESENT ADDRESS
Elena L. Sassu,
Division for Animal Health, Austrian Agency for Health and Food Safety (AGES), Mödling, Austria
Wilhelm Gerner,
The Pirbright Institute, Woking, United Kingdom

‡These authors have contributed equally to this work

SPECIALTY SECTION
This article was submitted to Comparative Immunology, a section of the journal Frontiers in Immunology

RECEIVED 27 September 2022
ACCEPTED 18 October 2022
PUBLISHED 08 November 2022

CITATION
Stas MR, Kreutzmann H, Stadler J, Sassu EL, Mair KH, Koch M, Knecht C, Stadler M, Dolezal M, Balka G, Zaruba M, Mötz M, Saalmüller A, Rümenapf T, Gerner W and Ladinig A (2022) Influence of PRRSV-1 vaccination and infection on mononuclear immune cells at the maternal-fetal interface. *Front. Immunol.* 13:1055048. doi: 10.3389/fimmu.2022.1055048

Influence of PRRSV-1 vaccination and infection on mononuclear immune cells at the maternal-fetal interface

Melissa R. Stas[1], Heinrich Kreutzmann[1], Julia Stadler[2], Elena L. Sassu[1†], Kerstin H. Mair[3,4], Michaela Koch[1], Christian Knecht[1], Maria Stadler[3], Marlies Dolezal[5], Gyula Balka[6], Marianne Zaruba[7], Marlene Mötz[7], Armin Saalmüller[3], Till Rümenapf[7], Wilhelm Gerner[3†‡] and Andrea Ladinig[1*‡]

[1]University Clinic for Swine, Department for Farm Animals and Veterinary Public Health, University of Veterinary Medicine Vienna, Vienna, Austria, [2]Clinic for Swine, Centre for Clinical Veterinary Medicine, Ludwig-Maximilians-University Munich, Oberschleissheim, Germany, [3]Department of Pathobiology, Institute of Immunology, University of Veterinary Medicine Vienna, Vienna, Austria, [4]Department of Pathobiology, Christian Doppler Laboratory for Optimized Prediction of Vaccination Success in Pigs, Institute of Immunology, University of Veterinary Medicine Vienna, Vienna, Austria, [5]Platform for Bioinformatics and Biostatistics, Department of Biomedical Sciences, University of Veterinary Medicine, Vienna, Austria, [6]Department of Pathology, University of Veterinary Medicine Budapest, Budapest, Hungary, [7]Department of Pathobiology, Institute of Virology, University of Veterinary Medicine Vienna, Vienna, Austria

Porcine reproductive and respiratory syndrome virus (PRRSV) is one of the most devastating viruses for the global swine industry. Infection during late gestation causes reproductive failure but the local immune response *in utero* remains poorly understood. In this study, an experimental PRRSV-infection model with two different PRRSV-1 field isolates was used to investigate the immune cell phenotypes at the maternal-fetal interface during late gestation. In addition, phenotypic changes induced by a modified live virus (MLV, ReproCyc® PRRS EU) vaccine were studied. Vaccinated (n = 12) and non-vaccinated pregnant gilts (n = 12) were challenged with either one of the PRRSV-1 field isolates (low vs. high virulent, LV or HV) or sham-inoculated at day 84 of gestation. Twenty-one days post infection all gilts were euthanized and the fetal preservation status for all fetuses per litter was assessed. Leukocytes from the maternal-fetal interface were isolated and PRRSV-induced changes were investigated using *ex vivo* phenotyping by flow cytometry. PRRSV load in tissue from the maternal endometrium (ME) and fetal placenta (FP) was determined by RT-qPCR. In the ME, a vast increase in CD8β T cells with $CD8\alpha^{pos}CD27^{dim}$ early effector phenotype was found for fetuses from the non-vaccinated LV and HV-challenged gilts, compared to non-treated and vaccinated-only controls. HV-challenged fetuses also showed significant increases of lymphocytes with effector phenotypes in the FP, including $NKp46^{pos}$ NK cells, $CD8\alpha^{high}$ γδ T cells, as well as $CD8\alpha^{pos}CD27^{pos/dim}$ CD4 and CD8 T cells. In vaccinated animals, this

common activation of effector phenotypes was more confined and the fetal preservation status significantly improved. Furthermore, a negative correlation between the viral load and CD163^{high}CD169^{pos} mononuclear phagocytic cells was observed in the FP of HV-infected animals. These results suggest that the strong expansion of effector lymphocytes in gilts that were only infected causes immune-pathogenesis rather than protection. In contrast, the attenuated MLV seems to dampen this effect, yet presumably induces memory cells that limit reproductive failure. This work provides valuable insights into changes of local immune cell phenotypes following PRRSV vaccination and infection.

KEYWORDS

PRRSV, porcine maternal-fetal interface, NK cells, γδ T cells, B cells, CD4 T cells, CD8 T cells

1 Introduction

Porcine reproductive and respiratory syndrome virus (PRRSV), belonging to the *Arteriviridae* family (1), is the cause of PRRS which has a massive negative economic impact on global swine industry (2–4). This enveloped, positive-stranded RNA virus preferentially infects cells of the monocytic lineage (1, 5); however, some dendritic cell populations have also been shown to be permissive for viral replication *in vitro* (6). PRRSV exists in two genetically distinct species, *Betaarterivirus suid 1* (PRRSV-1) and *Betaarterivirus suid 2* (PRRSV-2) (7–9). Between and within species, a high degree of genetic diversity has been described (10, 11), which might explain observed differences in virulence and severity of clinical outcome (12, 13). A high mutation rate and genetic recombination events contribute to PRRSV heterogeneity (11) and inevitably have repercussions on vaccine efficacy and design.

Modified live virus (MLV) vaccines are widely used as a preventive or therapeutic measure to mitigate clinical signs, financial losses and transmission of the virus. These vaccines are considered efficacious, especially when compared to killed vaccines (14), but no clear correlates of protection have been identified so far (5, 15). The PRRSV-specific antibody responses that occur early after infection are non-neutralizing and do not correlate with clinical protection (5, 15). Neutralizing antibodies (NAbs) occur late (about four weeks post infection) and can confer protection (5, 15). NAbs are mostly strain specific, although heterologous NAbs have been identified (16, 17). Interferon-γ (IFN-γ) producing T cells and NK cells are considered to be involved in protection (5, 15, 18–21). Furthermore, a recent study showed that local T cell responses in the lung are already induced ten days post infection (dpi) and seem to be linked to viral clearance (20).

As to date, several molecules have been implicated as potential receptors for PRRSV including: CD163, CD169 (also known as sialoadhesin or siglec-1), non-muscle myosin heavy chain 9, heparin sulfate, CD151, vimentin, and DC-SING (CD209) (22). The cysteine-rich scavenger receptor CD163 is considered as the main receptor for PRRSV internalization and disassembly (5, 22) as pigs with a complete CD163 knock-out are resistant to PRRSV infection (23). CD169 is considered as a co-receptor which may assist in viral attachment/internalization but is not a requirement to establish a PRRSV infection (5, 22). Momentarily, CD163 and CD169 are the most extensively studied. The potential role of the other mentioned co-receptors in context of PRRSV is reviewed here (22).

The reproductive form of PRRS is associated with transplacental infection of the fetuses and primarily occurs during late gestation (24–26). This might be related to the frequency of CD169^{pos} cells located at the maternal-fetal interface (27). An epithelial bilayer sequesters the porcine maternal-fetal interface and is considered as a tight, impermeable barrier (28). The mechanisms responsible for reproductive failure remain elusive, although several hypotheses exist (26, 29–32). Currently, it is thought that post-infection events at the maternal-fetal interface are the cause for fetal deterioration and demise (33–36).

We recently described lymphocyte phenotypes that reside at the maternal-fetal interface in healthy sows during late gestation (37). More NKp46^{pos} and NKP46^{neg} NK cells were identified in the maternal endometrium (ME) and fetal placenta (FP), compared to fetal spleens. In the FP, however, also NKp46^{high} NK cells were found. CD4, CD8, and γδ T cells in the ME predominantly exhibited differentiated effector phenotypes whereas in the FP naive phenotypes prevailed. Investigations concerning the PRRSV-mediated immune response at the

maternal-fetal interface are limited. Following infection, PRRSV-infected monocytes reach the endometrium *via* the endometrial vessels (5, 26). Hereafter, the virus replicates in $CD163^{pos}CD169^{pos}$ macrophages and causes apoptosis of infected cells and bystander cells (5, 26, 33). Ten dpi a higher number of these virus susceptible cells are found in the ME and FP of PRRSV-infected sows (33). Furthermore, an increase in $CD3^{neg}CD8\alpha^{pos}$ cells was also found in the ME of PRRSV-infected animals through immunofluorescence staining (33).

Due to these limited findings, we investigated local changes in immune cell phenotypes at the maternal-fetal interface in response to two PRRSV-1 field isolates, using *ex vivo* phenotyping by flow cytometry. With the same methodology, we also investigated the influence of a PRRSV-1 MLV (ReproCyc® PRRS EU) immunization prior to challenge infection, which was previously shown to partially prevent vertical transmission following heterologous PRRSV-1 AUT15-33 infection (38).

2 Material and methods

2.1 Animals and experimental design

Twenty-four healthy crossbred (Landrace × Large White) gilts were purchased from a specialized producer (PIC Deutschland GmbH) and housed in a commercial Austrian piglet-producing farm free of PRRSV, as confirmed by regular serological monitoring. All gilts were vaccinated against porcine parvovirus 1 in combination with *Erysipelothrix rhusiopathiae*, swine influenza A virus, and porcine circovirus type 2, as previously described (38). Prior to insemination (142 and 114 days prior to infection) and during mid-gestation (31 days prior to infection), twelve randomly selected gilts were vaccinated with a PRRSV MLV vaccine (ReproCyc® PRRS EU, Boehringer Ingelheim Vetmedica GmbH, Ingelheim am Rhein, Germany) according to the instructions of the manufacturer. Vaccinated and non-vaccinated gilts were housed separately but under identical housing conditions. At day 77/78 of gestation, vaccinated and non-vaccinated gilts were relocated to a biosafety level 2 unit of the University of Veterinary Medicine Vienna on two consecutive days. All gilts were randomly allocated into six groups: 1. non-vaccinated and non-infected, No.Vac_No.Chall; 2. vaccinated and non-infected, Vac_No.Chall; 3. non-vaccinated and infected with low virulent (LV) strain, No.Vac_Chall_LV; 4. vaccinated and infected with low virulent (LV) strain, Vac_Chall_LV; 5. non-vaccinated and infected high virulent (HV) strain, No.Vac_Chall_HV; 6. vaccinated and infected with high virulent (HV) strain, Vac_Chall_HV (n = 4/group). Each group was housed in individual rooms with isolated airspaces. After one-week of acclimation, experimental infection was performed as described previously (39). Eight gilts (4 vaccinated and 4 non-vaccinated) were inoculated intranasally and intramuscularly (50% IN, 50% IM), with an infectious dose of 3×10^5 $TCID_{50}$, with either one of two different PRRSV-1 field isolates (LV or HV) or sham-inoculated with cell culture medium (DMEM, Thermo Fischer Scientific, Carlsbad, CA, United States) at day 84 of gestation. An overview of the six groups is given in Table 1. All experiments were approved by institutional ethics and animal welfare committee (Vetmeduni Vienna) and the national authority according to §§26ff. of Animal Experiments Act, Tierversuchsgesetz 2012 – TVG 2012 (GZ 68.205/0142-WF/V/3b/2016).

2.2 Virus isolates for challenge

Two European PRRSV-1 field isolates with a documented history of reproductive pathogenesis, as communicated by veterinarians in the field, were used. The PRRSV-1 field isolate 720789 (Genbank Accession number OP529852, kindly provided by Christoph Keller, Boehringer Ingelheim Vetmedica GmbH), further referred to as the 'low virulent strain (LV)', was propagated in MARC-145 cells for seven passages. The PRRSV-1 field isolate AUT15-33 (GenBank

TABLE 1 Overview six treatment groups.

Groups	n	Vaccination PRRSV*	Infection PRRSV**
No.Vac_No.Chall	4	–	–
Vac_No.Chall	4	3 doses Reprocyc® PRRS EU	–
No.Vac_Chall_LV	4	–	LV dog 84, 50% IN + 50% IM
Vac_Chall_LV	4	3 doses Reprocyc® PRRS EU	LV dog 84, 50% IN + 50% IM
No.Vac_Chall_HV	4	–	HV dog 84, 50% IN + 50% IM
Vac_Chall_HV	4	3 doses Reprocyc® PRRS EU	HV dog 84, 50% IN + 50% IM

No.Vac_No.Chall, non-vaccinated and non-infected; Vac_No.Chall, vaccinated and non-infected; No.Vac_Chall_LV, non-vaccinated and infected with low virulent (LV) strain; Vac_Chall_LV, vaccinated and infected with low virulent (LV) strain; No.Vac_Chall_HV; non-vaccinated and infected high virulent (HV) strain; Vac_Chall_HV, vaccinated and infected with high virulent (HV) strain.
LV, low virulent; HV, high virulent; dog, day of gestation; IN, intranasal; IM, intramuscular.
*2 Reprocyc® PRRS EU doses prior to insemination and 1 dose mid-gestation.
**PRRSV infection dose 3×10^5 $TCID_{50}$.

Accession number MT000052), further referred to as the 'high virulent strain (HV)', was propagated for three passages in porcine alveolar macrophages as described before (9). Titers were determined on the respective cell line (MARC-145, MA-104 derived African Green monkey kidney cell line) or cells (porcine alveolar macrophages, PAMs) used for propagation.

2.3 Euthanasia and sample collection

Approximately 21 dpi (21 ± 2, gestation day 105 ± 2), gilts and their litters were anesthetized by intravenous injection of Ketamine (Narketan® 100 mg/mL, Vetoquinol Österreich GmbH, Vienna Austria, 10 mg/kg body weight) and Azaperone (Stresnil® 40 mg/mL, Elanco GmbH, Cuxhaven, Germany, 1.5 mg/kg body weight) and subsequently euthanized *via* intracardial injection of T61® (Intervet GesmbH, Vienna, Austria, 1 mL/10 kg body weight). To retrieve samples, the abdomen of the gilts was opened, and the uteri removed, placed into a trough, and rinsed with tap water to remove maternal blood. The uteri were incised and opened at the anti-mesometrial side. The position of each fetus, from the left and right uterine horn, was recorded as previously described (38, 40). Fetal preservation status for each individual fetus was assessed and categorized as viable (VIA), meconium-stained (MEC), decomposed (DEC), and autolyzed (AUT) as previously described (39). For investigations on immune cell populations at the maternal-fetal interface, two fetuses per gilt were randomly selected and removed with their umbilical cord, placenta, and a portion of the uterus adjacent to the umbilical stump. A 1 × 1 cm piece of the maternal-fetal interface, was embedded in Tissue-Tek® O.C.T compound (Sakura Fintek, Alphen aan den Rijn, The Netherlands) and immediately frozen in liquid isopentane whilst placed on dry ice and stored at −80 °C until further processing. The myometrium was trimmed off and the maternal endometrium (ME) and fetal placenta (FP) were mechanically separated with two forceps without contaminating either side. Once separated, 40 g of ME and 60 g of FP were collected in sterile collection cups (Greiner Bio-One, Frickenhausen, Germany) filled with medium (RPMI-1640 with stable L-glutamine supplemented with 100 IU/mL penicillin and 0.1 mg/mL streptomycin (PAN-Biotech, Aidenbach, Germany)). In addition, tissue pieces from the ME and FP for viral load quantification were snap-frozen in liquid nitrogen and stored at −80 °C until further processing.

2.4 Cell isolation

The procedure for the isolation of immune cells from the porcine maternal-fetal interface has been described previously (37). In brief, ME and FP tissues were cut into small pieces and incubated in tissue digestion medium [RPMI-1640 supplemented with 2% (v/v) heat-inactivated fetal calf serum (FCS; Sigma-Aldrich, Schnelldorf, Germany), 25 U/mL DNase type I (Thermo Fischer Scientific), 300 U/mL Collagenase type I (Thermo Fisher Scientific), 100 IU/mL penicillin (PAN-Biotech), and 0.1 mg/mL streptomycin (PAN-Biotech)] for 1 h at 37 °C and constant mixing. Remaining larger pieces of tissue and dead cells were removed by draining the cell suspensions through a coarse-meshed sieve and subsequent filtering through a layer of cotton wool. Suspensions were centrifuged (350 × *g*, 10 minutes, 4°C), resuspended in 40% Percoll (13 mL, Thermo Fisher Scientific), underlaid with 70% Percoll (13 mL, Thermo Fisher Scientific), and subjected to density gradient centrifugation (920 × *g*, 30 minutes, room temperature). Isolated leukocytes were washed four times (phosphate-buffered saline (PBS, 2x), RPMI-1640 + 5% FCS (1x), and RPMI-1640 + 10% FCS (1x)) and immediately used for immune phenotyping.

2.5 Viral load quantification *via* RT-qPCR

The extraction of PRRSV RNA from the ME and FP, and quantification of the viral load in these tissues has been described elsewhere (38). Briefly, tissues were homogenized in lysis buffer (QIAzol® lysis reagent, QIAGEN GmbH, Hilden, Germany) with three stainless steel beads using a TissueLyser II instrument (QIAGEN GmbH). The homogenates were centrifuged, chloroform was added, and the tubes were vigorously vortexed and subsequently spun (13 000 × *g*, 5 minutes) to ensure phase separation. The aqueous phase was collected, and viral RNA was obtained using the Cador Pathogen Kit (QIAGEN GmbH) in a QiaCubeHT device (QIAGEN GmbH) following the manufacturer's instructions. An ORF7-specific reverse transcription quantitative polymerase chain reaction (RT-qPCR) for the LV and HV strain, primers and probes listed in Table 2, was performed using the Luna Onestep RT PCR kit (New England Biolabs GmbH, Frankfurt am Main, Germany). The viral load, expressed as genome equivalents (GE), was determined based on the serial dilution of SP6 transcripts, specific to the PRRSV-1 isolates that were cloned into a

TABLE 2 Overview primers and probes used for PRRSV ORF7-specific RT-qPCR.

	Forward primer (5'-3')	Reverse primer (5'-3')	Probe
LV	TCAACTGTGCCAGTTGCTGG	TGCGGCTTCTCAGGCTTTTTC	5′Fam-CCCAGCGCCAGCAAYCTAGGG Tamra-3′
HV	TCAACTGTGCCAGTTGCTGG	TGRGGCTTCTCAGGCTTTTC	5′Fam-CCCAGCGYCRRCARCCTAGGG Tamra-3′

pGEM-T vector (pLS69, Promega GmbH, Walldorf, Germany) and amplified. The cloned product was digested with DNaseI (New England Biolabs GmbH) and viral SP6 RNA was purified with the RNeasy kit (QIAGEN GmbH). Hereafter, a Quantus fluorometer and RNA-specific fluorescent dye (Promega) were used to determine the RNA concentration. The RNA concentration was multiplied with Avogadro's number and divided by the molecular mass of the PRRSV-1 specific SP6 transcripts to determine the absolute quantity of GE.

2.6 Flow cytometry staining and analysis

Mononuclear immune cells (1.5×10^6 cells per isolation) from ME and FP, were transferred into a 96-well round bottom microtiter plate (Greiner Bio-One) and stained in a 5- or 6-step procedure. An overview of the primary monoclonal antibodies (mAbs) and secondary reagents used per panel is given in Table 3. All incubation steps (20 minutes, 4°C) were followed by two washes with cold PBS supplemented with 10% (v/v) porcine plasma (in-house preparation) or as specified. Surface antigens were stained with mAbs listed in Table 3 followed by incubation with secondary reagents. Free antibody sites of the isotype-specific secondary antibodies were blocked with 2 µg whole mouse IgG (ChromPure, Jackson ImmunoResearch, West Grove, PA, United States) and subsequently washed with PBS. Thereafter, a mixture of directly conjugated primary mAbs, streptavidin conjugates, and the Fixable Viability Dye eFluor 780 (Thermo Fisher Scientific) was applied. The BD Cytofix/Cytoperm kit (BD Biosciences, San Jose, CA, USA) was used to fix and permeabilize the cells. This was followed by a staining for intracellular antigens using directly conjugated mAbs. All samples were measured on a FACSCanto II flow cytometer (BD Biosciences) equipped with three lasers (405, 488, and 633 nm), and a minimum of 1×10^5 lymphocytes per sample were recorded. Single-stained samples were prepared and recorded for automatic calculation of compensation, using FACSDiva software version 6.1.3 (BD Biosciences). The obtained data was analyzed with FlowJo software version 10.8.1 (BD Biosciences) and a consecutive gating strategy was applied (Supplementary Figure 1). A time gate was applied and based on the light scatter properties [forward scatter area (FSC-A) vs. side scatter area (SSC-A)] lymphocytes were identified. A 2-step doublet discrimination was performed and subsequently cells with high auto fluorescent signal were excluded using a 530/30 nm bandpass filter in the excitation line of the violet laser. Dead cells were excluded by a high signal for the Fixable Viability dye eFluor 780.

2.7 Immunofluorescence histology staining

Tissue from the maternal-fetal interface was sectioned using a Leica CM1950 microtome (Leica Biosystems Nussloch GmbH, Nussloch, Germany). Sections were loaded onto a slide, air-dried

TABLE 3 Antibodies and secondary reagents used for FCM staining.

Antigen	Clone	Isotype	Source	Labeling	Fluorophore
Total mononuclear immune cells					
CD45	K252.1E4	IgG1	Bio-Rad	Direct	AlexaFluor647
Myeloid cells					
CD169	3B11/11	IgG1	Bio-Rad	Indirect[A]	AlexaFluor647
CD14	Tük4	IgG2a	Bio-Rad	Indirect[B]	PE-Cy7
CD163	2A10/11	IgG1	Bio-Rad	Direct	PE
CD172a	74-22-15A	IgG2b	In-house	Indirect[C,D]	BV421
NK cells					
CD3	BB23-8E6-8C8	IgG2a	BD biosciences	Direct	PerCP-Cy5.5
CD8α	11/295/33	IgG2a	In-house	Indirect[D]	BV421
CD172a	74-22-15	IgG1	In-house	Indirect[E]	PE
NKp46	VIV-KM1	IgG1	In-house	Direct	AlexaFluor647
CD16	G7	IgG1	Bio-Rad	Direct	FITC
B and T cells					
CD4	74-12-4	IgG2b	BD biosciences	Direct	PerCP-Cy5.5
CD8α	76-2-11	IgG2a	In-house	Indirect[B]	PE-Cy7
CD27	b30c7	IgG1	In-house	Direct	AlexaFluor647
CD79αcγ	HM57	IgG1	Thermo Fisher Scientific	Direct	PE
TCR-γδ	PPT16	IgG2b	In-house	Indirect[F]	AlexaFluor488
CD8β	PPT23	IgG1	In-house	Indirect[D]	BV421

[A]Goat-anti-mouse anti-IgG1-AlexaFluor647, Thermo Fisher Scientific, [B]Goat-anti-mouse anti-IgG2a-PE-Cy7, Southern Biotech, [C]Goat-anti-mouse anti-IgG2b-biotin, Southern Biotech, [D]Streptavidin-BV421, Biolegend, [E]Goat-anti-mouse anti-IgG1-PE, Southern Biotech, [F]Goat-anti-mouse anti-IgG2b-AlexaFluor488, Jackson Immuno Research.

at room temperature for 1 h, and fixed with methanol/acetone (1:1) for 30 minutes at -20°C. Slides were blocked with PBS + 5% goat serum (Vector Laboratories, Inc., Burlingame, CA, U.S.A.) for 30 minutes at room temperature. Mouse anti-PRRSV-NP mAb (IgG2a, clone P11/d72-c1, in-house, 1:2) was diluted in PBS and applied overnight (4°C). Thereafter, secondary goat anti-mouse IgG2a AlexaFluor488 (Thermo Fisher Scientific, 1:500) was diluted in PBS and applied for 40 minutes at room temperature. This was followed by a 2 h incubation with a rat anti-human/mouse Cytokeratin 8 mAb (1:500; IgG2a, clone TROMA-1, Merck KGaA, Darmstadt, Germany) and visualized by secondary goat-anti-rat IgG (H+L) AlexaFluor647 (1:500; Thermo Fisher Scientific), for 40 minutes, both at room temperature. After each incubation step, slides were washed three times in PBS for five minutes. Nuclei were stained with DAPI (Sigma Aldrich) for 3 minutes in the dark and the slides were washed twice with PBS. Finally, slides were washed once with dH_2O and covered with mounting medium (Mowiol®4-88, Polysciences Europe GmbH, Germany) and a cover glass. Tissue sections were scanned using an Axioimager Z.1 microscope (Carl Zeiss Micro imaging GmbH, Germany) equipped with TissueFAXS hardware and software (TissueGnostics GmbH, Austria).

2.8 Statistics and graphical representation

The frequencies of major immune cells lineages (NK, γδ, B, CD4 T, and CD8β T cells), as a measure within viable lymphocytes, were exported into Microsoft Excel (Office 2016, Microsoft, Redmond, WA, United States) and corrected for CD45 expression as previously described (37). Also, frequencies of immune cell subsets and myeloid phenotypes were exported into Microsoft Excel and imported into GraphPad Prism version 9.2.0 (GraphPad Software Inc., San Diego, CA, United States) for the graphical presentation highlighting animal-to-animal variation. Statistical analysis was performed with R version *R v4.0.2* (41).

2.8.1 Viral load quantification *via* RT-qPCR

We analyzed $\log_{10}$ transformed RT-qPCR measured viral loads, after adding a constant of one to every observation in the ME and FP tissue, *via* two separate univariate linear mixed effects models applying function *lmer* in R package *lme4 v1.1-27.1* (42) fitting a fixed categorical effect of treatment with the four factor levels involving a challenge: No.Vac_Chall_LV, Vac_Chall_LV, No.Vac_Chall_HV, and Vac_Chall_HV, respectively. We further included a random intercept for gilt with 16 factor levels (four gilts in each of the four treatment groups) as we had measures from two fetuses per gilt. Option *REML* was set to false to request maximum likelihood estimation. We then calculated estimated marginal means for each challenge group using function *emmeans* in package *emmeans v1.7.5* Lenth (43) and requested hypothesis testing for all pairwise contrasts between estimated marginal means of treatment levels using option *pairwise*. Default multiple testing correction for these pairwise contrasts was turned off (option *adjust = "none"*). We performed a False Discovery Rate (FDR) multiple testing correction (44) across all p-values for all pairwise treatment contrasts across the two analyzed tissues. The multiple testing load was 12 tests total (six group comparisons × two tissues) and significance was declared at 10% FDR.

Results of the models are visualized *via* bar plots of estimated marginal means on a $\log_{10}$ transformed level using packages *RColorBrewer v1.1-2* (45), *ggplot2 v3.3.5* (46), and *ggpubr v0.4.0* (47) in which the fitted model is shown as the height of the bar plot. The black dots and whiskers represent upper and lower 95% confidence intervals of estimated marginal means. P-value brackets display contrasts significant at 10% FDR. Figures were exported as scalable vector graphics using package *svglite v2.0.0* (48).

2.8.2 Viral load and $CD163^{high}CD169^{pos}$ phenotypes

To investigate the relationships between viral loads and $CD163^{high}CD169^{pos}$ phenotypes in both the ME and FP tissue, we produced scatterplots and calculated Spearman correlation coefficients on $\log_{10}$ transformed viral loads and $\log_{10}$ transformed $CD163^{high}CD169^{pos}$ phenotypes separately for each challenged group (No.Vac_Chall_LV, Vac_Chall_LV, No.Vac_Chall_HV, and Vac_Chall_HV), after adding a constant of 1 to every observation for both the viral load and cell type data. P-values in these plots were not corrected for multiple testing. Plots were produced using packages *RColorBrewer v1.1-2* (45), *ggplot2 v3.3.5* (46), and exported in svg format using package *svglite v2.0.0* (48).

2.8.3 Immune cells

Our data comprised two different types of measurements. Frequencies of major immune cell lineages (*e.g.* total NK, total γδ T, total B, total CD4, and total CD8β T cells), phenotypes of the myeloid lineage (*e.g.* $CD14^{pos}CD172a^{neg}$, $CD14^{pos}CD163^{high}CD169^{pos}$, and $CD14^{neg}CD163^{high}CD169^{pos}$ cells), which were investigated in separate samples (Table 3) and frequencies of immune cell subsets as compositional data, derived from a single sample. Compositional data (CoDa) were transformed into log-ratios, to get rid of the constant sum constraint, allowing standard uni- and multivariate model employment for hypothesis testing (49).

For compositions of two components, which are perfectly negatively correlated (correlation coefficient of –1), and with components of the same effect sizes but with opposing signs (in our study $CD8\alpha^{neg/dim}$ *vs.* $CD8\alpha^{high}$ γδ T cells and

$CD14^{pos}CD172a^{pos}$ *vs.* $CD14^{neg}CD172a^{pos}$ cells), we chose the former in each composition due to its higher discriminative power after log_{10} transformation during hypothesis testing. Immune cell subsets representing compositions of three components included NK cells (*i.e.* NKp46-defined subsets: $NKp46^{neg}$, $NKp46^{pos}$, and $NKp46^{high}$), CD4 T cells (*i.e.* CD8α/CD27-defined subsets: $CD8\alpha^{neg}CD27^{pos}$, $CD8\alpha^{pos}CD27^{pos}$, and $CD8\alpha^{pos}CD27^{neg}$), and CD8 T cells (*i.e.* CD8α/CD27-defined subsets: $CD8\alpha^{pos}CD27^{high}$, $CD8\alpha^{pos}CD27^{pos}$, and $CD8\alpha^{pos}CD27^{neg}$). Each composition was subjected to centered log ratio (clr) transformation using function *clr* in package *compositions v2.0-4* (50, 51) after turning them into a package specific class of type *Aitchison compositions* using function *acomp*. Clr transformed data was then reformatted into "long data format" applying functions from package *dplyr v1.0.7* (52).

We then analyzed every measured immune cell type individually, either log_{10} transformed after adding a constant of one to every observation or clr transformed for the compositional data, fitting univariate linear mixed models applying function *lmer* in R package *lme4 v1.1-27.1* (42) changing the optimizer to *"nloptwrap"* with 100,000 iterations and setting option *REML* to false to perform maximum likelihood estimation to yield the most accurate estimates for the fixed effects part of the model. The fixed effects part of our models contained a main effect of treatment with six factor levels (No.Vac_No.Chall, Vac_No.Chall, No.Vac_Chall_LV, Vac_Chall_LV, No.Vac_Chall_HV, Vac_Chall_HV), a fixed effect of tissue type with levels ME and FP, and the interaction between treatment and tissue type. We further fitted a random intercept effect of day of experiment (six levels) to reduce any potential technical noise in our data. A random intercept of gilt (24 levels) was added to account for the covariance structure in our data (each gilt had measures of two fetuses each measured in the two tissues). As each level of random intercept of gilt had two observations per tissue, we added a dummy coded, centered, random slope for tissue as recommended by Barr et al. (53). Variance homogeneity of the residuals, normal distribution of residuals, fitted random intercepts, and slopes were verified with custom R scripts.

We then calculated estimated marginal means for all treatment levels for both tissues and tested for all pairwise differences (option *pairwise~treatment|tissue*) between treatment levels within tissue with function *emmeans* in package *emmeansv1.7.5* (43). Default multiple testing correction for these pairwise contrasts was turned off (option *adjust = "none"*). We then selected pairwise biological contrasts of interest, excluding the contrasts "Vac_Chall_LV *vs.* No.Vac_Chall_HV" and "No.Vac_Chall_LV *vs.* Vac_Chall_HV", and collected all p-values for all contrasts of interest, measured in all cell types for both tissues before applying a False Discovery Rate (FDR) multiple testing correction (44). Multiple testing correction was performed across all major immune cell lineages, myeloid phenotypes, and separately across all immune cell subsets. The multiple testing load was 234 tests total (13 group comparisons × nine phenotypes × two tissues). Significance was declared at 10% FDR. Modelling results were visualized with bar plots as described for viral load (in section 2.8.1).

2.8.4 Graphical representation

All figures were assembled using Inkscape software version 1.1.1 (URL https://inkscape.org/)

3 Results

3.1 Viral load at the maternal-fetal interface and fetal preservation

The viral load in tissues from the maternal-fetal interface was determined using RT-qPCR for PRRSV ORF7, with primers specific for the LV or the HV strain. Since no viral RNA for any strain could be detected in the ME and FP from gilts in the No.Vac_No.Chall and the Vac_No.Chall group (data not shown) only the challenged groups (No.Vac_Chall_LV, Vac_Chall_LV, No.Vac_Chall_HV, and Vac_Chall_HV) are displayed in Figure 1. Our analysis revealed that the emmeans for the viral load were significantly higher for the No.Vac_Chall_HV group as compared to the No.Vac_Chall_LV, Vac_Chall_LV, and Vac_Chall_HV group within ME and FP, respectively (Figures 1A, B). Of note, at the maternal-fetal interface from fetuses originating from Vac_Chall_LV gilts no viral RNA could be detected (Supplementary Figure 2). For Vac_Chall_HV gilts, viral RNA could be detected in the ME from a few fetuses from two different litters (gilts 15 and 16) and for gilt 15 in affected fetuses the virus was transmitted to the FP (Supplementary Figure 2), highlighting vertical transmission. Furthermore, there was a substantial negative impact on the fetal preservation status in the No.Vac_Chall_HV gilts (Supplementary Figure 2). Only 56% of these fetuses were designated as viable whereas in the other groups the vast majority (>90%) of fetuses were viable (data for the No.Vac_No.Chall and Vac_No.Chall group not shown). A clear difference in impact on the fetal preservation status between the two PRRSV-1 field isolates (LV and HV) was observed and demonstrated a divergence in virulence.

3.2 $CD172a^{pos}$ cells at the maternal-fetal interface and their correlation with viral load

Since PRRSV infects cells of the myeloid lineage, we sought to investigate their phenotype at the maternal-fetal interface. Following FCM staining, myeloid cells at the maternal-fetal interface were identified based on their CD172a expression and were subsequently divided into $CD14^{pos}$ and $CD14^{neg}$ subsets

(Figures 2A, B). No significant differences were observed for the CD14^{pos} cells within total CD172a^{pos} cells in the ME whereas a significant decrease was observed in the FP of No.Vac_Chall_HV group as compared to No.Vac_No.Chall group (Figure 2C, top panel). In addition, a high degree of variation between individual fetuses, especially within the ME, was identified (Figure 2C, bottom panel, scatterplots). Both CD14-defined subsets were further analyzed for their co-expression of CD163 and CD169, both molecules involved in viral entry, and CD163^{high}CD169^{pos} mononuclear phagocytes (MPCs) were identified (Figures 2A, B). The abundance of these CD163^{high}CD169^{pos} MPC phenotypes in the respective CD14-defined populations in ME was rather low (Figures 2A, D left) and no differences in emmeans for either macrophage phenotypes was observed between the six groups (Figure 2D left, top panel). A high abundance of CD163^{high}CD169^{pos} phenotypes within CD14^{pos} and CD14^{neg} CD172a^{pos} cells was found in the FP, especially in the No.Vac_No.Chall and the Vac_No.Chall groups (Figures 2B, D right, bottom panel). A significant drop for CD163^{high}CD169^{pos} cells within CD14^{pos} CD172a^{pos} MPCs was seen in the FP of fetuses from the No.Vac_Chall_HV as compared to the No.Vac_No.Chall, Vac_No.Chall, and No.Vac_Chall_LV groups (Figures 2B, D right, top panel). For CD163^{high}CD169^{pos} cells within CD14^{neg} MPCs in the FP a similar drop was observed for the No.Vac_Chall_HV as compared to the No.Vac_No.Chall group (Figures 2B, D right, top panel). These significant contrasts for both MPC subsets in the FP (Figure 2D right) prompted us to investigate a correlation with viral load. For this purpose, a spearman correlation was performed for all challenged groups and both anatomic locations (Figure 2E). A strong negative correlation (R = –0.76, p = 0.03) between both MPC phenotypes and the viral load was revealed

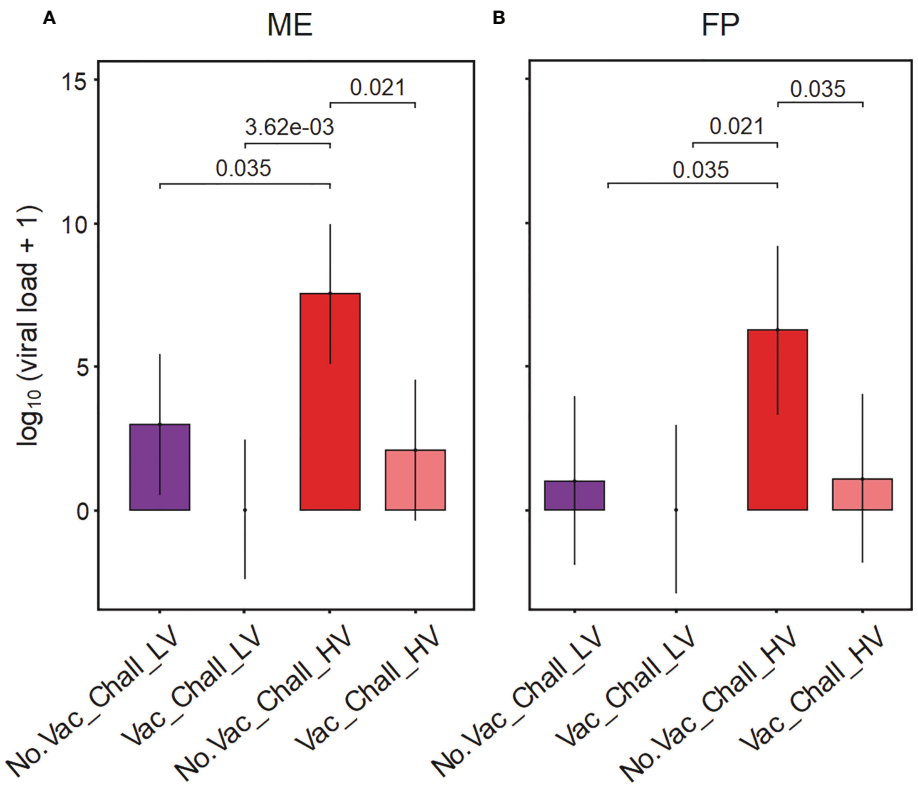

FIGURE 1
Viral RNA at the maternal-fetal interface of infected and vaccinated-infected gilts. Porcine reproductive and respiratory syndrome virus (PRRSV) RNA was extracted from tissue from the maternal endometrium (ME) and fetal placenta (FP). The viral load within the respective tissues was determined using an ORF7 PRRSV-1 field isolate specific RT-qPCR. PRRSV RNA was not detected in tissue samples from the No.Vac_No.Chall and Vac_No.Chall group and are therefore not shown. A linear mixed effects model fitting a fixed categorical effect (treatment) and random intercept for gilt (16 levels) was applied for the ME and FP separately. Results for the viral load are summarized in bar plots for the ME **(A)** and FP **(B)**. The y-axes show the estimated marginal means (emmeans) of the viral load (genome equivalents/g tissue) on a $\log_{10}$ scale, after adding a constant of + 1, for the four different treatment groups. Only significant p-values ($p < 0.1$) corrected for multiple testing, using a false discovery rate approach, across all pairwise comparisons of contrasts, across both tissues, are shown above the brackets. The whiskers depict the 95% confidence intervals of the emmeans. Depicted treatment groups: No.Vac_Chall_LV (dark purple, non-vaccinated and infected low virulent strain), Vac_Chall_LV (light purple, vaccinated and infected low virulent strain), No.Vac_Chall_HV (dark red, non-vaccinated and infected high virulent strain), and Vac_Chall_HV (light red, vaccinated and infected high virulent strain).

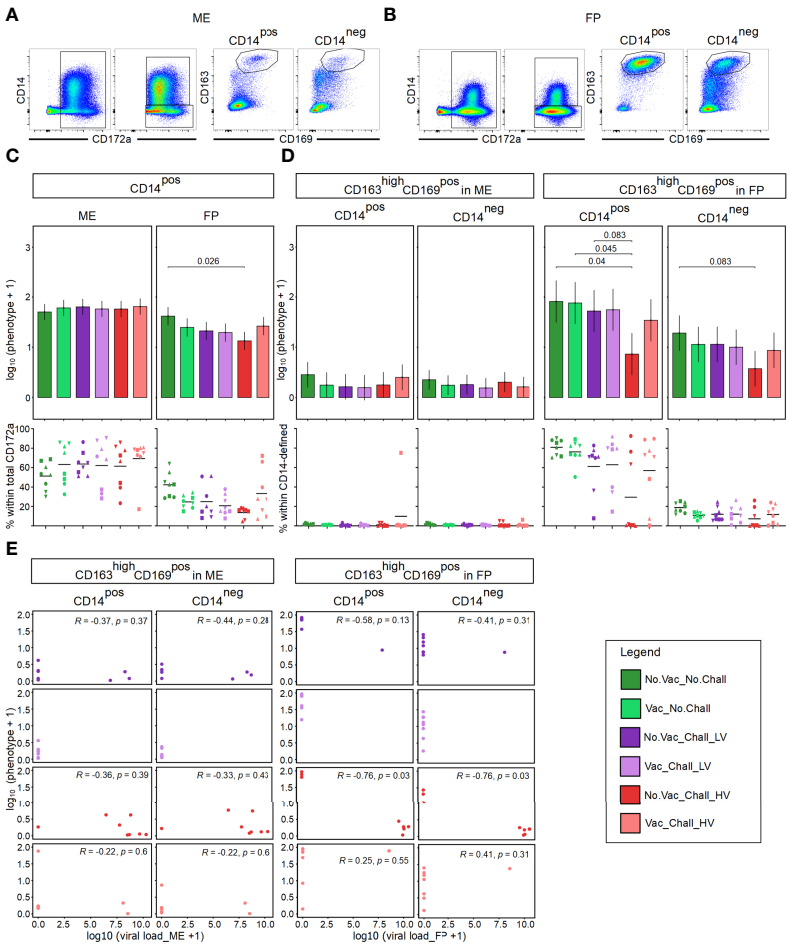

FIGURE 2
Mononuclear phagocytes at the maternal-fetal interface and their correlation to viral load. **(A, B)** A time gate was applied and mononuclear phagocytes (MPCs) were gated based on their SSC-A (side scatter area) versus FSC-A (forward scatter area) characteristics and following a consecutive gating strategy was applied to exclude doublets, cells with high autofluorescence, and dead cells (Supplementary Figure 1). MPCs were further analyzed for their expression of CD172a and subsequently sub-gated for $CD14^{pos}CD172a^{pos}$ and $CD14^{neg}CD172a^{pos}$ MPCs. The two CD14-defined MPC populations were further analyzed for their co-expression of CD163 and CD169. For both CD14-defined MPCs a $CD163^{high}CD169^{pos}$ subset was identified at the maternal fetal interface. Representative pseudocolor plots from the maternal endometrium (ME) in **(A)** and fetal placenta (FP) in **(B)** from a No.Vac_No.Chall fetus are shown. **(C)** A linear mixed effects model considering the fixed effects of treatment, tissue, and the interaction between both was applied. A random intercept (gilt) was fitted and estimated marginal means (emmeans) were calculated. Results for total $CD14^{pos}$ MPCs within the ME (left) and FP (right) are presented as bar plots on top. On the y-axes the estimated marginal means (emmeans) for $CD14^{pos}$ MPCs on a $\log_{10}$ scale, after adding a constant of + 1, are depicted. The graphs below depict the frequency of $CD14^{pos}$ MPCs within total $CD172a^{pos}$ cells for the individual fetuses within each treatment group in the ME (left) and FP (right). **(D)** A linear mixed effects model considering the fixed effects of treatment, tissue, and the interaction between both was applied. A random intercept (gilt) was fitted and estimated marginal means (emmeans) were calculated. Results for $CD163^{high}CD169^{pos}$ MPCs within $CD14^{pos}$ and $CD14^{neg}$ cells within the ME (left) and FP (right) are shown. The y-axes in the bar plots (on top) represent the emmeans of the $CD163^{high}CD169^{pos}$ MPCs within CD14-defined subsets on a $\log_{10}$ + 1 scale. The frequencies of the $CD163^{high}CD169^{pos}$ MPCs within CD14-defined subsets for the individual fetuses and anatomic locations are given in the graphs below. For all bar plots only significant p-values ($p < 0.1$), corrected for multiple testing using a false discovery rate approach across all 234 pairwise comparisons of contrasts, are shown above the brackets. The whiskers depict the 95% confidence intervals of the emmeans. For all graphs showing the frequencies of a specific cell subset, results for the fetuses from one gilt are represented by different symbols. The black bars in the graphs display the mean within the respective treatment group within the specified anatomic location. **(E)** Spearman correlation coefficients were estimated, to investigate the relationship between $\log_{10}$ transformed $CD163^{high}CD169^{pos}$ CD14-defined MPCs and $\log_{10}$ transformed viral load, for all challenged groups and both anatomic locations. Results for the spearman correlation in the ME are shown on the left and FP on the right. The correlation coefficients (R) and p-values ($p < 0.1$) not corrected for multiple testing are depicted. For all bar plots, graphs, and scatterplots the depicted treatment groups are: No.Vac_No.Chall (dark green, non-vaccinated and non-infected), Vac_No.Chall (light green, vaccinated and non-infected), No.Vac_Chall_LV (dark purple, non-vaccinated and infected low virulent strain), Vac_Chall_LV (light purple, vaccinated and infected low virulent strain), No.Vac_Chall_HV (dark red, non-vaccinated and infected high virulent strain), and Vac_Chall_HV (light red, vaccinated and infected high virulent strain).

inthe FP from No.Vac_Chall_HV fetuses. Furthermore, virus infected cells, as identified with a monoclonal antibody targeting PRRSV-NP, were predominantly detected in the FP (Supplementary Figure 3).

3.3 Major lymphocyte subsets at the maternal-fetal interface in response to an infection with PRRSV

Next to MPCs, major lymphocyte subsets were investigated by flow cytometry and the applied gating strategy is illustrated in Supplementary Figure 1. A $CD3^{neg}CD8\alpha^{pos}CD16^{pos}CD172a^{neg}$ phenotype was used to identify NK cells. During steady state conditions (No.Vac_No.Chall), total NK cells were present in similar frequencies within total lymphocytes in both the ME and FP (Figure 3, Scatter plots). With regards to PRRSV-mediated changes, no significant contrasts were detected in the ME, possibly due to the high degree of animal-to-animal variation. Significant higher emmeans for total NK cells could be observed in the FP from No.Vac_Chall_HV fetuses. Significant contrasts for the FP were found between No.Vac_Chall_HV vs No.Vac_No.Chall, No.Vac_Chall_HV vs Vac_No.Chall, and No.Vac_Chall_HV vs Vac_Chall_HV (Figure 3B). Porcine γδ T cells at the maternal-fetal interface were identified with a monoclonal antibody targeting a T-cell receptor γδ-specific CD3ε chain (clone PPT16) (54). Emmeans for the total γδ T cells in the ME were lower for both non-vaccinated challenged groups (No.Vac_Chall_LV and No.Vac_Chall_HV) as compared to the No.Vac_No.Chall group. Furthermore, the vaccination seemed to have prevented this loss in total γδ T cells in the Vac_Chall_HV group. These differences in emmeans were also visible in the scatterplots showing the percentages of γδ T cells within lymphocytes (Figure 3A). Total γδ T cells were significantly reduced in the FP of fetuses from the No.Vac_Chall_HV group as compared to No.Vac_No.Chall, Vac_No.Chall, and vaccinated counterpart (Vac_Chall_HV) (Figure 3B). Total B cells at the maternal-fetal interface were identified using the pan-B cell marker CD79α. For this phenotype, no PRRSV-associated changes were observed neither in the ME nor in the FP (Figure 3). CD4 and CD8 T cells, were characterized by gating on total CD4 and total CD8β expressing T cells (Supplementary Figure 1). No significant PRRSV-induced contrasts for both T cell phenotypes in the ME could be identified by our statistical model. However, for the total CD8β T cells a high degree of animal-to-animal variation was observed for most groups except for the Vac_Chall_HV group. A significant reduction in total CD4 T cells could be observed in the FP from the No.Vac_Chall_HV group as compared to the No.Vac_No.Chall and Vac_No.Chall groups. For CD8β T cells, we only observed a significant increase in the No.Vac_Chall_LV group in comparison to the No.Vac_No.Chall group (Figure 3B).

3.4 NKp46-defined NK cell phenotypes

Total $CD3^{neg}CD8\alpha^{pos}CD16^{pos}CD172a^{neg}$ NK cells in the FP were further investigated for their expression of NKp46. Three NK cell subsets, $NKp46^{neg}$, $NKp46^{pos}$, and $NKp46^{high}$ were identified. Representative pseudocolor plots for one fetus from the No.Vac_No.Chall and No.Vac_Chall_HV group are shown in Figure 4A. Considering that the relative frequencies of the three NKp46-defined NK cell subsets are interdependent, a univariate CoDa was performed. Therefore, to correct for this interdependence our data was transformed to centered log ratios (clr). The output of our model, showed a significant increase in NK cells with a $NKp46^{pos}$ phenotype in the No.Vac_Chall_HV as compared to the Vac_No.Chall group (Figure 4B). For the other two NKp46-defined NK cell phenotypes, no significant changes were observed. When considering the raw frequency data, however, a visual reduction in the $NKp46^{neg}$ NK cells in the FP from the No.Vac_Chall_HV group could be observed. Notably, considerable variation between individual fetuses was observed. Data on NKp46-defined NK cell phenotypes in the ME are not shown, since no significant changes were observed.

3.5 CD8α-defined γδ T cell phenotypes

Total γδ T cells were analyzed for their expression of CD8α which enabled us to identify a $CD8\alpha^{neg/dim}$ and $CD8\alpha^{high}$ expressing subset in the ME and FP. Representative pseudocolor plots for the two investigated anatomic locations are shown in Figures 5A, B. $CD8\alpha^{high}$ expressing γδ T cells were the main phenotype in the ME (Figure 5A) whereas the $CD8\alpha^{neg/dim}$ expressing γδ T cells were more abundant in the FP (Figure 5B). For the statistical analysis, only γδ T cells with a $CD8\alpha^{neg/dim}$ phenotype were included since the effect size of the $CD8\alpha^{high}$ γδ T cells is dependent on the $CD8\alpha^{neg/dim}$ phenotype. In the ME no significant difference was found for the $CD8\alpha^{neg/dim}$ phenotype (Figure 5A). Nonetheless, a significant reduction for this phenotype and thus an increase in $CD8\alpha^{high}$ γδ T was observed in the FP of fetuses from the No.Vac_Chall_HV group as compared to the No.Vac_No.Chall, Vac_No.Chall, and No.Vac_Chall_LV group (Figure 5B).

3.6 The activation and differentiation state of porcine CD4 T cells

Total CD4 T cells at the maternal-fetal interface were investigated for their expression of CD8α and CD27 (Figure 6). This enabled us to delineate three subsets with a $CD8\alpha^{neg}CD27^{pos}$ naive, $CD8\alpha^{pos}CD27^{pos}$ early effector or central memory (Tcm), and $CD8\alpha^{pos}CD27^{neg}$ late effector or effector memory phenotype (Tem) (Figures 6A, B), representative pseudocolor plots are shown). Since the three CD8α/CD27-defined CD4 T cell subsets

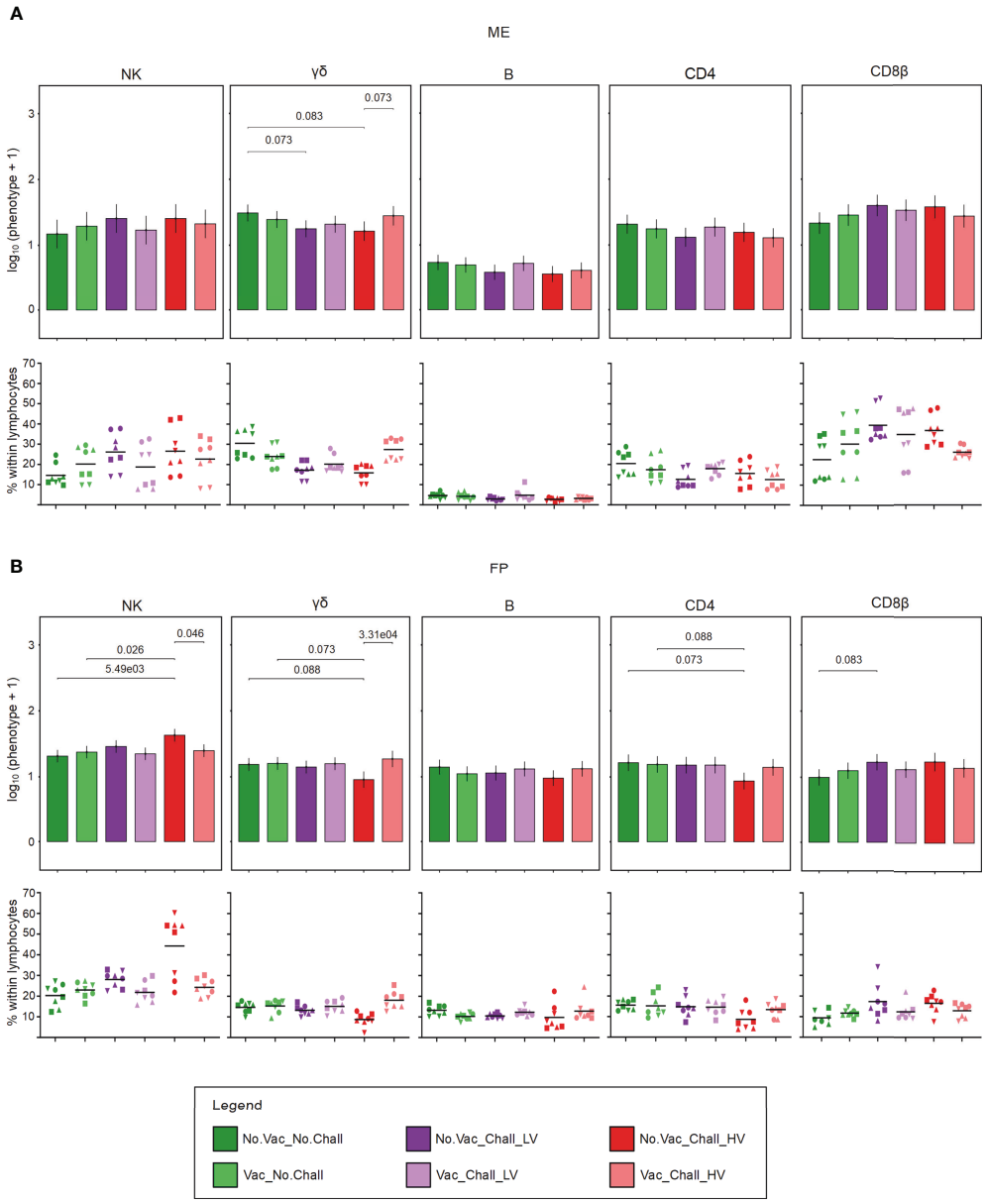

FIGURE 3
Major lymphocyte subsets at the maternal-fetal interface. Following the applied consecutive gating strategy (Supplementary Figure 1) NK cells, γδ T cells, B cells, CD4 T cells, and CD8β T cells were identified in the ME **(A)** and FP **(B)**. A linear mixed effects model considering the fixed effects of treatment, tissue, and the interaction between both was applied. A random intercept (gilt) was fitted and estimated marginal means (emmeans) were calculated. The bar plots (top panel; **(A)** ME; **(B)** FP) depict the results for the obtained major lymphocyte subsets across all treatment groups and are presented as emmeans of each subset on a $\log_{10}$ + 1 scale as depicted on the y-axes. Only significant p-values ($p < 0.1$), corrected for multiple testing using a false discovery rate approach, across all 234 pairwise comparisons of contrasts, are shown above the brackets. The whiskers depict the 95% confidence intervals of the emmeans. Frequencies of the major lymphocyte subsets, within viable lymphocytes corrected for CD45 expression, are given (bottom panel; **(A)** ME; **(B)** FP). For all graphs, results for each individual fetus are shown and different symbols indicate fetuses from different gilts. The black bars in the graphs display the mean within the respective treatment group within the specified anatomic location. For all bar plots and graphs shown, the depicted treatment groups are: No.Vac_No.Chall (dark green, non-vaccinated and non-infected), Vac_No.Chall (light green, vaccinated and non-infected), No.Vac_Chall_LV (dark purple, non-vaccinated and infected low virulent strain), Vac_Chall_LV (light purple, vaccinated and infected low virulent strain), No.Vac_Chall_HV (dark red, non-vaccinated and infected high virulent strain), and Vac_Chall_HV (light red, vaccinated and infected high virulent strain).

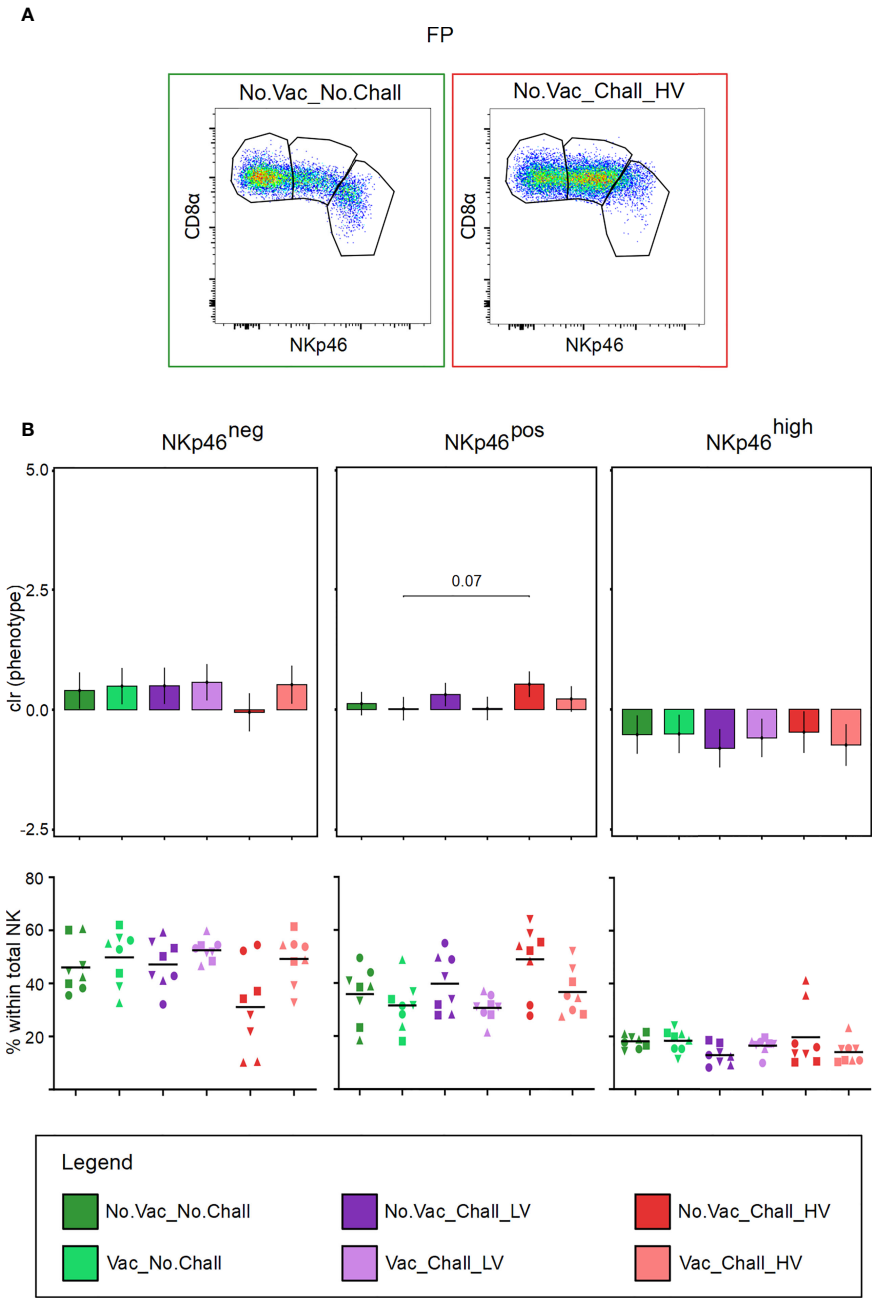

FIGURE 4
NKp46-defined NK cell subsets in the fetal placenta. **(A)** $CD3^{neg}CD8\alpha^{pos}CD16^{pos}CD172a^{neg}$ NK cells in the fetal placenta (FP) were investigated for their expression of NKp46. Three NK cell subsets were identified: $NKp46^{neg}$, $NKp46^{pos}$, and $NKp46^{high}$ (from left to right). Representative pseudocolor plots for the FP from a No.Vac_No.Chall and No.Vac_Chall_HV fetus are shown. **(B)** Univariate compositional data analysis was performed for the three NKp46-defined NK cell subsets. Results are represented in the bar charts (top panel). The y-axes depict the estimated marginal means (emmeans) of the centered log ratios (clr) transformed $NKp46^{neg}$, $NKp46^{pos}$, and $NKp46^{high}$ NK cell subsets (from left to right). Only significant p-values ($p < 0.1$), corrected for multiple testing using a false discovery rate approach, across all pairwise comparisons of contrasts for all (nine) compositional cell subsets and both tissues, are shown above the brackets. The whiskers depict the 95% confidence intervals of the clr-transformed data. The graphs in the bottom panel show the frequencies of the three NKp46-defined subsets within total NK cells. For all graphs, results for each individual fetus are shown and different symbols indicate fetuses from different gilts. The black bars in the graphs display the mean within the respective treatment group. For all bar plots and graphs shown, the depicted treatment groups are: No.Vac_No.Chall (dark green, non-vaccinated and non-infected), Vac_No.Chall (light green, vaccinated and non-infected), No.Vac_Chall_LV (dark purple, non-vaccinated and infected low virulent strain), Vac_Chall_LV (light purple, vaccinated and infected low virulent strain), No.Vac_Chall_HV (dark red, non-vaccinated and infected high virulent strain), and Vac_Chall_HV (light red, vaccinated and infected high virulent strain).

are interdependent on each other, the components of the compositions were clr transformed before hypothesis testing to deal with the constant sum constraints. No significant changes in the CD8α/CD27-defined CD4 T cell subsets were observed in the ME (Figure 6A). In the FP, however, a significant decrease in $CD8\alpha^{neg}CD27^{pos}$ naive CD4 T cells and a concurrent increase in $CD8\alpha^{pos}CD27^{pos}$ Tcm cells was observed in the No.Vac_Chall_HV group as compared to the No.Vac_No.Chall, Vac_No.Chall, and No.Vac_Chall_LV group (Figure 6B). Of note, the five FP tissues with the highest $CD8\alpha^{pos}CD27^{pos}$ percentages tested PRRSV positive in this tissue (fetuses G22 L7, G22 R10, G23 L5, G23 R11, and G24 L2, Supplementary Figure 2) and showed a reduced number of $CD163^{high}CD169^{pos}$ MPCs (Figure 2D). Furthermore, the significant loss in $CD8\alpha^{neg}CD27^{pos}$ naive CD4 T cells was also observed as compared to the Vac_Chall_HV. However, in this case the increase in $CD8\alpha^{pos}CD27^{pos}$ Tcm cells in the No.Vac_Chall_HV compared to the Vac_Chall_HV was not significant.

3.7 CD8β T cell phenotypes

As CD8 T cells are major effector cells in many viral infections, we sought to investigate their phenotype at the maternal-fetal interface. Therefore, the expression of CD8α and CD27 on the identified CD8β T cells was evaluated. CD8β T cells with a $CD8\alpha^{pos}CD27^{pos}$, $CD8\alpha^{pos}CD27^{dim}$, and $CD8\alpha^{pos}CD27^{neg}$ phenotype were identified (Figures 7A, B, representative pseudocolor plots are shown) and represent CD8β T cells with a naive, early effector, and late effector phenotype, respectively (55, 56). The interdependency between the three CD8β T cell phenotypes was corrected for with CoDa. Several significant contrasts were identified in both investigated anatomic compartments. In the ME a significant loss of CD8β T cells with a $CD8\alpha^{pos}CD27^{pos}$ naive phenotype and an accompanying increase of $CD8\alpha^{pos}CD27^{dim}$ early effector phenotype was observed from No.Vac_Chall_HV fetuses as compared to the No.Vac_No.Chall and Vac_No.Chall group (Figure 7A). A similar increase of

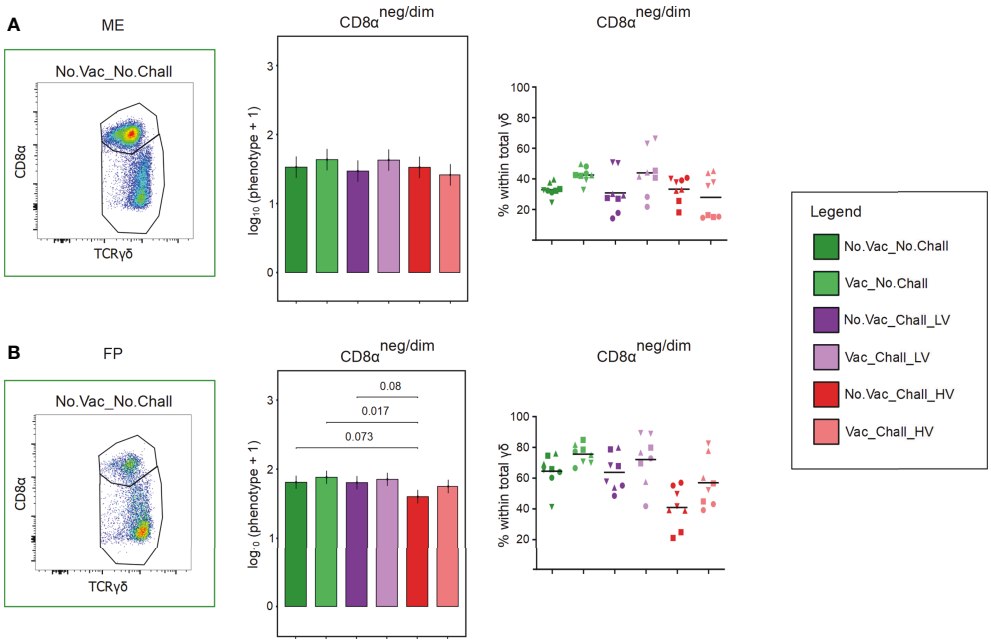

FIGURE 5
CD8α-defined γδ T cell phenotypes at the maternal-fetal interface. **(A, B)** Total γδ T cells were analyzed for their CD8α surface expression and separated into a $CD8\alpha^{neg/dim}$ and a $CD8\alpha^{high}$ γδ T cell subset. Representative pseudocolor plots for the **(A)** maternal endometrium (ME) and the **(B)** fetal placenta (FP) from a No.Vac_No.Chall fetus are given. A linear mixed effects model considering the fixed effects of treatment, tissue, and the interaction between both was applied. A random intercept (gilt) was fitted and estimated marginal means (emmeans) were calculated. The bar plots (middle panel; **(A)** ME; **(B)** FP), depict the results for the obtained $CD8\alpha^{neg/dim}$ γδ T phenotype across all treatment groups and are presented as emmeans of the $CD8\alpha^{neg/dim}$ γδ T cells on a $\log_{10}$ + 1 scale as depicted on the y-axes. Only significant p-values ($p < 0.1$), corrected for multiple testing using a false discovery rate approach, across all 234 pairwise comparisons of contrasts, are shown above the brackets. The whiskers depict the 95% confidence intervals of the emmeans. The frequencies of this $CD8\alpha^{neg/dim}$ phenotype within total γδ T cells are given in the graph (right panel; **(A)** ME; **(B)** FP). For all graphs, results for each individual fetus are given and different symbols indicate fetuses from different gilts. The black bars in the graphs display the mean within the respective treatment group within the specified anatomic location. For all bar plots and graphs shown, the depicted treatment groups are: No.Vac_No.Chall (dark green, non-vaccinated and non-infected), Vac_No.Chall (light green, vaccinated and non-infected), No.Vac_Chall_LV (dark purple, non-vaccinated and infected low virulent strain), Vac_Chall_LV (light purple, vaccinated and infected low virulent strain), No.Vac_Chall_HV (dark red, non-vaccinated and infected high virulent strain), and Vac_Chall_HV (light red, vaccinated and infected high virulent strain).

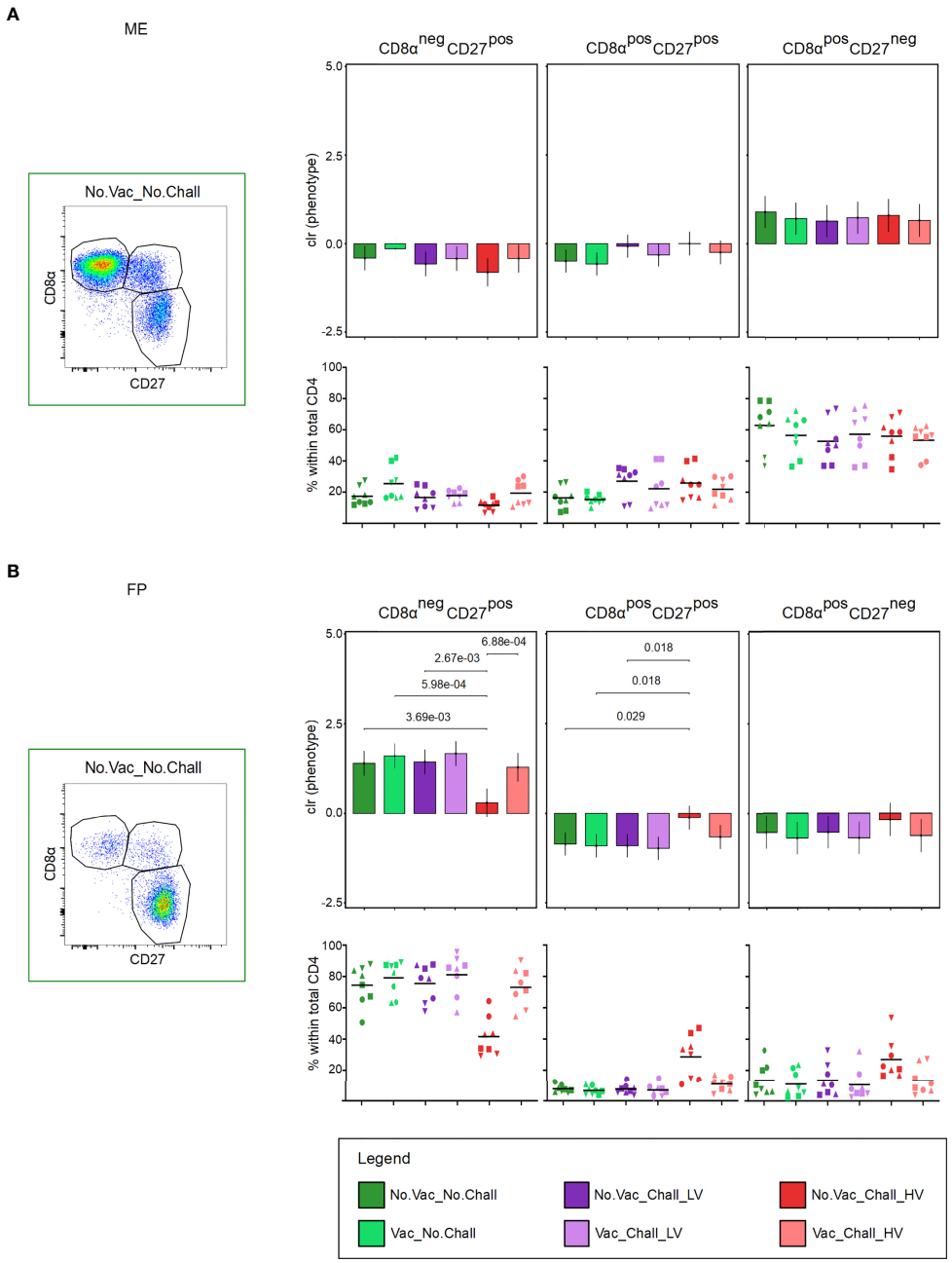

FIGURE 6
CD8α and CD27 expression of CD4 T cells at the maternal-fetal interface. **(A, B)** Total CD4 T cells were investigated for their expression of CD8α and CD27. CD8α^{neg}CD27^{pos} (representing naive), CD8α^{pos}CD27^{pos} (representing early effectors or central memory, Tcm), and CD8α^{pos}CD27^{neg} (representing late effectors of effector memory, Tem) cells were identified. Representative pseudocolor plots for the **(A)** maternal endometrium (ME) and the **(B)** fetal placenta (FP) from a No.Vac_No.Chall fetus are shown. Univariate compositional data analysis was performed for the three CD8α/CD27-defined CD4 T cell subsets. Results are represented in the bar charts (top panel; **(A)** ME; **(B)** FP). The y-axes depict the estimated marginal means (emmeans) of the centered log ratios (clr) for the specified CD4 T cell subset. Only significant p-values ($p < 0.1$), corrected for multiple testing using a false discovery rate approach, across all pairwise comparisons of contrasts for all (nine) compositional cell subsets and both tissues, are shown above the brackets. The whiskers depict the 95% confidence intervals of the clr-transformed data. The graphs in the bottom panel **(A)** ME; **(B)** FP) show the frequencies of the CD8α/CD27-defined CD4 T cell subsets within total CD4 T cells. For all graphs, results for each individual fetus are shown and different symbols indicate fetuses from different gilts. The black bars in the graphs display the mean within the respective treatment group. For all bar plots and graphs shown, the depicted treatment groups are: No.Vac_No.Chall (dark green, non-vaccinated and non-infected), Vac_No.Chall (light green, vaccinated and non-infected), No.Vac_Chall_LV (dark purple, non-vaccinated and infected low virulent strain), Vac_Chall_LV (light purple, vaccinated and infected low virulent strain), No.Vac_Chall_HV (dark red, non-vaccinated and infected high virulent strain), and Vac_Chall_HV (light red, vaccinated and infected high virulent strain).

CD8α^{pos}CD27^{dim} early effector CD8β T cells was observed for the ME from No.Vac_Chall_LV group as compared to the No.Vac_No.Chall and Vac_No.Chall groups (Figure 7A). In addition, significant contrasts for CD8β T cells with a CD8α^{pos}CD27^{dim} early effector phenotype were observed between the non-vaccinated challenged groups, No.Vac_Chall_HV and No.Vac_Chall_LV, and their vaccinated counterparts, Vac_Chall_HV and Vac_Chall_LV, respectively (Figure 7A). Furthermore, a significant but limited increase in CD8β T cells with a CD8α^{pos}CD27^{dim} early effector phenotype was observed in the Vac_Chall_HV and Vac_Chall_LV groups as compared to the No.Vac_No.Chall and Vac_No.Chall groups (Figure 7A). In the FP, a significant loss of CD8α^{pos}CD27^{pos} naive CD8β T cells in the No.Vac_Chall_HV group as compared to the Vac_No.Chall group concurred with a strong increase in CD8β T cells with a CD8α^{pos}CD27^{dim} early effector phenotype (Figure 7B). Also for No.Vac_Chall_LV group a significant increase of CD8β T cells with a CD8α^{pos}CD27^{dim} early effector phenotype was observed (Figure 7B). Similarly to the ME, significant contrasts in the FP were observed between the non-vaccinated challenged groups, No.Vac_Chall_HV and No.Vac_Chall_LV, and their vaccinated counterparts, Vac_Chall_HV and Vac_Chall_LV, respectively (Figure 7B). Compared to the other investigated lymphocyte subsets, CD8α^{pos}CD27^{dim} early effector CD8β T cells showed the strongest response to infection with the two PRRSV-1 strains.

4 Discussion and conclusions

Research on PRRSV-specific immune responses *in utero* is sparse. By using our previously established method of ME and FP separation (37), we were able to provide an in-depth characterization of the mononuclear immune cells at the maternal-fetal interface following experimental infection and vaccination.

In this study, two PRRSV-1 field isolates were used, designated in hindsight as LV and HV. Initially, we did not expect to see a difference in terms of reproductive failure, as both PRRSV-1 field isolates caused severe clinical signs in affected farms (9), as communicated by veterinarians in the field. However, viral loads measured in the ME and FP for the LV strain were significantly lower as compared to the HV strain for non-vaccinated animals (Figure 1). Furthermore, for the LV infected gilts viral transmission from the ME to the FP was only observed in five fetuses. In addition, only two fetuses from LV infected gilts had an impaired fetal preservation status whereas in the HV infected gilts the fetal preservation was affected in many (n=30) fetuses (Supplementary Figure 2). An obvious explanation for these observed differences might be the *in vitro* passaging of the LV strain on MARC-145 cells (MA-104 derived African Green monkey kidney cell line), whereas the HV strain was passaged on porcine alveolar macrophages. It has been shown that PRRSV loses its virulence due to adaptation to MARC-145 cells *in vitro* resulting in an attenuated phenotype *in vivo* (57). Furthermore, PRRS MLVs can be generated by *in vitro* passaging leading to attenuation (58, 59). The LV strain has a 99.76% sequence homology to the PRRSV field isolate IVI-1173 (Genbank Accession number KX622783.1) that caused a PRRSV outbreak in Switzerland (2012) (60). Although not planned at the outset, these differences in virulence allowed valuable insights into the response of the investigated immune cell phenotypes, as outlined above, and discussed in the following.

In our reproductive gilt model, the PRRSV-1 based MLV (ReproCyc® PRRS EU) completely or partially prevented reproductive signs following heterologous challenge with the LV PRRSV-1 field isolate and HV PRRSV-1 field isolate, respectively. Nevertheless, for gilts from the Vac_Chall_HV group viral transmission to the FP only occurred in one out of four litters. For the viral load, in the ME and FP, no significant difference could be found between the No.Vac_Chall_LV and the Vac_Chall_LV groups (Figure 1). However, when considering the fetal preservation status and viral load of each given individual fetus it becomes apparent that no viral RNA could be detected at the maternal-fetal interface from Vac_Chall_LV gilts (Supplementary Figure 2). This is due to the fact that all observations for viral load in the Vac_Chall_LV gilts were zero resulting in the absence of variation in this group. In the Vac_Chall_HV group the viral load in the ME and FP was significantly lower as compared to the non-vaccinated counterpart. Furthermore, the fetal preservation status substantially improved when the gilts were vaccinated prior PRRSV infection (Supplementary Figure 2).

We focused mainly on immune cell phenotypes *in utero*. Humoral-mediated effector mechanisms were not investigated but could also have contributed to the protective effects of the MLV. Following a similar vaccination scheme, PRRSV-specific antibodies were readily detected in the serum of vaccinated gilts after two MLV doses, which did not drastically change after a third dose (38). Combining the three dose MLV with the experimental infection with a PRRSV-1 field isolate significantly increased the antibody response in these gilts (38). In addition, serum transfer experiments in gestating females have shown that vertical transmission can be prevented by PRRSV-specific Nabs (61). Therefore, it is conceivable that PRRSV-specific antibodies, as detected in the serum, could be locally active *in utero* in the Vac_Chall_HV and Vac_Chall_LV group, and contribute to the protective effect of the vaccine.

As cells from the myeloid lineage are the primary targets for the virus; we characterized them using CD14, CD163, CD169 and CD172a. In the ME, CD172a^{pos} cells with a CD14^{pos} and CD14^{neg} phenotype were identified; however, the frequency of CD163^{high}CD169^{pos} MPCs was rather low as compared to the FP (Figures 2C, D). Similarly, other researchers evaluated the presence of CD163^{pos} and CD169^{pos} cells at the maternal-fetal interface and reported that they were significantly enriched in

10.3389/fimmu.2022.1055048

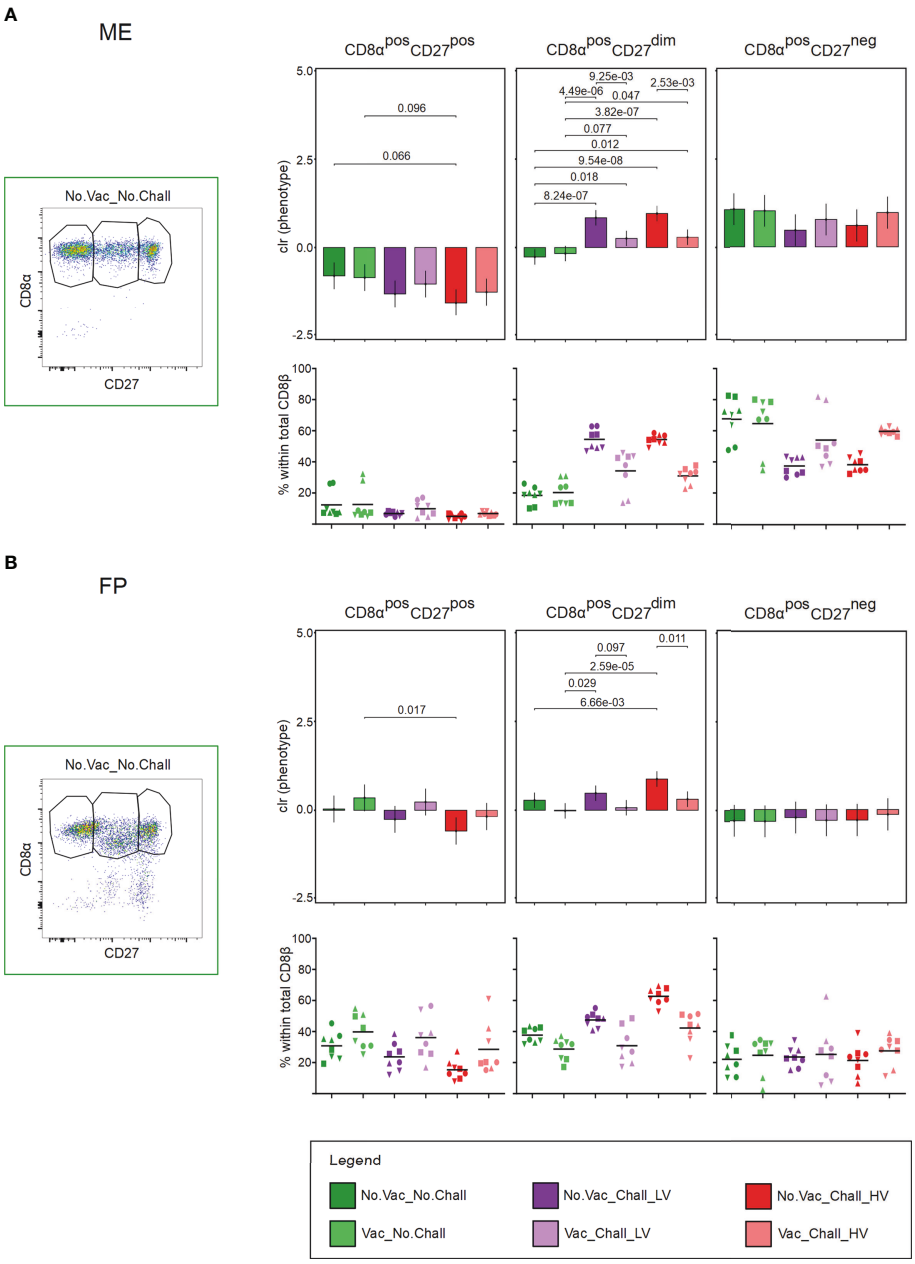

FIGURE 7
CD8α and CD27 expression of CD8β T cells at the maternal-fetal interface **(A, B)** Total CD8β T cells were investigated for their expression of CD8α and CD27. CD8β T cells with a CD8α^{pos}CD27^{pos}, CD8α^{pos}CD27^{dim}, and CD8α^{pos}CD27^{neg} phenotype were identified and presumably represent naive, early effector, and late effector CD8 T cells, respectively. Representative pseudocolor plots for the **(A)** maternal endometrium (ME) and the **(B)** fetal placenta (FP) from a No.Vac_No.Chall fetus are shown. Representative pseudocolor plots for the **(A)** ME and the **(B)** FP from a No.Vac_No.Chall fetus are shown. Univariate compositional data analysis was performed for the three CD8α/CD27-defined CD8β T cell subsets. Results are represented in the bar charts (top panel; **(A)** ME; **(B)** FP). The y-axes depict the estimated marginal means (emmeans) of the centered log ratios (clr) transformed specified CD8β T cell subset. Only significant p-values ($p < 0.1$), corrected for multiple testing using a false discovery rate approach, across all pairwise comparisons of contrasts for all (nine) compositional cell subsets and both tissues, are shown above the brackets. The whiskers depict the 95% confidence intervals of the clr-transformed data. The graphs in the bottom panel **(A)** ME; **(B)** FP) show the frequencies of the CD8α/CD27-defined subsets within total CD8β T cells. For all graphs, results for each individual fetus are shown and different symbols indicate fetuses from different gilts. The black bars in the graphs display the mean within the respective treatment group. For all bar plots and graphs shown, the depicted treatment groups are: No.Vac_No.Chall (dark green, non-vaccinated and non-infected), Vac_No.Chall (light green, vaccinated and non-infected), No.Vac_Chall_LV (dark purple, non-vaccinated and infected low virulent strain), Vac_Chall_LV (light purple, vaccinated and infected low virulent strain), No.Vac_Chall_HV (dark red, non-vaccinated and infected high virulent strain), and Vac_Chall_HV (light red, vaccinated and infected high virulent strain).

the FP during steady state and even 21 dpi with PRRSV-2 (31). In our study, the MPCs identified in the ME did not seem to be affected by the vaccination or infection since no significant differences were found. In contrast, in the ME of PRRSV-2 infected gilts an increase of $CD163^{pos}$ and $CD169^{pos}$ cells was found 21 dpi (31). In addition, another study demonstrated the increase in $CD169^{pos}$ cells in both the ME and FP from PRRSV-1 inoculated sows as compared to controls at 10 dpi whereas the $CD163^{pos}$ cell count was not altered (33). They also showed a decrease in $CD14^{pos}$ cells in the FP of PRRSV-infected animals (33), this decrease is in line with the outcome of our study (Figure 2D). Furthermore, we observed a significant loss in $CD163^{high}CD169^{pos}$ MPCs in the FP of the No.Vac_Chall_HV group, which was inversely associated to the viral load (Figure 2E). The latter would be in line with the inverse relationship between placental $CD163^{pos}$ cells and viral load in the fetal thymus (31). It has been shown that PRRSV induces apoptosis of PRRSV-infected cells, expressing CD163, and bystander apoptosis of virus-negative cells (34). Therefore, our data suggests that viral replication in the FP accounts for the observed loss of $CD163^{high}CD169^{pos}$ MPCs. The discrepancies observed as compared to the other studies, might be explained by the different methodologies used. So far, most investigations utilized immunofluorescence microscopy, which is limited in the number of cellular markers that can be investigated simultaneously. Flow cytometry enabled us to include multiple parameters for the characterization of the immune cells, although, at the cost of the spatial information in the tissue. Furthermore, our data indicates that there is a high degree of MPC heterogeneity at the maternal-fetal interface, which illustrates a need for more sophisticated phenotypical, transcriptional, and functional analyses in the context of PRRSV.

NK cells form a first line of defense in many viral infections (62). Previous work has shown that an increase of $CD3^{neg}CD8\alpha^{pos}$ NK cells in the ME of PRRSV-infected pregnant gilts can be observed 10 dpi (33). In the current study, however, we did not observe any increase of $CD3^{neg}CD8\alpha^{pos}CD16^{pos}CD172a^{neg}$ NK cells in the ME 21 dpi (Figure 3A). A plausible explanation for that might be that between 10 and 21 dpi a shift from innate to adaptive responses may have occurred. Furthermore, we also considered the expression of the activating receptor NKp46 (63) and found an increase of $NKp46^{pos}$ NK cells in the FP from No.Vac_Chall_HV fetuses (Figure 4B). This increase coincided with a drop in $NKp46^{neg}$ NK cells, which could either be explained by the reacquisition of NKp46 on these cells or the influx of more $NKp46^{pos}$ cells. *In vitro* experiments have demonstrated that NKp46 expression can be induced on sorted $NKp46^{neg}$ NK cells following cytokine stimulation (63). For $NKp46^{pos}$ NK cells in blood and spleen, it has been shown that their capacity to produce cytokines and cytolytic activity is higher compared to $NKp46^{neg}$ NK cells (64). $NKp46^{high}$ expressing NK cells are considered to be superior in context of cytokine production and cytolytic activity (64), but recent data suggests that NKp46 downregulation occurs during porcine NK cell differentiation (Schmuckenschlager et al., manuscript in preparation). In addition, we have also demonstrated that all NK cells at the maternal-fetal interface contain perforin (37). Therefore, it seems likely that the NK cells in the FP are combatting the virus. Further investigations are needed to prove this hypothesis.

The exact role of γδ T cells in context of PRRSV infection is not fully understood. In this study, total γδ T cells were significantly lower at the maternal-fetal interface of No.Vac_Chall_HV fetuses as compared to the Vac_Chall_HV and No.Vac_No.Chall fetuses (Figure 3). Moreover, in the FP of No.Vac_Chall_HV fetuses, there was a significant change towards a dominance of $CD8\alpha^{high}$ γδ T cells at the expense of the $CD8\alpha^{neg/dim}$ γδ T cells (Figure 5B). Based on our previous data, where CD8α expression was mainly associated with a $CD2^{pos}$ phenotype (37), we presume that the $CD8\alpha^{high}$ and $CD8\alpha^{neg/dim}$ γδ T closely correspond to a $CD2^{pos}$ and $CD2^{neg}$ phenotype, respectively. Distinct cytokine production profiles have been associated with the two γδ T cell subsets (65). A $CD2^{pos}$ phenotype is associated with a higher capacity to produce IFN-γ (65), and exclusively expresses perforin (66). The latter was also demonstrated for $CD2^{pos}$ γδ T cells at the maternal-fetal interface (37). This suggests that the identified increase in $CD8\alpha^{high}$ γδ T cells in the FP might have exhibited inflammatory and potentially cytotoxic functions in No.Vac_Chall_HV fetuses.

CD4 T cells can promote the B cell and CD8 T cell function in context of antiviral immunity (67). In the current study, the CD8α/CD27-expression pattern was used to assess $CD8\alpha^{pos}CD27^{pos}$ early effector or central memory (Tcm) and $CD8\alpha^{pos}CD27^{neg}$ late effector or effector memory phenotype at the maternal-fetal interface. A clear increase in CD4 T cells with an early effector phenotype was observed for No.Vac_Chall_HV fetuses, and coincided with a drop of $CD8\alpha^{neg}CD27^{pos}$ naive CD4 T cells (Figure 6). It seems that this increase in early effector T cells is a response to HV PRRSV infection. However, further functional characteristics and PRRSV-specificity of CD4 T cells need to be characterized. CD8 T cells are important components of the adaptive immune system responsible for the elimination of virus-infected cells. CD8β-expressing T cells with a putative $CD8\alpha^{pos}CD27^{dim}$ early effector phenotype were the main responders at the maternal-fetal interface of No.Vac_Chall_HV and No.Vac_Chall_LV fetuses (Figure 7). Furthermore, our previous work has shown that CD8β T cells with an early effector phenotype readily express perforin (37), which is indicative of a cytotoxic potential. Overall, research addressing local CD8 T cell responses is limited. Previously, it has been shown that peripheral blood CD8 T cells, isolated 21 dpi, readily proliferate upon restimulation *in vitro* (68). However their capacity to kill PRRSV-infected macrophages only occurred 49 dpi (68). Recent work has shown that CD8 T cells might play a pivotal role at the site of infection, particularly in lung and brochoalveolar lavage (20, 69). Future work is needed to address the PRRSV-specific CD8 T cell responses and their functional capacity *in utero*.

Hence, the results of our study indicate that the HV PRRSV-1 field isolate causes an influx of early effector phenotypes at the maternal-fetal interface, including NKp46^{pos} NK cells, CD8α^{high} γδ T cells, as well as CD8α^{pos}CD27$^{pos/dim}$ CD4 and CD8 T cells. We postulate that this substantial increase in effector phenotypes is an indicator of local tissue damage potentially resulting in focal detachment of the placenta and consequently fetal demise. Of note, in the ME of vaccinated gilts (*e.g.* Vac_Chall_LV and Vac_Chall_HV), this increase of CD4 and CD8 early effector T cell phenotypes compared to No.Vac_No.Chall and Vac_No.Chall groups was more contained. This may suggest that the challenge infection lead to a re-activation of pre-existing memory T cells, induced by the MLV vaccine, that was "just about right" to control viral replication yet avoided an excessive inflammatory response. However, depending on the PRRSV field strain and response to vaccination, in some gilts/sows the local response might not be sufficient to prevent vertical transmission (as observed in gilt #15, Supplementary Figure 2).

In conclusion, using flow cytometry, we have shown that PRRSV induces changes in immune cell phenotypes that reside at the maternal-fetal interface. Our study suggests that the local activation of effector phenotypes in response to high-virulent PRRSV strains might cause immune-pathogenesis, as the result of local inflammation, apoptosis and bystander apoptosis, causing focal detachment of the maternal-fetal interface, contributing to reproductive failure. In addition, our data indicates that vaccination by MLVs may limit such local immune activation with potentially beneficial or detrimental consequences. However, functional aspects of the addressed immune cell phenotypes need further investigation, as it is assumed that PRRSV utilizes various immune modulatory mechanisms (5, 70–72).

Data availability statement

The original contributions presented in the study are included in the article/Supplementary Material. Further inquiries can be directed to the corresponding author.

Ethics statement

The animal study was reviewed and approved by institutional ethics and animal welfare committee (Vetmeduni Vienna) and the national authority according to §§26ff. of Animal Experiments Act, Tierversuchsgesetz 2012 – TVG 2012 (GZ 68.205/0142-WF/V/3b/2016).

Author contributions

MRS, KM, JS, AS, TR, WG, and AL were in charge of the study design. HK, CK, JS, GB, and AL organised the animal experiment and were responsible for the sample collection. ES, KM, MK, MS, MZ, MM, and TR performed the laboratory work. MRS, WG, and AL analysed the data and MD performed the statistical analysis. MRS, WG, and AL discussed and interpreted the data and prepared the manuscript. All authors read and approved the final manuscript.

Funding

The authors declare that this research was funded by Boehringer Ingelheim Vetmedica GmbH. However, the funder was not involved in the study design, data analysis and interpretation, the writing process, or the decision to submit the manuscript for publication. GB was supported by the János Bolyai Research Scholarship of the Hungarian Academy of Sciences.

Acknowledgments

We would like to express our gratitude to all people involved in the animal experiment, particularly during sample collection at necropsy and sample processing in the lab. In addition, we would also like to thank Simona Winkler for providing us with the immunofluorescence microscopy picture.

Conflict of interest

The authors declare that the research was conducted in the absence of any commercial or financial relationships that could be construed as a potential conflict of interest.

Publisher's note

Supplementary material

The Supplementary Material for this article can be found online at: https://www.frontiersin.org/articles/10.3389/fimmu.2022.1055048/full#supplementary-material

References

1. Snijder EJ, Kikkert M, Fang Y. Arterivirus molecular biology and pathogenesis. *J Gen Virol* (2013) 94:2141–63. doi: 10.1099/vir.0.056341-0

2. Holtkamp DJ, Kliebenstein JB, Neumann EJ, Zimmerman JJ, Rotto HF, Yoder TK, et al. Assessment of the economic impact of porcine reproductive and respiratory syndrome virus on united states pork producers. *JSHAP.* (2013) 21 (2):72–84. https://www.aasv.org/library/swineinfo/Content/SHAP/2013/v21n2p72.pdf

3. Nathues H, Alarcon P, Rushton J, Jolie R, Fiebig K, Jimenez M, et al. Cost of porcine reproductive and respiratory syndrome virus at individual farm level - an economic disease model. *Prev Vet Med* (2017) 142:16–29. doi: 10.1016/j.prevetmed.2017.04.006

4. Nieuwenhuis N, Duinhof TF, van Nes A. Economic analysis of outbreaks of porcine reproductive and respiratory syndrome virus in nine sow herds. *Vet Rec.* (2012) 170(9):225. doi: 10.1136/vr.100101

5. Lunney JK, Fang Y, Ladinig A, Chen N, Li Y, Rowland B, et al. Porcine reproductive and respiratory syndrome virus (PRRSV): Pathogenesis and interaction with the immune system. *Annu Rev Anim Biosci* (2016) 4:129–54. doi: 10.1146/annurev-animal-022114-111025

6. Loving CL, Brockmeier SL, Sacco RE. Differential type I interferon activation and susceptibility of dendritic cell populations to porcine arterivirus. *Immunology.* (2007) 120(2):217–29. doi: 10.1111/j.1365-2567.2006.02493.x

7. Adams MJ, Lefkowitz EJ, King AM, Harrach B, Harrison RL, Knowles NJ, et al. Ratification vote on taxonomic proposals to the international committee on taxonomy of viruses (2016). *Arch Virol* (2016) 161(10):2921–49. doi: 10.1007/s00705-016-2977-6

8. Kuhn JH, Lauck M, Bailey AL, Shchetinin AM, Vishnevskaya TV, Bao Y, et al. Reorganization and expansion of the nidoviral family arteriviridae. *Arch Virol* (2016) 161(3):755–68. doi: 10.1007/s00705-015-2672-z

9. Sinn LJ, Klingler E, Lamp B, Brunthaler R, Weissenböck H, Rümenapf T, et al. Emergence of a virulent porcine reproductive and respiratory syndrome virus (PRRSV) 1 strain in lower Austria. *Porcine Health Manage* (2016) 2:28. doi: 10.1186/s40813-016-0044-z

10. Balka G, Podgórska K, Brar MS, Bálint A, Cadar D, Celer V, et al. Genetic diversity of PRRSV 1 in central Eastern Europe in 1994-2014: origin and evolution of the virus in the region. *Sci Rep* (2018) 8(1):7811. doi: 10.1038/s41598-018-26036-w

11. Paploski IAD, Corzo C, Rovira A, Murtaugh MP, Sanhueza JM, Vilalta C, et al. Temporal dynamics of Co-circulating lineages of porcine reproductive and respiratory syndrome virus. *Front Microbiol* (2019) 10:2486. doi: 10.3389/fmicb.2019.02486

12. de Abin MF, Spronk G, Wagner M, Fitzsimmons M, Abrahante JE, Murtaugh MP. Comparative infection efficiency of porcine reproductive and respiratory syndrome virus field isolates on MA104 cells and porcine alveolar macrophages. *Can J Vet Res* (2009) 73(3):200–4.

13. Martínez-Lobo FJ, Díez-Fuertes F, Segalés J, García-Artiga C, Simarro I, Castro JM, et al. Comparative pathogenicity of type 1 and type 2 isolates of porcine reproductive and respiratory syndrome virus (PRRSV) in a young pig infection model. *Vet Microbiol* (2011) 154(1-2):58–68. doi: 10.1016/j.vetmic.2011.06.025

14. Chae C. Commercial PRRS modified-live virus vaccines. *Vaccines (Basel)* (2021) 9(2):185. doi: 10.3390/vaccines9020185

15. Loving CL, Osorio FA, Murtaugh MP, Zuckermann FA. Innate and adaptive immunity against porcine reproductive and respiratory syndrome virus. *Vet Immunol Immunopathol* (2015) 167(1-2):1–14. doi: 10.1016/j.vetimm.2015.07.003

16. Martínez-Lobo FJ, Díez-Fuertes F, Simarro I, Castro JM, Prieto C. The ability of porcine reproductive and respiratory syndrome virus isolates to induce broadly reactive neutralizing antibodies correlates with *In vivo* protection. *Front Immunol* (2021) 12:691145. doi: 10.3389/fimmu.2021.691145

17. Robinson SR, Li J, Nelson EA, Murtaugh MP. Broadly neutralizing antibodies against the rapidly evolving porcine reproductive and respiratory syndrome virus. *Virus Res* (2015) 203:56–65. doi: 10.1016/j.virusres.2015.03.016

18. Kreutzmann H, Dürlinger S, Knecht C, Koch M, Cabana M, Torrent G, et al. Efficacy of a modified live virus vaccine against porcine reproductive and respiratory syndrome virus 1 (PRRSV-1) administered to 1-Day-Old piglets in front of heterologous PRRSV-1 challenge. *Pathogens* (2021) 10(10):1342. doi: 10.3390/pathogens10101342

19. Martelli P, Gozio S, Ferrari L, Rosina S, De Angelis E, Quintavalla C, et al. Efficacy of a modified live porcine reproductive and respiratory syndrome virus (PRRSV) vaccine in pigs naturally exposed to a heterologous European (Italian cluster) field strain: Clinical protection and cell-mediated immunity. *Vaccine.* (2009) 27(28):3788–99. doi: 10.1016/j.vaccine.2009.03.028

20. Nazki S, Khatun A, Jeong CG, Mattoo SUS, Gu S, Lee SI, et al. Evaluation of local and systemic immune responses in pigs experimentally challenged with porcine reproductive and respiratory syndrome virus. *Vet Res* (2020) 51(1):66. doi: 10.1186/s13567-020-00789-7

21. Bautista EM, Molitor TW. IFN gamma inhibits porcine reproductive and respiratory syndrome virus replication in macrophages. *Arch Virol* (1999) 144 (6):1191–200. doi: 10.1007/s007050050578

22. Su CM, Rowland RRR, Yoo D. Recent advances in PRRS virus receptors and the targeting of receptor-ligand for control. *Vaccines (Basel).* (2021) 9(4):354. doi: 10.3390/vaccines9040354

23. Whitworth KM, Rowland RR, Ewen CL, Trible BR, Kerrigan MA, Cino-Ozuna AG, et al. Gene-edited pigs are protected from porcine reproductive and respiratory syndrome virus. *Nat Biotechnol* (2016) 34(1):20–2. doi: 10.1038/nbt.3434

24. Terpstra C, Wensvoort G, Pol JM. Experimental reproduction of porcine epidemic abortion and respiratory syndrome (mystery swine disease) by infection with lelystad virus: Koch's postulates fulfilled. *Vet Q* (1991) 13(3):131–6. doi: 10.1080/01652176.1991.9694297

25. Kranker S, Nielsen J, Bille-Hansen V, Bøtner A. Experimental inoculation of swine at various stages of gestation with a Danish isolate of porcine reproductive and respiratory syndrome virus (PRRSV). *Vet Microbiol* (1998) 61(1-2):21–31. doi: 10.1016/S0378-1135(98)00176-X

26. Karniychuk UU, Nauwynck HJ. Pathogenesis and prevention of placental and transplacental porcine reproductive and respiratory syndrome virus infection. *Vet Res* (2013) 44:95. doi: 10.1186/1297-9716-44-95

27. Karniychuk UU, Nauwynck HJ. Quantitative changes of sialoadhesin and CD163 positive macrophages in the implantation sites and organs of porcine embryos/fetuses during gestation. *Placenta.* (2009) 30(6):497–500. doi: 10.1016/j.placenta.2009.03.016

28. Kim YB. Developmental immunity in the piglet. *Birth Defects Orig Artic Ser* (1975) 11(1):549–57.

29. Suleman M, Novakovic P, Malgarin CM, Detmer SE, Harding JCS, MacPhee DJ. Spatiotemporal immunofluorescent evaluation of porcine reproductive and respiratory syndrome virus transmission across the maternal-fetal interface. *Pathog Dis* (2018) 76(5):fty060. doi: 10.1093/femspd/fty060

30. Wang T, Fang L, Zhao F, Wang D, Xiao S. Exosomes mediate intercellular transmission of porcine reproductive and respiratory syndrome virus. *J Virol* (2018) 92(4):e01734–17. doi: 10.1128/JVI.01734-17

31. Novakovic P, Harding JC, Ladinig A, Al-Dissi AN, MacPhee DJ, Detmer SE. Relationships of CD163 and CD169 positive cell numbers in the endometrium and fetal placenta with type 2 PRRSV RNA concentration in fetal thymus. *Vet Res* (2016) 47(1):76. doi: 10.1186/s13567-016-0364-7

32. Barrera-Zarate J, Detmer SE, Pasternak JA, Hamonic G, MacPhee DJ, Harding JCS. Detection of PRRSV-2 alone and co-localized with CD163 positive macrophages in porcine placental areolae. *Vet Immunol Immunopathol* (2022) 250:110457. doi: 10.1016/j.vetimm.2022.110457

33. Karniychuk UU, De Spiegelaere W, Nauwynck HJ. Porcine reproductive and respiratory syndrome virus infection is associated with an increased number of Sn-positive and CD8-positive cells in the maternal-fetal interface. *Virus Res* (2013) 176(1-2):285–91. doi: 10.1016/j.virusres.2013.05.005

34. Karniychuk UU, Saha D, Geldhof M, Vanhee M, Cornillie P, Van den Broeck W, et al. Porcine reproductive and respiratory syndrome virus (PRRSV) causes apoptosis during its replication in fetal implantation sites. *Microb Pathog* (2011) 51(3):194–202. doi: 10.1016/j.micpath.2011.04.001

35. Novakovic P, Harding JC, Al-Dissi AN, Detmer SE. Type 2 porcine reproductive and respiratory syndrome virus infection increases apoptosis at the maternal-fetal interface in late gestation pregnant gilts. *PloS One* (2017) 12(3): e0173360. doi: 10.1371/journal.pone.0173360

36. Guidoni PB, Pasternak JA, Hamonic G, MacPhee DJ, Harding JCS. Effect of porcine reproductive and respiratory syndrome virus 2 on tight junction gene expression at the maternal-fetal interface. *Theriogenology.* (2022) 184:162–70. doi: 10.1016/j.theriogenology.2022.03.011

37. Stas MR, Koch M, Stadler M, Sawyer S, Sassu EL, Mair KH, et al. NK and T cell differentiation at the maternal-fetal interface in sows during late gestation. *Front Immunol* (2020) 11:582065. doi: 10.3389/fimmu.2020.582065

38. Kreutzmann H, Stadler J, Knecht C, Sassu EL, Ruczizka U, Zablotski Y, et al. Phenotypic characterization of a virulent PRRSV-1 isolate in a reproductive model with and without prior heterologous modified live PRRSV-1 vaccination. *Front Vet Sci* (2022) 9:820233. doi: 10.3389/fvets.2022.820233

39. Ladinig A, Wilkinson J, Ashley C, Detmer SE, Lunney JK, Plastow G, et al. Variation in fetal outcome, viral load and ORF5 sequence mutations in a large scale study of phenotypic responses to late gestation exposure to type 2 porcine reproductive and respiratory syndrome virus. *PloS One* (2014) 9(4):e96104. doi: 10.1371/journal.pone.0096104

40. Ladinig A, Detmer SE, Clarke K, Ashley C, Rowland RR, Lunney JK, et al. Pathogenicity of three type 2 porcine reproductive and respiratory syndrome virus strains in experimentally inoculated pregnant gilts. *Virus Res* (2015) 203:24–35. doi: 10.1016/j.virusres.2015.03.005

41. R Core Team. R: A language and environment for statistical computing, in: *R foundation for statistical computing* (2020). Vienna, Austria. Available at: https://www.R-project.org/ (Accessed 15 September 2022).

42. Bates D, Mächler M, Bolker B, Walker S. Fitting linear mixed-effects models using lme4. *J Stat Soft.* (2015) 67(1):1–48. doi: 10.18637/jss.v067.i01

43. Lenth RV. Emmeans: Estimated marginal means, aka least-squares means, in: *R package version 1.7.5* (2022). Available at: https://CRAN.R-project.org/package=emmeans (Accessed 15 September 2022).

44. Benjamini Y, Hochberg Y. Controlling the false discovery rate: a practical and powerful approach to multiple testing. *J R Stat Soc Ser B (Methodological).* (1995) 57(1):289–300. doi: 10.1111/j.2517-6161.1995.tb02031.x

45. Neuwirth E. RColorBrewer: ColorBrewer palettes, in: *R package version 1.1-2* (2014). Available at: https://CRAN.R-project.org/package=RColorBrewer (Accessed 15 September 2022).

46. Wickham H. *Ggplot2: Elegant graphics for data analysis*. New York: Springer-Verlag (2016).

47. Kassambara A. Ggpubr: 'ggplot2' based publication ready plots, in: *R package version 0.4.0* (2020). Available at: https://CRAN.R-project.org/package=ggpubr (Accessed 15 September 2022).

48. Wickham H, Henry L, Lin Pedersen T, Luciami TJ, Decorde M, et al. Svglite: An 'SVG' graphics device, in: *R package version 2.0.0* (2021). Available at: https://CRAN.R-project.org/package=svglite (Accessed 15 September 2022).

49. Pawlowsky-Glahn V, Egoycue J. Compositional data and their analysis: an introduction. In: Buccianti A, Mateu-Figueras G, Pawlowsky-Glahn V, editors. *Compositional data analysis in the geosciences: From theory to practice. geological society*, vol. 264 . London: Special Publications (2006). p. 1–10.

50. van den Boogaart G, Tolosana-Delgado R. Compositions: A unified r package to analyze compositional data. *Comp Geosci* (2008) 34(4):320–38. doi: 10.1016/j.cageo.2006.11.017

51. van den Boogaart G, Tolosana-Delgado R, Bren M. Compositions: Compositional data analysis, in: *R package version 2.0-4* (2022). Available at: https://CRAN.R-project.org/package=compositions (Accessed 15 September 2022).

52. Wickham H, François R, Henry L, Müller K. Dplyr: A grammar of data manipulation, in: *R package version 1.0.6* (2021). Available at: https://CRAN.R-project.org/package=dplyr (Accessed 15 September 2022).

53. Barr DJ, Levy R, Scheepers C, Tily HJ. Random effects structure for confirmatory hypothesis testing: Keep it maximal. *J Mem Lang.* (2013) 68(3). doi: 10.1016/j.jml.2012.11.001

54. Yang H, Parkhouse RM, Wileman T. Monoclonal antibodies that identify the CD3 molecules expressed specifically at the surface of porcine gammadelta-T cells. *Immunology.* (2005) 115(2):189–96. doi: 10.1111/j.1365-2567.2005.02137.x

55. Talker SC, Käser T, Reutner K, Sedlak C, Mair KH, Koinig H, et al. Phenotypic maturation of porcine NK- and T-cell subsets. *Dev Comp Immunol* (2013) 40(1):51–68. doi: 10.1016/j.dci.2013.01.003

56. Lagumdzic E, Pernold C, Viano M, Olgiati S, Schmitt MW, Mair KH, et al. Transcriptome profiling of porcine naive, intermediate and terminally differentiated CD8(+) T cells. *Front Immunol* (2022) 13:849922. doi: 10.3389/fimmu.2022.849922

57. Lee SC, Choi HW, Nam E, Noh YH, Lee S, Lee YJ, et al. Pathogenicity and genetic characteristics associated with cell adaptation of a virulent porcine reproductive and respiratory syndrome virus nsp2 DEL strain CA-2. *Vet Microbiol* (2016) 186:174–88. doi: 10.1016/j.vetmic.2016.03.002

58. Zhang H, Xiang L, Xu H, Li C, Tang YD, Gong B, et al. Lineage 1 porcine reproductive and respiratory syndrome virus attenuated live vaccine provides broad cross-protection against homologous and heterologous NADC30-like virus challenge in piglets. *Vaccines (Basel)* (2022) 10(5):752. doi: 10.3390/vaccines10050752

59. Leng X, Li Z, Xia M, He Y, Wu H. Evaluation of the efficacy of an attenuated live vaccine against highly pathogenic porcine reproductive and respiratory syndrome virus in young pigs. *Clin Vaccine Immunol* (2012) 19(8):1199–206. doi: 10.1128/CVI.05646-11

60. Nathues C, Perler L, Bruhn S, Suter D, Eichhorn L, Hofmann M, et al. An outbreak of porcine reproductive and respiratory syndrome virus in Switzerland following import of boar semen. *Transbound Emerg Dis* (2016) 63(2):e251–61. doi: 10.1111/tbed.12262

61. Osorio FA, Galeota JA, Nelson E, Brodersen B, Doster A, Wills R, et al. Passive transfer of virus-specific antibodies confers protection against reproductive failure induced by a virulent strain of porcine reproductive and respiratory syndrome virus and establishes sterilizing immunity. *Virology.* (2002) 302(1):9–20. doi: 10.1006/viro.2002.1612

62. Vivier E, Tomasello E, Baratin M, Walzer T, Ugolini S. Functions of natural killer cells. *Nat Immunol* (2008) 9(5):503–10. doi: 10.1038/ni1582

63. Mair KH, Essler SE, Patzl M, Storset AK, Saalmüller A, Gerner W. NKp46 expression discriminates porcine NK cells with different functional properties. *Eur J Immunol* (2012) 42(5):1261–71. doi: 10.1002/eji.201141989

64. Mair KH, Müllebner A, Essler SE, Duvigneau JC, Storset AK, Saalmüller A, et al. Porcine CD8αdim/-NKp46high NK cells are in a highly activated state. *Vet Res* (2013) 44:13. doi: 10.1186/1297-9716-44-13

65. Sedlak C, Patzl M, Saalmüller A, Gerner W. CD2 and CD8α define porcine γδ T cells with distinct cytokine production profiles. *Dev Comp Immunol* (2014) 45 (1):97–106. doi: 10.1016/j.dci.2014.02.008

66. Rodríguez-Gómez IM, Talker SC, Käser T, Stadler M, Reiter L, Ladinig A, et al. Expression of T-bet, eomesodermin, and GATA-3 correlates with distinct phenotypes and functional properties in porcine γδ T cells. *Front Immunol* (2019) 10:396. doi: 10.3389/fimmu.2019.00396

67. Swain SL, McKinstry KK, Strutt TM. Expanding roles for CD4(+) T cells in immunity to viruses. *Nat Rev Immunol* (2012) 12(2):136–48. doi: 10.1038/nri3152

68. Costers S, Lefebvre DJ, Goddeeris B, Delputte PL, Nauwynck HJ. Functional impairment of PRRSV-specific peripheral CD3+CD8high cells. *Vet Res* (2009) 40 (5):46. doi: 10.1051/vetres/2009029

69. Kick AR, Amaral AF, Cortes LM, Fogle JE, Crisci E, Almond GW, et al. The T-cell response to type 2 porcine reproductive and respiratory syndrome virus (PRRSV). *Viruses* (2019) 11(9):796. doi: 10.3390/v11090796

70. Montaner-Tarbes S, Del Portillo HA, Montoya M, Fraile L. Key gaps in the knowledge of the porcine respiratory reproductive syndrome virus (PRRSV). *Front Vet Sci* (2019) 6:38. doi: 10.3389/fvets.2019.00038

71. Crisci E, Fraile L, Montoya M. Cellular innate immunity against PRRSV and swine influenza viruses. *Vet Sci* (2019) 6(1):26. doi: 10.3390/vetsci6010026

72. Rahe MC, Murtaugh MP. Mechanisms of adaptive immunity to porcine reproductive and respiratory syndrome virus. *Viruses*. (2017) 9(6):148. doi: 10.3390/v9060148

frontiers

Supplementary Material

Influence of PRRSV-1 vaccination and infection on mononuclear immune cells at the maternal-fetal interface

Melissa R Stas[1], Heinrich Kreutzmann[1], Julia Stadler[2], Elena L Sassu[1,¥], Kerstin H Mair[3,4], Michaela Koch[1], Christian Knecht[1], Maria Stadler[3], Marlies Dolezal[5], Gyula Balka[6], Marianne Zaruba[7], Marlene Mötz[7],Armin Saalmüller[3], Till Rümenapf[7], Wilhelm Gerner[3,§,Ŧ], and Andrea Ladinig[1,Ŧ]

Correspondence: Andrea Ladinig (Andrea.ladinig@vetmeduni.ac.at)

Ŧ These authors have contributed equally to this work

1 Supplementary Figures

Supplementary Figure 1 | Consecutive gating strategy applied for the identification of lymphocytes at the maternal-fetal interface. For the characterization of the major lymphocyte subsets a similar gating hierarchy was applied. Each individual sample was inspected using the time parameter in order to ensure a stable flow of cells was established. A time gate was applied in order to exclude areas with a poor flow (e.g. due to a clog or an air bubble). Hereafter, lymphocytes and larger leukocytes were identified according to their light scatter properties (forward scatter area (FSC-A) vs. side scatter area (SSC-A) and a double doublet discrimination (forward scatter area (FSC-A) vs. forward scatter height (FSC-H) and side scatter (SSC-A) vs. side scatter height (SSC-H)) was performed. Cells with high autofluorescence were excluded using the 510/50 bandpass filter in the excitation line of the violet laser and dead cells were excluded based on the staining with the fixable viability dye eFluor780®. Firstly, total $CD45^{pos}$ cells within viable lymphocytes were identified (black box) using the same lymphocyte identification gate for each individual sample. The frequency obtained for total $CD45^{pos}$ cells was used to calculate the CD45 correction factor to correct the obtained cell lineage frequencies. Major lymphocyte subsets were identified within viable lymphocytes. B cells were gated based on their expression of CD79α. The T cell subsets were gated based on their expression of TCR-γδ, CD4, and CD8β for the identification of total γδ T cells, CD4 T cells, and CD8β T cells, respectively. For the characterization of NK cells, $CD16^{pos}CD172a^{neg}$ cells were selected and sub-gated for a $CD3^{neg}CD8\alpha^{pos}$ phenotype. Myeloid cells were identified based upon their CD172a expression. Representative pseudocolor plots for their hierarchical structure is shown for the maternal endometrium (ME) in **(A)** and fetal placenta (FP) in **(B)** from a No.Vac_No.Chall fetus.

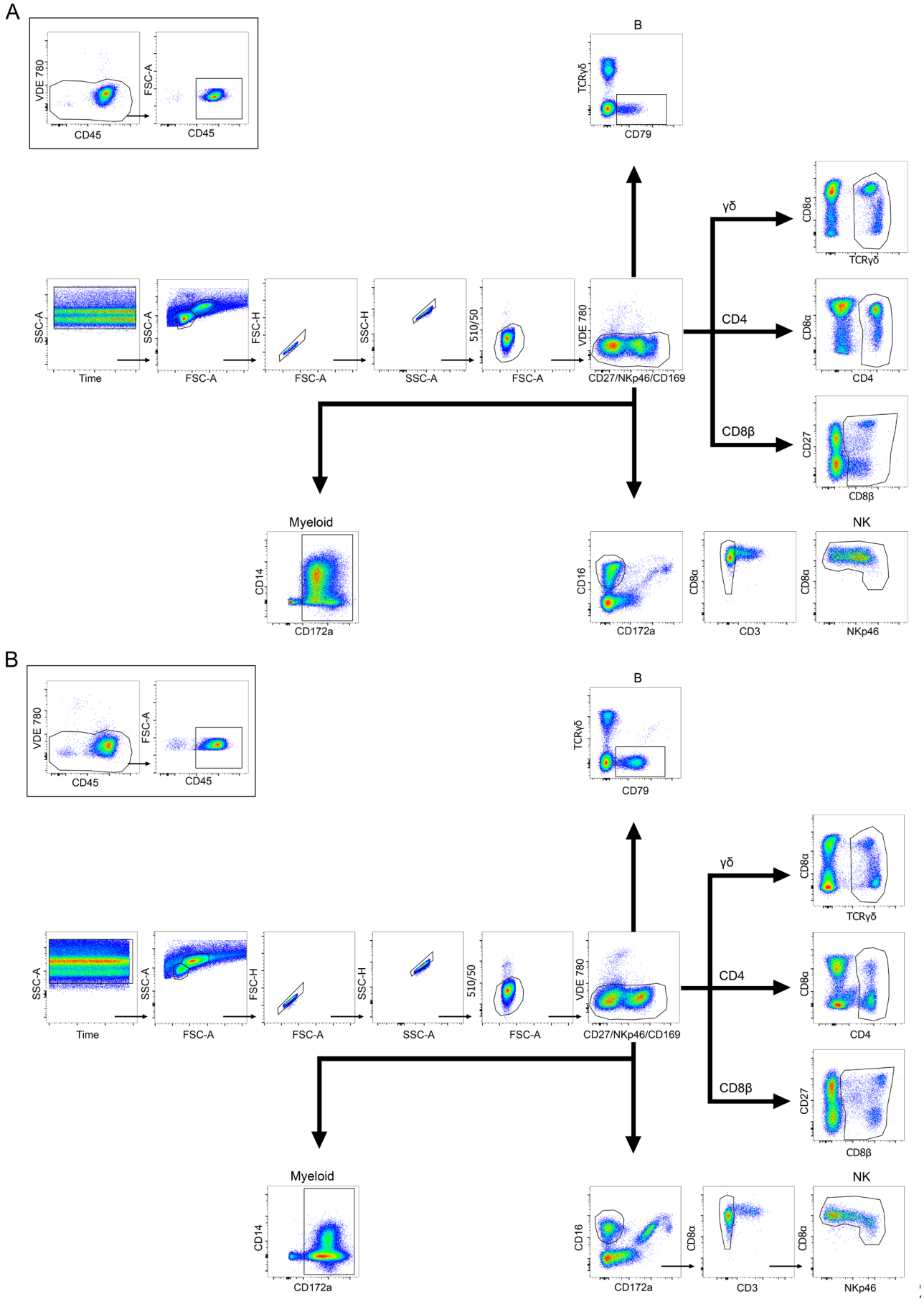
A
VDE 780
CD45
FSC-A
CD45
B
TCRγδ
CD79
γδ
CD4
CD8β
CD8α
TCRγδ
CD8α
CD4
CD27
CD8β
SSC-A
Time
SSC-A
FSC-A
FSC-H
FSC-A
SSC-H
SSC-A
510/50
FSC-A
VDE 780
CD27/NKp46/CD169
Myeloid
CD14
CD172a
CD16
CD172a
CD8α
CD3
NK
CD8α
NKp46
B
VDE 780
CD45
FSC-A
CD45
B
TCRγδ
CD79
γδ
CD4
CD8β
CD8α
TCRγδ
CD8α
CD4
CD27
CD8β
SSC-A
Time
SSC-A
FSC-A
FSC-H
FSC-A
SSC-H
SSC-A
510/50
FSC-A
VDE 780
CD27/NKp46/CD169
Myeloid
CD14
CD172a
CD16
CD172a
CD8α
CD3
NK
CD8α
NKp46

Supplementary Figure 2 | Fetal preservation status and viral load at the maternal-fetal interface of individual fetuses. Following the opening of the uteri, the position of each fetus, within the left and right uterine horn, was recorded and the fetal preservation status was evaluated. The categories for the fetal preservation status included VIA, MEC, DEC, and AUT in order to identify the viable, meconium stained, decomposed, and autolyzed fetuses, respectively. The viral load for the maternal endometrium (ME) and fetal placenta (FP) for each individual fetus was determined using an ORF7 PRRSV-1 isolate specific RT-qPCR. The results for the viral load are given as genome equivalents per gram tissue (log_{10} transformed). The color codes indicate the magnitude of the viral load. (*) means below the detection limit and (-) sample was not taken. Within one color coded frame (e.g. No.Vac_Chall_LV), each line depicts the results for the fetal preservation status, viral load in the ME, and viral load in the FP for one litter. The first column always indicates the gilt ID. Fetuses used for *ex vivo* phenotyping are indicated in bold and blue (section of fetal preservation). The depicted treatment groups are: No.Vac_Chall_LV (dark purple, non-vaccinated and infected low virulent strain), Vac_Chall_LV (light purple, vaccinated and infected low virulent strain), No.Vac_Chall_HV (dark red, non-vaccinated and infected high virulent strain), and Vac_Chall_HV (light red, vaccinated and infected high virulent strain).

No.Vac_Chall_LV

Fetal preservation

	Left uterine horn											Right uterine horn												
Gilt	L1	L2	L3	L4	L5	L6	L7	L8	L9	L10	L11	R14	R13	R12	R11	R10	R9	R8	R7	R6	R5	R4	R3	R2	R1
17	VIA	VIA	VIA	VIA	VIA	VIA	VIA												VIA	VIA	VIA	VIA	VIA	VIA	VIA
18																							AUT	VIA	VIA
19	VIA	VIA	VIA	VIA	VIA	VIA	VIA	VIA	VIA	VIA	MEC								VIA	VIA	VIA	VIA	VIA	VIA	VIA
20	VIA	VIA	VIA	VIA	VIA	VIA	VIA	VIA	VIA								VIA	VIA	VIA	VIA	VIA	VIA	VIA	VIA	VIA

Viral load ME

17	(*)	7,5	(*)	(*)	7,5	(*)	8,8												9,0	(*)	(*)	7,8	8,4	7,7	8,3
18																							7,8	6,9	(*)
19	(*)	(*)	(*)	(*)	6,7	7,5	(*)	(*)	8,0	(*)	5,4								8,7	4,5	(*)	(*)	(*)	5,2	8,3
20	(*)	(*)	8,7	(*)	(*)	(*)	(*)	8,4	(*)								(*)	(*)	(*)	(*)	(*)	(*)	(*)	(*)	(*)

Viral load FP

17	(*)	(*)	(*)	(*)	(*)	8,8	(*)												(*)	(*)	(*)	(*)	(*)	(*)	8,5
18																							9,7	8,0	(*)
19	(*)	(*)	(*)	(*)	(*)	(*)	(*)	(*)	(*)	(*)	9,9								(*)	(*)	(*)	(*)	(*)	(*)	(*)
20	(*)	(*)	(*)	(*)	(*)	(*)	(*)	(*)	(*)								(*)	(*)	(*)	(*)	(*)	(*)	(*)	(*)	(*)

Vac_Chall_LV

Fetal preservation

	Left uterine horn											Right uterine horn												
Gilt	L1	L2	L3	L4	L5	L6	L7	L8	L9	L10	L11	R14	R13	R12	R11	R10	R9	R8	R7	R6	R5	R4	R3	R2	R1
9	VIA	VIA	AUT	MEC	VIA	VIA	VIA								VIA	VIA	VIA	VIA	VIA	VIA	VIA	VIA	VIA	VIA	VIA
10	VIA	VIA	VIA	VIA	VIA	VIA	VIA											VIA	VIA	VIA	VIA	VIA	VIA	VIA	VIA
11	VIA	VIA	VIA	VIA	VIA	VIA	VIA	VIA										VIA	VIA	VIA	VIA	VIA	VIA	VIA	VIA
12	VIA	VIA	VIA	VIA	VIA	VIA	VIA	VIA	VIA	VIA		VIA	VIA	VIA	VIA	VIA	VIA	VIA	VIA	VIA	VIA	VIA	AUT	VIA	MEC

Viral load ME

9	(*)	(*)	(*)	(*)	(*)	(*)	(*)								(*)	(*)	(*)	(*)	(*)	(*)	(*)	(*)	(*)	(*)	(*)
10	(*)	(*)	(*)	(*)	(*)	(*)	(*)											(*)	(*)	(*)	(*)	(*)	(*)	(*)	(*)
11	(*)	(*)	(*)	(*)	(*)	(*)	(*)	(*)										(*)	(*)	(*)	(*)	(*)	(*)	(*)	(*)
12	(*)	(*)	(*)	(*)	(*)	(*)	(*)	(*)	(*)	(*)		(*)	(*)	(*)	(*)	(*)	(*)	(*)	(*)	(*)	(*)	(*)	(*)	(*)	(*)

Viral load FP

9	(*)	(*)	(*)	(*)	(*)	(*)	(*)								(*)	(*)	(*)	(*)	(*)	(*)	(*)	(*)	(*)	(*)	(*)
10	(*)	(*)	(*)	(*)	(*)	(*)	(*)											(*)	(*)	(*)	(*)	(*)	(*)	(*)	(*)
11	(*)	(*)	(*)	(*)	(*)	(*)	(*)	(*)										(*)	(*)	(*)	(*)	(*)	(*)	(*)	(*)
12	(*)	(*)	(*)	(*)	(*)	(*)	(*)	(*)	(*)	(*)		(*)	(*)	(*)	(*)	(*)	(*)	(*)	(*)	(*)	(*)	(*)	(*)	(*)	(*)

No.Vac_Chall_HV

Fetal preservation

	Left uterine horn											Right uterine horn												
Gilt	L1	L2	L3	L4	L5	L6	L7	L8	L9	L10	L11	R14	R13	R12	R11	R10	R9	R8	R7	R6	R5	R4	R3	R2	R1
21	VIA	VIA	VIA	VIA	VIA	VIA	VIA	VIA											VIA	VIA	VIA	VIA	DEC	AUT	MEC
22	MEC	DEC	MEC	DEC	MEC	MEC	VIA	AUT							MEC	MEC	VIA	DEC	VIA	MEC	MEC	AUT	MEC	AUT	AUT
23	VIA	VIA	VIA	VIA	MEC	AUT	DEC	AUT							MEC	AUT	VIA	VIA	MEC	AUT	VIA	VIA	VIA	VIA	VIA
24	MEC	MEC	VIA	VIA	VIA	VIA	VIA											AUT	VIA	VIA	VIA	VIA	VIA	VIA	VIA

Viral load ME

21	7,7	(*)	8,2	(*)	(*)	9,8	7,7	9,1											(*)	8,8	(*)	9,6	(*)	9,1	9,0
22	10,3	9,3	10,3	8,9	9,8	9,5	9,7	8,5							10,1	10,3	9,1	9,5	9,8	8,9	9,0	10,3	9,3	7,8	8,8
23	6,4	(*)	(*)	9,2	8,5	7,3	8,2	7,8							8,7	8,3	8,2	7,7	7,9	(*)	8,2	8,7	(*)	(*)	(*)
24	8,6	8,8	8,1	(*)	(*)	(*)	(*)											(*)	(*)	(*)	(*)	6,5	(*)	(*)	(*)

Viral load FP

21	(*)	(*)	(*)	8,8	(*)	(*)	(*)	(*)											(*)	(*)	(*)	(*)	9,7	(*)	10,2
22	10,9	10,6	10,0	8,8	9,4	8,6	9,4	(-)							9,4	10,5	9,0	(-)	7,4	9,6	9,8	(-)	10,0	9,4	(-)
23	(*)	7,7	(-)	9,5	10,0	9,3	10,2	8,9							10	8,0	8,7	9,3	9,7	7,3	9,4	9,3	(*)	(*)	(*)
24	9,1	9,5	8,1	(*)	(*)	6,4	(*)											(*)	(*)	(*)	(*)	(*)	(*)	(*)	(*)

Vac_Chall_HV

Fetal preservation

	Left uterine horn											Right uterine horn												
Gilt	L1	L2	L3	L4	L5	L6	L7	L8	L9	L10	L11	R14	R13	R12	R11	R10	R9	R8	R7	R6	R5	R4	R3	R2	R1
13	VIA	VIA	VIA	VIA																			VIA	VIA	VIA
14	VIA	VIA	VIA	VIA	VIA	VIA	VIA	VIA	VIA									VIA	VIA	VIA	VIA	VIA	VIA	VIA	VIA
15	VIA	VIA	VIA	VIA	VIA	VIA	VIA												DEC	MEC	MEC	VIA	VIA	VIA	VIA
16	VIA	VIA	VIA	VIA	VIA	VIA	VIA	VIA	VIA	VIA	VIA					VIA	VIA	VIA	VIA	VIA	VIA	VIA	VIA	VIA	VIA

Viral load ME

13	(*)	(*)	(*)	(*)																			(*)	(*)	(*)
14	(*)	(*)	(*)	(*)	(*)	(*)	(*)	(*)	(*)									(*)	(*)	(*)	(*)	(*)	(*)	(*)	(*)
15	(*)	(*)	(*)	(*)	(*)	(*)	(*)												8,0	8,8	9,0	8,5	(*)	(*)	(*)
16	(*)	(*)	(*)	(*)	(*)	(*)	(*)	(*)	(*)	(*)	8,1					(*)	(*)	(*)	(*)	(*)	(*)	(*)	7,9	7,9	8,0

Viral load FP

13	(*)	(*)	(*)	(*)																			(*)	(*)	(*)
14	(*)	(*)	(*)	(*)	(*)	(*)	(*)	(*)	(*)									(*)	(*)	(*)	(*)	(*)	(*)	(*)	(*)
15	(*)	(*)	(*)	(*)	(*)	(*)	(*)												9,9	9,1	9,8	8,6	(*)	(*)	(*)
16	(*)	(*)	(*)	(*)	(*)	(*)	(*)	(*)	(*)	(*)	(*)					(*)	(*)	(*)	(*)	(*)	(*)	(*)	(*)	(*)	(*)

log_{10} GE/g tissue

<6,0 | 6,0-6,9 | 7,0-7,9 | 8,0-8,9 | 9,0-9,9 | 10,0-10,9

Supplementary Figure 3 | Detection of porcine reproductive and respiratory syndrome virus at the maternal-fetal interface using immunofluorescence. Cryopreserved tissue from a No.Vac_Chall_HV fetus was sectioned (6 µm thick) and immunofluorescence was performed. A staining for nuclei (DAPI, blue), PRRSV-NP (IgG2a, clone P11/d72-c1, green), and cytokeratin-8 ((CK8), TROMA-1, grey) was applied. Stained sections were scanned using an Axioimager Z.1 wide field microscope (Zeiss, Germany) equipped with a mercury lamp, using a LD Plan-Neofluar 20x/0.40 air NA lens coupled to an ultra-compact 14 bit CCD camera (PCO PixelFlyUSB, PCO AG, Kelheim, Germany) to obtain images. For the detection of DAPI, PRRSV-NP, and CK8 the exposure time was set to 80 ms for all three channels and signal was detected using the DAPI, GFP and Cy5 filters, respectively. CK8, strongly stains the endometrial epithelium and was used to identify the maternal and fetal boundaries of the fetal-maternal junction (FMJ). The maternal endometrium (ME) and fetal placenta (FP) were identified. Yellow arrowheads indicate viral antigen, which is predominantly located in the FP, in close proximity to the FMJ. MSF = maternal secondary fold, UG = uterine glands. Scale bar = 200 µm.

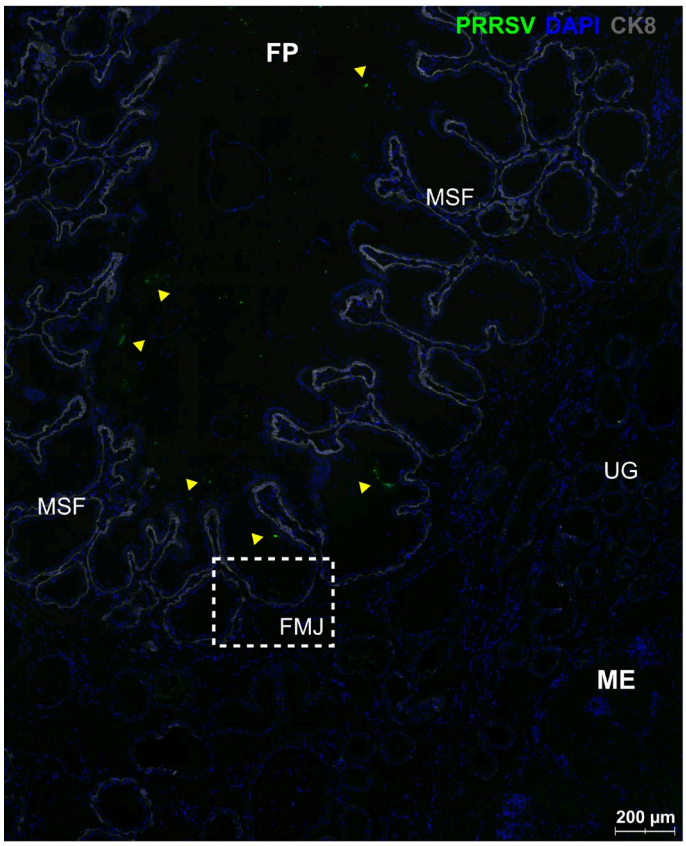

4. Discussion and Conclusion

4.1. Novel methodology for the study of immune cells isolated from the maternal-fetal interface

As to date, immune cells that reside at the porcine maternal-fetal interface have barely been investigated. NK cells and various T cell subsets have been identified during early gestation, however, only a few markers were used for their identification. During late gestation, the extent on available literature on immunophenotypic characterization of local leukocytes is limited and has mainly been performed in context of PRRSV research. The vast majority of investigations have focused on $CD163^{+}$ and or $CD169^{+}$ macrophages and $CD3^{-}CD8\alpha^{+}$ NK cells using fluorescence microscopy or immunohistochemistry (102, 116, 121, 122). These techniques provide information on the spatial localization of the cells but are limited in the number of cellular makers that can be targeted. Standard immunofluorescence labelling usually combines up to four fluorescent signals including a nuclei stain. In addition, a cytokeratin staining is necessary to discriminate between the ME and FP which restricts the number of cellular markers to be used even more and complicates the identification of certain immune cell subsets (i.e. those without lineage specific markers, e.g. NK cells) or the activation/differentiation status *in situ*. Therefore, a methodology tailored to the porcine epitheliochorial placenta was established with the goal to characterize the isolated leukocytes from the maternal-fetal interface via multicolor flow cytometry during steady state conditions (**Figure 5**).

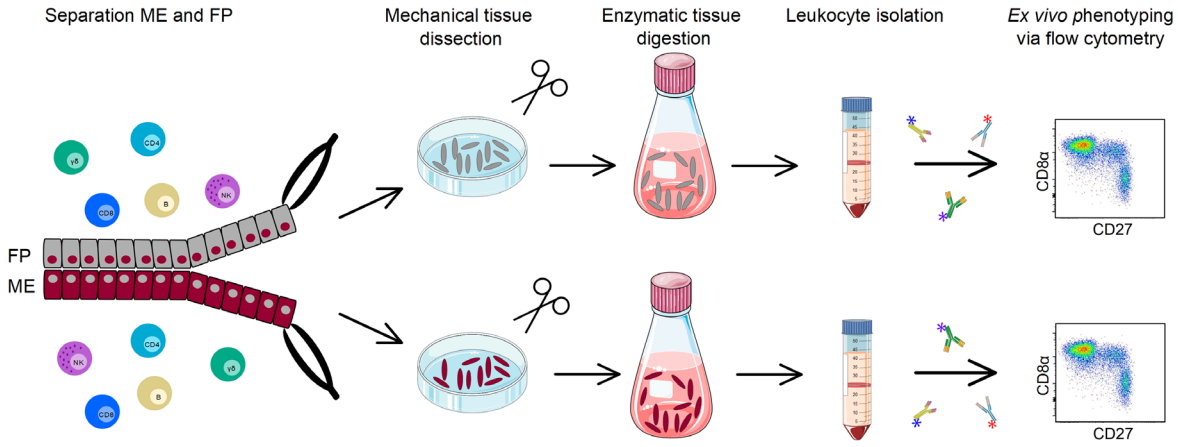

Figure 5 | Methodology for the separation of the porcine epitheliochorial placenta. The maternal-fetal interface from randomly selected fetuses from healthy sows was collected and maternal endometrium (ME) and fetal placenta (FP) were mechanically separated. A forceps for each epithelial layer was used for the separation without contaminating either side and separated tissue was collected in a sterile cup. In the lab, ME and FP tissue was transferred to a sterile petri dish on ice and mechanically dissected using scissors. The tissue pieces were then transferred into a flask containing digestion medium, containing DNase and collagenase, followed by an incubation for one hour at 37ºC during constant shaking. Hereafter, remaining tissue pieces were removed and leukocytes, obtained from the cell suspension, were isolated via density gradient centrifugation. For the *ex vivo* phenotypic characterisation of various immune cell subsets, isolated cells were labelled with fluorophore-linked antibodies and subsequently analysed by flow cytometry. This

figure was created with Inkscape. Parts of the figure were drawn and adapted using pictures from Servier Medical Art, provided by servier, licensed under a Creative Commons Attribution 3.0 unported license (https://smart.servier.com/).

We successfully established a methodological approach which allowed us to study the immune cell composition separately in the ME and FP. We have tested the efficiency of our mechanical separation method using three male fetuses. ME and FP tissue were separated using a single forceps for each individual side. Separated ME was tested for contamination of male DNA using a sex typing method via PCR as described elsewhere (124). Furthermore, we routinely use a cytokeratin staining in order to discriminate the uterine epithelium and trophoblast layer *in situ*. As this cytokeratin marker exclusively demarcates the uterine epithelium, this staining was applied on separated FP tissue. Overall, the results indicated that the contaminations observed are negligible (unpublished findings). Therefore, we are convinced that this separation method provides a reliable methodology for further immunological investigations.

4.2. Lymphocytes in late gestation under steady state conditions

4.2.1. NK cells

Phenotypic characterization of various immune cell subsets was initially performed on the ME and FP samples obtained from healthy sows during late gestation. In addition, maternal blood (mBld) and fetal spleen (fSpln) were also included for comparison. NK cells were identified by a $CD3^{-}CD16^{+}CD8\alpha^{+}CD172a^{-}$ phenotype and analyzed for variable expression of NKp46. Peripheral human NK cells can be divided into two subsets based on the expression of CD16 and CD56 (46). The majority of human NK cells have a $CD16^{+}CD56^{dim}$ phenotype and these cells have a high killing capacity (46). A smaller subset is $CD16^{-}CD56^{bright}$, which mainly secretes cytokines (46). Human uNK cells share certain features of both subsets and express additional surface markers including CD9, CD49a, and 40% express CD69 (46). Human uNK cells lack the expression of CD16 and are highly positive for CD56 (46). In contrast to the human uNK cells, porcine NK cells regardless of their location, do express CD16 which is an Fc receptor leading to NK cell-activation. Human uNK cells are all $NKp46^{+}$, whereas in pigs expression is variable. Overall, our analysis showed that NK cells that reside at the maternal-fetal interface have a similar phenotype as their peripheral counterpart. Tools to target CD49a or NK cell-inhibitory receptors on porcine NK cells are lacking. Recently, monoclonal antibodies specific for porcine CD9 and CD69 were generated (125, 126). *Ex vivo* phenotyping experiments revealed that porcine blood derived NK cells do not express CD9, whereas a variable expression was found on T cells and B cells (125). Whether or not porcine NK cells residing at the maternal-fetal interface express CD9, remains to be elucidated. However, the fact that porcine peripheral blood NK cells lack the expression of CD9 (125), would be in line with the findings for human peripheral blood NK cells (46). Additional *ex vivo* phenotyping experiments combined with transcriptional profiling might provide more in-depth insights as it

would allow the investigation of translated transcripts (e.g. CD56, CD49a, killer-cell immunoglobulin-like receptor (KIR), and leukocyte immunoglobulin-like receptor (LILR)) for which tools to detect them on the protein level are still lacking.

4.2.2. T cell subsets and their differentiation and function

Our in-depth phenotyping for T cells highlighted major differences between anatomic locations, especially when comparing maternal *versus* fetal compartments. Our findings demonstrated that the maternal compartments mainly harbored antigen experienced phenotypes, whereas naive phenotypes prevailed in both fetal compartments. Some similarities between the human decidua and porcine ME were found despite the differences in placentation (i.e. hemochorial vs. epitheliochorial). For instance, on average a higher proportion of CD8 T cells as compared to CD4 T cells can be found in both the human decidua (55, 56) and porcine ME, although, in our studies we observed some animal-to-animal variation. Indeed, for some animals a 1:1 ratio of CD4 and CD8 T cells was found. In humans, a few studies have shown that the frequency of CD4 T cells at term is higher as compared to the frequency of CD8 T cells (63) and this is thought to play a role in parturition (66). In addition, our data demonstrate that the majority of T cells residing at the porcine ME display highly differentiated phenotypes (e.g. $CD2^{+}CD8\alpha^{+}CD27^{dim/-}$perforin^{+} γδ T cells, $CD27^{-}$perforin^{+} CD8 T cells, and T-$bet^{+}CD8\alpha^{+}CD27^{-}$ Tem cells), which is in line with data obtained from the human field (59-61, 63). However, the memory status of human T cells is mostly assessed using the CD45RA and CCR7 expression pattern followed by a subcategorization of effector memory cells using CD27 and CD28 (59-61). A recent study showed that the CD45RA/CCR7 expression pattern as it is applied to assess the differentiation stages of human CD8 T cells, is also applicable to pigs (24). This phenotypic characterization may, in the future, provide an alternative strategy comparable to the human field, to discriminate porcine CD8 T cell differentiation stages. In our first study, we showed that differentiated CD8 T cells originating from the ME have a comparable perforin expression level as their peripheral counterpart, which directly contrasts the reduced expression of perforin found in human-derived dCD8 T cells (59, 60, 68). In human dCD8 T cells, this reduced expression seems to be post-translationally regulated but can be overcome in a T cell activating environment (e.g. local infection) (59). This indicates that in CD8 T cells in the porcine ME cytolytic protein expression is not coordinated in a similar manner as in human dCD8 T cells, which might indicate that other regulatory mechanisms are involved as fetuses are not rejected in healthy steady state conditions. The topic on regulatory mechanisms will be discussed in more detail later. In the porcine ME the vast majority (~80-90%) of CD4 T cells with a $CD8\alpha^{+}CD27^{-}$ Tem phenotype expressed the Th1 defining transcription factor T-bet, indicative of a local Th1 enrichment which is another resemblance to term human decidua (62, 63). Other potential polarization states, as defined by transcription factor and cytokine expression profiles (e.g. Th2, Th17, *etc.*), have not yet been addressed so far and may be an avenue for future investigations.

Generally, the paradigm of CD4 T cell polarization in pigs is less well characterized but seems to be similar as compared to the human/murine counterpart. To add another layer of complexity, CD4 T cells possess phenotypic plasticity which means that these cells can simultaneously acquire Th cell characteristics of more than one of the defined subsets or repolarize in order to adapt to changes in the microenvironment (20). For example, IL-9 producing Th9 cells derive from Th2 cells under the influence of transforming growth factor-β (20) and their reduction at term might be involved in parturition (65). Also in the pig CD4 T cells may exhibit phenotypic and functional plasticity (14) which would be interesting to be further explored, both systemically and at the maternal-fetal interface. Human and murine T follicular helper (Tfh) cells can be characterized by their expression of the transcription factor B-cell lymphoma 6 (bcl-6), inducible co-stimulatory molecule (ICOS), the chemokine receptor CXCR5, and programmed cell death protein-1 (PD-1) (65). These cells are specialized in providing help to B cells. Literature indicates that compared to non-pregnant women, the frequency of circulating Tfh cells in pregnant women is higher during the last trimester (127). In mice, an increase of $CD4^{+}CXCR5^{hi}PD\text{-}1^{hi}$ and $CD4^{+}CXCR5^{hi}ICOS^{hi}$ phenotypes at the maternal-fetal interface was found during late gestation; their exact role locally, however, remains to be elucidated (128). Unfortunately, tools for the detection of porcine CXCR5 and PD-1 are currently lacking, hampering the identification of circulating Tfh cells in pigs. Nevertheless, porcine Tfh cells were identified using Bcl-6 and ICOS in lymph nodes, yet, as in mice and humans no Bcl-6 expressing CD4 T cells were found in blood (129). However, the authors also showed that the sorted circulating $ICOS^{+}$ CD4 T cells were able to stimulate B cells to differentiate into immunoglobulin secreting blast cells and have a transcriptional profile reminiscent of Tfh cells (129). This will allow the investigation of this cell subset during porcine gestation in the future.

Potential regulatory mechanisms described for the porcine maternal-fetal interface have been mentioned in the introduction of this PhD thesis. In the ME, we were able to detect $Foxp3^{+}CD25^{hi}$ CD4 T cells which mainly displayed an antigen-experienced phenotype, and is comparable to findings from the human field (63). An interesting avenue for further investigations would be to address their origin (natural *vs.* induced), their phenotype, and their function over the course of gestation. In addition it would also be worthwhile to see if seminal fluid would induce paternal/fetus-specific Tregs. In the porcine field it is difficult to study the immune system in a comparable manner as to human and murine studies since reagents to detect for example the checkpoint molecule (PD-1) are lacking. Recently, *in situ* immune checkpoint expression of cytotoxic T-lymphocyte-associated protein 4 (CTLA-4), T cell immunoglobulin and mucin-domain containing 3 (TIM-3), and the ligand of PD-1 was identified in the thymus of piglets (130). An alternative approach one could follow is to combine *ex vivo* phenotyping experiments, functional assays, and single cell RNA sequencing in order to gain

the maximal amount of information. Together, they might reveal a high level of heterogeneity within immune cell subsets and give an indication of different functionalities.

As the maternal-fetal interface is a highly vascularized transient organ it should be questioned if the highly differentiated T cells found at the maternal-fetal interface are tissue-resident memory (Trm) cells or just passing through at that exact moment. Trm cells represent a cell population that does not re-enter the blood circulation but instead takes residency in (mucosal) tissues (e.g. lung, skin, intestine) (131, 132). These cells differ from their recirculating counterpart on a transcriptional, phenotypic, and functional level. Trm cells are usually identified by the expression of CD69 and CD103 (also known as integrin αEβ7) (131, 132). The latter, however, is not expressed on all Trm CD8 T cells and depending on the tissue only a small fraction of Trm CD4 T cells is positive for this marker (131). Trm cells upregulate markers associated with tissue retention (e.g. CD49a) and inhibitory and regulatory molecules (e.g. PD-1 and IL-10), and down regulate molecules that would promote tissue egression (e.g. CD62L, S1PR1, and S1PR5) (131, 132). Furthermore, Trm cells significantly contribute to protective immunity against local invading pathogens (131, 132). Investigations of porcine Trm cells are not as straightforward due to the lack of identifying markers. Therefore, an alternative approach to study porcine Trm CD8 T cells was applied (24). Herein, pigs received an intravenous infusion of anti-porcine CD3 monoclonal antibodies (1mg/kg bodyweight) prior to euthanasia which would allow for the identification of T cells in the circulation (24). T cells that were not labeled with CD3 via the infusion were considered Trm cells (24). This approach could be used to identify Trm cells in the porcine ME, but based on the bodyweight of pregnant females a high quantity of antibodies for infusion would be needed. Furthermore, immune cells residing in the FP would not be labeled via this approach as the porcine placenta does not allow the transfer of antibodies. Therefore, other approaches might suit these further investigations better.

We also investigated the capacity of our isolated leukocytes to produce IFN-γ via an ELISpot assay with or without stimuli. The level of antigen-experienced phenotypes identified in the maternal compartments was also reflected by the functional capacity of these cells, because even without the presence of stimuli a substantial amount of IFN-γ producing cells was observed. IFN-γ producing cells originating from the fetal compartments were only observed in response to the stimuli used, reflective of an overall naive immune cell composition. The ELISpot assay gives a good indication on cytokine production, however, it does not allow to identify the phenotype of cytokine-producing cells. For instance, T cells, NK cells, and macrophages are all able to secrete IFN-γ. As to date, the cytokine production profiles of immune cells that reside at the porcine maternal-fetal interface, and potential gestational changes, remain to be elucidated.

4.2.3. T cell specificities at the maternal-fetal interface and their implications

Further research needs to focus on the specificity of the T cells that reside at the porcine maternal-fetal interface, especially in the ME as the vast majority displays a highly differentiated phenotype. Originally the uterus was described to be a sterile environment but this notion is challenged as evidence for an endometrial microbiome is rising (133). In pigs the uterine microbiome has not yet been studied, however, literature for various mammalian species (e.g. human, equine, bovine, canine) on this topic is available (134). Furthermore, semen (human and mice) has been shown to have a unique microbiome, and in some instances it can be a source of pathogenic micro-organisms (135). The pregnant females included in our studies were routinely vaccinated against Porcine Parvovirus (PPV), Porcine Circovirus Type 2, and the bacterium *Erysipelothrix rhusiopathiae*. These pathogens can cause reproductive complications (e.g. abortions) in pregnant females (136-138). Therefore, it is possible that a proportion of the local antigen-experienced T cells have a specificity to certain pathogens/micro-organisms and patrol the local environment and might have the capacity to swiftly respond to a local infection. For PPV, literature indicates that when animals are vaccinated (or, in the course of their life, naturally exposed) reproductive signs upon infection are negligible, whereas maternal reproductive failure occurs in unvaccinated animals (137). The presence of virus-specific CD8 T cells in the human decidua has been demonstrated for HCMV and Epstein-Barr virus (69). In addition, there is ample evidence in humans and mice that pregnancy induces T cells with fetal/paternal/placental specificity. Fetal antigens may include paternally derived MHC, minor histocompatibility antigens (e.g. male antigens encoded on the Y chromosome), blood group antigens, and fetal/placental-specific antigens (139). These antigens can reach the maternal system via direct expression on trophoblasts, they can be released by the trophoblasts, and via microchimerism (139). Fetal specific CD8 T cells have been identified in the maternal circulation and decidua of humans (61, 140). In healthy progressing pregnancies, fetal rejection does not occur despite the presence of fetal-specific T cells. HLA-C mismatched pregnancies resulted in a higher frequency of activated CD4 T cells and an expansion of functional $CD4^{+}CD25^{bright}$ Tregs in the decidua (71, 141). Mouse models show that fetal/paternal-specific Tregs are expanded during pregnancy and are primed upon exposure to seminal fluid (72, 73). Furthermore, human decidual Tregs have been shown to suppress T cell effector functions and seem to be a heterogeneous population, and not all of them express Foxp3 (61, 71, 74, 141). Other mechanisms that control local effector functions include the expression of checkpoint molecules like PD-1, TIM-3, CTLA-4, and lymphocyte-activation gene 3 (LAG-3) (59, 61, 142, 143). Some T cells have been shown to also express NK cell inhibitory and activating receptors which might implicate alternative means of regulation (56). Whether or not fetus-specific T cells reside in the porcine ME remains a question to be addressed.

4.2.4. Considerations on maternal-fetal trafficking of immune cells

Maternal-fetal trafficking of immune cells, also known as microchimerism, is a well-accepted notion during human and murine pregnancy. Due to the impermeable nature of the porcine placenta, it is currently debatable if maternal-fetal trafficking across the porcine maternal-fetal interface is possible, as available literature on this topic is inconsistent and would challenge textbook knowledge (144, 145). Even though the majority of immune cells in the FP displayed a naive phenotype, also highly differentiated phenotypes (e.g. $CD2^{+}CD8\alpha^{+}CD27^{dim/-}perforin^{+}$ γδ T cells, $CD27^{-}perforin^{+}$ CTLs, and $T\text{-}bet^{+}CD8\alpha^{+}CD27^{-}$ Tem cells) were found in this anatomic location. These effector T cells may originate from the ME. Alternatively, these cells might also be of fetal origin but then the triggers that resulted in their differentiation remain unknown. Our results from the fSpln indicate that the adaptive immune system *in utero* remains unchallenged and coincides with the sterile womb hypothesis. Porcine fetuses are considered immunocompetent around day 70 of gestation and for porcine parvovirus it has been shown that infection after this point does not result in fetal death (137). PPV might, in case of exposure (> gd 70), reside at the maternal-fetal interface and steer the T cell differentiation in the FP. The assumption that womb is a sterile environment, however, has been challenged as amniotic fluid has been shown to contain bacterial DNA (146). In addition, differentiated T cell phenotypes in human fSpln, fetal liver, and fetal intestine were identified using high dimensional mass-cytometry (147). Microchimersim could, if it occurs, allow the generation of fetal-specific T cells in the porcine ME. In human pregnancy, trophoblast-derived extracellular vesicles might also be a way to maintain maternal-fetal tolerance (148). In the pig, the composition of extracellular vesicles still needs to be characterized (148) but might be a way by which maternal cells are exposed to fetal antigens (and maybe vice versa).

4.3. Influence of PRRSV infection and vaccination on maternal-fetal immune cell phenotypes

4.3.1. PRRSV vaccines and their limitations

Following an in-depth characterization of various immune cell subsets during steady state conditions, the second aim of this PhD thesis was to address the phenotypic changes in context of infection and vaccination. PRRSV was chosen as it still is one of the most important viruses affecting the swine industry worldwide. One current problem in the context of PRRSV immunology, despite the extensive amount of PRRSV literature, is the lack of understanding the cell-mediated mechanisms that provide protection. The high degree of PRRSV heterogeneity may impact the efficacy and development of vaccines and may explain the differences in results between PRRSV studies.

In many species, vaccination strategies are widely used either to prevent disease, to limit clinical signs, or as a therapeutic measure with the goal to mitigate economic losses. As to date, commercially available PRRSV vaccines include killed vaccines and modified live virus (MLV) vaccines developed for both PRRSV species (149). MLVs contain live virus which has

been adapted/attenuated so it has the ability to replicate in the host and induce an immune response similar to a mild natural infection (150), but without the typical associated clinical signs. Some safety issues are associated with the use of MLVs; nevertheless, according to a statement from the European Medicines Agency (EMA) the benefits of using the MLV still outweigh the risks (151). MLVs are commonly used in the field as they are considered more efficacious, compared to killed vaccines. They can confer complete or at least partial protection against homologous or heterologous challenge, respectively (149). Even though these vaccines are often used, correlates of protection remain elusive (87, 152). The fact that these MLVs confer some degree of protection indicates the involvement of the humoral and cell-mediated immune response. Approximately ten days post-vaccination or post-infection PRRSV antibodies can be measured (153, 154), however, these antibodies are not protective (87, 152). Following infection, neutralizing antibodies (nAbs) only appear four weeks later but can confer protection (87, 152). Furthermore, passive transfer of PRRSV-specific antibodies in sows (at an end-point titer of 1:8) prevented viremia and protected the fetuses (152, 155). Whilst in piglets an end-point titer of 1:32 is needed to fully protect piglets from infection which might be due to their susceptibility and higher permissiveness of target cells (152). In most cases nAbs only protect against the homologous strain, but recently also broadly nAbs have been identified (156, 157). Further research focusing on the role of Tfh cells following vaccination and or infection is a prerequisite to further understand humoral immunity which has become possible due to their recent characterization. On the other hand, viremia can be resolved prior to the appearance of nAbs which might implicate the involvement of the cell-mediated immunity (149). As IFN-γ has been shown to limit viral replication, IFN-γ-producing cells might be considered as a correlate of protection (87, 152, 158-161). Another limiting factor is that we do not yet know the T cell epitope landscape of the virus which is further complicated by the swine leukocyte antigen (SLA)-background of the pigs. Several studies are working on the identification of PRRSV antigens (162, 163), which will make it easier to study PRRSV-specific responses and may inform future vaccine development.

4.3.2. Placental infections

In our second study, we investigated the phenotypic changes of immune cells in the maternal-fetal interface that occur following PRRSV infection and or vaccination. Two different PRRSV-1 field isolates were used and based on the study outcome (e.g. difference in reproductive failure based on fetal preservation status) these were designated as 'low' versus 'high' virulent (LV *vs.* HV). Without prior vaccination, we observed a strong and common activation of effector phenotypes and hypothesized that cells with these phenotypes may contribute to excessive inflammatory responses, damaging the maternal-fetal interface and thereby facilitate fetal demise. In fact, during human pregnancy certain pathogens can be vertically transmitted to the fetus which can negatively impact fetal or neonatal life (164). Furthermore, local infections may alter the local microenvironment at the maternal-fetal interface which

could affect the activation status of local immune cells and therefore may hamper the mechanisms that evoke maternal-fetal tolerance (165). Infections, depending on the gestational stage and pathogen, can cause local inflammation which can result in preterm labor and pregnancy loss (164). For instance infection with the bacterium *Treponema pallidum*, causing syphilis, results in inflammation and autolytic changes of placental tissues which have been associated with pregnancy loss and intra-uterine fetal demise (164). In mice, infection with *Listeria monocytogenes* during mid-gestation induced the expression of the chemokine ligand CXCL19 by local innate immune cells promoting the selective infiltration of fetal specific CD8 T cells into the decidua causing fetal losses (166). *Trypanosoma cruzi*, the parasite that causes Chagas disease, can damage and focally detach the maternal-fetal interface (164). Currently, it is thought that this damage is due to apoptosis, and parasite-derived exosomes have also been implicated in inflammation-mediated damage of the placenta (164). The risk for congenital transmission of HCMV, following primary infection, is highest during the third trimester (40-70%) of pregnancy as compared to first and second trimester (30 - 40%) (167). Infection during the early stages of gestation negatively impacts the ability of the trophoblasts to invade (168). The virus can induce local cytokine changes (IL-10, TNF-α, and monocyte-attractant protein-1 (=MIP-1)) and has been shown to downregulate the expression of MHC I molecules expressed by the trophoblasts (168). In context of HCMV, the increase in TNF-α can induce trophoblast apoptosis and the inflammatory response induced by these cytokines might break the maternal-fetal tolerance mechanisms and damage the placenta (168). In addition, modulating the expression of MHC I molecules in trophoblasts might make them a target for NK cells (168). Lastly, HCMV has also been shown to inhibit the activity of indolamine 2,3-dioxygenase, which is also involved in regulating the maternal immune response towards the fetus (168). These may all be mechanisms by which HCMV-infection may cause reproductive complications like fetal loss (168). The transmission rate of Parvovirus B19 is dependent on the gestational stage and in most cases congenital infection is resolved (164). Nevertheless, Parvovirus B19 has been shown to infect trophoblasts and induces apoptosis in these cells and in this case, fetal demise is caused by placental damage (164). Taken together, this indicates that local infections may indeed result in placental damage and that immune-mediated mechanisms can be involved.

4.3.3. Local immune response to PRRSV following infection/vaccination

Depending on the virus strain used, the MLV vaccine provided complete or partial protection in our experimental challenge model. Vaccinated infected gilts were able to mount a local immune response but the magnitude, based on the increase of early effector phenotypes, was reduced compared to non-vaccinated infected gilts. Since the gilts were vaccinated three times prior to infection, we postulated that the subsequent challenge reactivated the memory response induced by the vaccine. The aim of the induced immune memory, in this case the probable induction of PRRSV-specific T (and B) cell responses, is to mount a swift and more

efficient response following the re-exposure to PRRSV. Our analysis focused on phenotypic changes in NK and T cell subsets, the question if the vaccine induced immunological memory remains to be investigated. *In vitro* recall assays using the MLV and/or PRRSV-based peptide pools for restimulation could potentially be used to elucidate the virus-specific T cell responses. In order to answer the question of immunological memory induced by the vaccine, the *in vitro* recall response should be investigated prior to challenge and/ or immediately after challenge following a frequent sampling schedule. Generally, mucosal immunization (e.g. providing the vaccine via the natural route of pathogen entry) has been shown to be superior to systemic immunization to induce Trm cells (169). In our study, three doses of MLV vaccine were applied i.m. prior to infection. Following the injection of an MLV vaccine, which mimics a natural infection, the modified pathogen enters the blood circulation and results in viremia, independent on the route of application (170). Once viremic, the attenuated pathogen disseminates to various organs, including the endometrium, meaning that antigen-presenting cells at multiple sites are activated (170). These cells migrate to the respective lymph nodes where they activate the T cells that will migrate to the site of infection in order to fight the infection (171, 172). When the pathogen is cleared, some of these cells might become Trm cells (171, 172). Furthermore, some T cells in the lymph node might already have been poised to become Trm early on during the infection phase (171, 172). Therefore, it is conceivable that some of the vaccine-induced memory T cells migrated to the ME and acquired features of Trm cells. Upon site-specific re-exposure to a pathogen, these cells can rapidly respond and accelerate the immune response resolving the infection (131, 132). In humans, virus-specific CD8 T cells accumulate in the decidua and protect the fetus (69). Therefore, the potential presence of local and systemic virus-specific memory cells might have contributed to the improved reproductive status. Of note, we did not address PRRSV-specific antibody responses which might have contributed to the protective effects of the vaccine. Clinical parameters and serological responses of the gilts included in our study (with the exception of the low virulent infected groups) in response to vaccination and infection were evaluated in another study (153). Antibodies against PRRSV-1 nucleoprotein were measured using a commercially available ELISA kit (IDEXX PRRS X3 Ab Test®, IDEXX Europe B.V., Hoofddorp, Netherlands) and evaluated via the obtained S/P ratios which are based on a calculation that uses optical density values (153). This study showed that the measured antibody response remained rather stable following three MLV doses (153). Following vaccination and infection the measured antibody response was considerably higher as compared to non-vaccinated animals. Furthermore, vaccinated gilts mounted a quicker antibody response as compared to non-vaccinated gilts (6 dpi *vs*. 14 dpi) (153).

Phenotypic changes following infection and or vaccination were identified. Primary infection with PRRSV induced a stronger effector response compared to vaccinated gilts. An additional aspect, that would need to be elucidated, is the functionality of the isolated cells to eliminate

the virus. For instance, blood-derived NK cells and peripheral $CD3^{+}CD8\alpha^{high}$ CTLs lacked the ability to kill PRRSV-infected pulmonary alveolar macrophages (173, 174). In the study from Cao and colleagues, blood-derived NK cells and PAMs were procured from PRRSV-naive animals (174). The inability of the sorted and *in vitro* activated NK cells to efficiently degranulate and kill PRRSV-infected PAMs in this study was attributed to the expression of viral proteins by the target cells as neither the secretome of PRRSV-infected macrophages nor the MHC class I expression was altered (174). Costers and colleagues aimed to assess the ability of PRRSV-1-specific T cells to eliminate PRRSV-infected macrophages. PAMs were collected from six week old healthy piglets via *in vivo* lung lavages and at 13 weeks of age these piglets were challenged. After challenge a frequent sampling scheme to procure PBMC (total of 12 time points, 0-56 dpi) was applied. Following a five-day *in vitro* restimulation period of total PBMC with the virus, the authors found an increase in the % of $Ki\text{-}67^{+}CD8\alpha^{high}$ lymphocytes, starting 7 dpi, using cytospin and immunofluorescence microscopy. Although an increase in proliferating $CD8\alpha^{high}$ lymphocytes was found, no cytolytic activity towards autologous infected PAMs could be shown until 56 dpi. It is currently not known if this functional impairment of peripheral immune cells in context of PRRSV would also apply to the cells locally residing at the maternal-fetal interface. Besides the killing capacity or degranulation capacity, of for instance NK and CD8 T cells, in T cells the capacity to produce IFN-γ, TNF-α, and IL-2 could also be measured following *in vitro* restimulation. This would allow for the identification of single, co- and triple-cytokine producing T cells. Such multifunctional T cells produce more of these effector molecules as compared to the single-producers (17). Furthermore, multifunctional T cells perform enhanced effector functions which correlates with a protective immune response (175). Unfortunately, limited data is available on T cell phenotypes and function in tissues in context of PRRSV. As to date, one can only speculate about the specificity and functionality of immune cells in response to the local PRRSV infection. Overall, infections can induce virus-specific T cells but besides that also other T cells, which are not specific to the virus of interest, may be activated via a phenomenon that is called bystander activation (176). Bystander activation of T cells is an antigen-independent process which can be mediated by certain cytokines. For instance, type I interferons, IL-12, IL-18, and IL-15 have been shown to be play a role in bystander activation (176, 177). Alternatively, bystander activation may also be achieved via stimulation of Toll like receptors expressed on effector/memory T cells (176). However, evidence for toll-like receptor mediated bystander activation in context of viral infections still needs to be corroborated (176). These bystander activated T cells may either mediate protective or damaging responses (176).

In situ immunofluorescence experiments demonstrated the increase of $CD3^{-}CD8\alpha^{+}$ NK cells in PRRSV-infected females already 10 dpi (116). These cells were mostly localized in close proximity of blood vessels and the uterine epithelium (116). Based on previous findings that

porcine endometrial NK cells were able to kill early gestation trophoblasts (80), the authors postulated that due to the close proximity of these potential NK cells to the uterine epithelium, these cells could potentially damage the maternal-fetal interface (116). A time course experiment using immunofluorescence microscopy after PRRSV-2 infection of late-term pregnant gilts has demonstrated that the virus can already be detected in the FP two days following infection of the dam (122). It would be interesting to study various immune cell subsets in a similar manner, as it could provide insight in the local changes that occur (e.g. shift from innate to adaptive responses). Although many studies showed a delay in the peripheral adaptive immune cell responses towards PRRSV, local T cells in the lung could already be observed 10 dpi and appear to be linked to viral clearance (160). Another interesting aspect to explore would be the possible imbalance between effector and regulatory mechanisms caused by infection.

4.4. Outlook

Overall, this PhD project investigated immune cell phenotypes that reside at the porcine maternal-fetal interface during late gestation and highlighted distinctive differences between the maternal- and fetal compartment. Primary exposure to PRRSV resulted in a local activation of effector phenotypes which might negatively impact the integrity of the maternal-fetal interface and might therefore play a role in the pathogenesis of reproductive failure. On the other hand, pre-exposure via vaccination conferred protection; however, depending on the virus strain this might not be sufficient. In addition, this work also raised a lot of questions that need to be addressed, for example the specificity of cells at the maternal-fetal interface, the function of the cells over the course of gestation, microchimerism, and the role of CD8 T cells in inducing placental pathology following PRRSV-infection. Furthermore, this work also provides a methodological approach which could be extrapolated to other pathogens that can be transmitted *in utero*.

5. References

1. Denyer MS, Wileman TE, Stirling CM, Zuber B, Takamatsu HH. Perforin expression can define CD8 positive lymphocyte subsets in pigs allowing phenotypic and functional analysis of natural killer, cytotoxic T, natural killer T and MHC un-restricted cytotoxic T-cells. Vet Immunol Immunopathol. 2006;110(3-4):279-92.
2. Mair KH, Essler SE, Patzl M, Storset AK, Saalmüller A, Gerner W. NKp46 expression discriminates porcine NK cells with different functional properties. Eur J Immunol. 2012;42(5):1261-71.
3. Mair KH, Müllebner A, Essler SE, Duvigneau JC, Storset AK, Saalmüller A, et al. Porcine CD8adim/-NKp46high NK cells are in a highly activated state. Vet Res. 2013;44:13.
4. Sedlak C, Patzl M, Saalmüller A, Gerner W. CD2 and CD8a define porcine gd T cells with distinct cytokine production profiles. Dev Comp Immunol. 2014;45(1):97-106.
5. Rodríguez-Gómez IM, Talker SC, Käser T, Stadler M, Reiter L, Ladinig A, et al. Expression of T-Bet, Eomesodermin, and GATA-3 Correlates with distinct phenotypes and functional properties in porcine gd T Cells. Front Immunol. 2019;10:396.
6. Bonneville M, O'Brien RL, Born WK. Gammadelta T cell effector functions: a blend of innate programming and acquired plasticity. Nat Rev Immunol. 2010;10(7):467-78.
7. Vantourout P, Hayday A. Six-of-the-best: unique contributions of gammadelta T cells to immunology. Nat Rev Immunol. 2013;13(2):88-100.
8. Stepanova K, Sinkora M. Porcine gammadelta T lymphocytes can be categorized into two functionally and developmentally distinct subsets according to expression of CD2 and level of TCR. J Immunol. 2013;190(5):2111-20.
9. Uehlein S, Ding X, Flosser J, Schmidt S, Steitz J, Bille M, et al. Human-like Response of Pig T Cells to Superagonistic Anti-CD28 Monoclonal Antibodies. J Immunol. 2021;207(10):2473-88.
10. Swain SL, McKinstry KK, Strutt TM. Expanding roles for CD4(+) T cells in immunity to viruses. Nat Rev Immunol. 2012;12(2):136-48.
11. Rodríguez-Gómez IM, Talker SC, Käser T, Stadler M, Hammer SE, Saalmüller A, et al. Expression of T-bet, Eomesodermin and GATA-3 in porcine αβ T cells. Dev Comp Immunol. 2016;60:115-26.
12. Reutner K, Leitner J, Müllebner A, Ladinig A, Essler SE, Duvigneau JC, et al. CD27 expression discriminates porcine T helper cells with functionally distinct properties. Vet Res. 2013;44:18.
13. Ebner F, Rausch S, Scharek-Tedin L, Pieper R, Burwinkel M, Zentek J, et al. A novel lineage transcription factor based analysis reveals differences in T helper cell subpopulation development in infected and intrauterine growth restricted (IUGR) piglets. Dev Comp Immunol. 2014;46(2):333-40.

14. Gerner W, Mair KH, Schmidt S. Local and Systemic T Cell Immunity in Fighting Pig Viral and Bacterial Infections. Annu Rev Anim Biosci. 2022;10:349-72.
15. Gerner W, Talker SC, Koinig HC, Sedlak C, Mair KH, Saalmüller A. Phenotypic and functional differentiation of porcine ab T cells: current knowledge and available tools. Mol Immunol. 2015;66(1):3-13.
16. Saalmüller A, Werner T, Fachinger V. T-helper cells from naive to committed. Vet Immunol Immunopathol. 2002;87(3-4):137-45.
17. Talker SC, Koinig HC, Stadler M, Graage R, Klingler E, Ladinig A, et al. Magnitude and kinetics of multifunctional $CD4^+$ and $CD8\beta^+$ T cells in pigs infected with swine influenza A virus. Vet Res. 2015;46:52.
18. Kick AR, Amaral AF, Cortes LM, Fogle JE, Crisci E, Almond GW, et al. The T-Cell Response to Type 2 Porcine Reproductive and Respiratory Syndrome Virus (PRRSV). Viruses. 2019;11(9):796.
19. Talker SC, Käser T, Reutner K, Sedlak C, Mair KH, Koinig H, et al. Phenotypic maturation of porcine NK- and T-cell subsets. Dev Comp Immunol. 2013;40(1):51-68.
20. DuPage M, Bluestone JA. Harnessing the plasticity of CD4(+) T cells to treat immune-mediated disease. Nat Rev Immunol. 2016;16(3):149-63.
21. Käser T, Gerner W, Hammer SE, Patzl M, Saalmüller A. Phenotypic and functional characterisation of porcine CD4(+)CD25(high) regulatory T cells. Vet Immunol Immunopathol. 2008;122(1-2):153-8.
22. Schmidt S, Kreutzmann H, Stadler M, Mair KH, Stas MR, Koch M, et al. T-Cell Cytokine Response in Salmonella Typhimurium-Vaccinated versus Infected Pigs. Vaccines (Basel). 2021;9(8).
23. Lagumdzic E, Pernold C, Viano M, Olgiati S, Schmitt MW, Mair KH, et al. Transcriptome Profiling of Porcine Naive, Intermediate and Terminally Differentiated CD8(+) T Cells. Front Immunol. 2022;13:849922.
24. Martini V, Edmans M, Gubbins S, Jayaraman S, Paudyal B, Morgan S, et al. Spatial, temporal and molecular dynamics of swine influenza virus-specific CD8 tissue resident memory T cells. Mucosal Immunol. 2022;15(3):428-42.
25. Wong P, Pamer EG. CD8 T cell responses to infectious pathogens. Annu Rev Immunol. 2003;21:29-70.
26. Schmidt ME, Varga SM. The CD8 T Cell Response to Respiratory Virus Infections. Front Immunol. 2018;9:678.
27. Ezquerra A, Revilla C, Alvarez B, Perez C, Alonso F, Dominguez J. Porcine myelomonocytic markers and cell populations. Dev Comp Immunol. 2009;33(3):284-98.
28. Su CM, Rowland RRR, Yoo D. Recent Advances in PRRS Virus Receptors and the Targeting of Receptor-Ligand for Control. Vaccines (Basel). 2021;9(4):354.

29. Geisert RD, Sutvosky P, Lucy MC, Bartol FF, Meyer AE. Reproductive physiology of swine. In: Bazer F.W. LGC, Wu G., editors, editor. Animal Agriculture: London: Academic Press; 2020. p. 263–81.
30. Almeida F, Dias A. Pregnancy in pigs: the journey of an early life. Domest Anim Endocrinol. 2022;78:106656.
31. Karniychuk UU, Nauwynck HJ. Pathogenesis and prevention of placental and transplacental porcine reproductive and respiratory syndrome virus infection. Vet Res. 2013;44:95.
32. Bazer FW, Johnson GA. Pig blastocyst-uterine interactions. Differentiation. 2014;87(1-2):52-65.
33. Tan C, Huang Z, Xiong W, Ye H, Deng J, Yin Y. A review of the amino acid metabolism in placental function response to fetal loss and low birth weight in pigs. J Anim Sci Biotechnol. 2022;13(1):28.
34. Mathew DJ, Lucy MC, R DG. Interleukins, interferons, and establishment of pregnancy in pigs. Reproduction. 2016;151(6):R111-22.
35. Fiorimanti MR, Cristofolini AL, Moreira-Espinoza MJ, Rabaglino MB, Barbeito CG, Merkis CI. Placental vascularization in middle and late gestation in the pig. Reprod Fertil. 2022;3(1):57-66.
36. Furukawa S, Kuroda Y, Sugiyama A. A comparison of the histological structure of the placenta in experimental animals. J Toxicol Pathol. 2014;27(1):11-8.
37. Mor G, Aldo P, Alvero AB. The unique immunological and microbial aspects of pregnancy. Nat Rev Immunol. 2017;17(8):469-82.
38. Ander SE, Diamond MS, Coyne CB. Immune responses at the maternal-fetal interface. Sci Immunol. 2019;4(31).
39. Ochoa-Bernal MA, Fazleabas AT. Physiologic Events of Embryo Implantation and Decidualization in Human and Non-Human Primates. Int J Mol Sci. 2020;21(6).
40. Ng SW, Norwitz GA, Pavlicev M, Tilburgs T, Simon C, Norwitz ER. Endometrial Decidualization: The Primary Driver of Pregnancy Health. Int J Mol Sci. 2020;21(11).
41. Kim YB. Developmental immunity in the piglet. Birth Defects Orig Artic Ser. 1975;11(1):549-57.
42. Spencer TE, Kelleher AM, Bartol FF. Development and Function of Uterine Glands in Domestic Animals. Annu Rev Anim Biosci. 2019;7:125-47.
43. Schumacher A, Sharkey DJ, Robertson SA, Zenclussen AC. Immune Cells at the Fetomaternal Interface: How the Microenvironment Modulates Immune Cells To Foster Fetal Development. J Immunol. 2018;201(2):325-34.
44. Shah NM, Herasimtschuk AA, Boasso A, Benlahrech A, Fuchs D, Imami N, et al. Changes in T cell and dendritic cell phenotype from mid to late pregnancy are indicative of a shift from immune tolerance to immune activation. Front Immunol. 2017;8:1138.

45. Tilburgs T, Claas FH, Scherjon SA. Elsevier Trophoblast Research Award Lecture: Unique properties of decidual T cells and their role in immune regulation during human pregnancy. Placenta. 2010;31 Suppl:S82-6.
46. Gaynor LM, Colucci F. Uterine Natural Killer cells: functional distinctions and influence on pregnancy in humans and mice. Front Immunol. 2017;8:467.
47. de Mendonca Vieira R, Meagher A, Crespo AC, Kshirsagar SK, Iyer V, Norwitz ER, et al. Human Term Pregnancy Decidual NK Cells Generate Distinct Cytotoxic Responses. J Immunol. 2020;204(12):3149-59.
48. Hanna J, Goldman-Wohl D, Hamani Y, Avraham I, Greenfield C, Natanson-Yaron S, et al. Decidual NK cells regulate key developmental processes at the human fetal-maternal interface. Nat Med. 2006;12(9):1065-74.
49. Anacker J, Segerer SE, Hagemann C, Feix S, Kapp M, Bausch R, et al. Human decidua and invasive trophoblasts are rich sources of nearly all human matrix metalloproteinases. Mol Hum Reprod. 2011;17(10):637-52.
50. Siewiera J, El Costa H, Tabiasco J, Berrebi A, Cartron G, Le Bouteiller P, et al. Human cytomegalovirus infection elicits new decidual natural killer cell effector functions. PLoS Pathog. 2013;9(4):e1003257.
51. Tilburgs T, Evans JH, Crespo AC, Strominger JL. The HLA-G cycle provides for both NK tolerance and immunity at the maternal-fetal interface. Proc Natl Acad Sci U S A. 2015;112(43):13312-7.
52. Crespo AC, Strominger JL, Tilburgs T. Expression of KIR2DS1 by decidual natural killer cells increases their ability to control placental HCMV infection. Proc Natl Acad Sci U S A. 2016;113(52):15072-7.
53. Crespo AC, Mulik S, Dotiwala F, Ansara JA, Sen Santara S, Ingersoll K, et al. Decidual NK Cells Transfer Granulysin to Selectively Kill Bacteria in Trophoblasts. Cell. 2020;182(5):1125-39 e18.
54. Sen Santara S, Crespo AC, Mulik S, Ovies C, Boulenouar S, Strominger JL, et al. Decidual NK cells kill Zika virus-infected trophoblasts. Proc Natl Acad Sci U S A. 2021;118(47).
55. Vassiliadou N, Bulmer JN. Quantitative analysis of T lymphocyte subsets in pregnant and nonpregnant human endometrium. Biol Reprod. 1996;55(5):1017-22.
56. Tilburgs T, van der Mast BJ, Nagtzaam NM, Roelen DL, Scherjon SA, Claas FH. Expression of NK cell receptors on decidual T cells in human pregnancy. J Reprod Immunol. 2009;80(1-2):22-32.
57. Terzieva A, Dimitrova V, Djerov L, Dimitrova P, Zapryanova S, Hristova I, et al. Early Pregnancy Human Decidua is Enriched with Activated, Fully Differentiated and Pro-Inflammatory Gamma/Delta T Cells with Diverse TCR Repertoires. Int J Mol Sci. 2019;20(3).
58. Saito S, Nishikawa K, Morii T, Narita N, Enomoto M, Ito A, et al. A study of CD45RO, CD45RA and CD29 antigen expression on human decidual T cells in an early stage of pregnancy. Immunol Lett. 1994;40(3):193-7.

59. van der Zwan A, Bi K, Norwitz ER, Crespo AC, Claas FHJ, Strominger JL, et al. Mixed signature of activation and dysfunction allows human decidual $CD8^+$ T cells to provide both tolerance and immunity. Proc Natl Acad Sci U S A. 2018;115(2):385-90.
60. Tilburgs T, Schonkeren D, Eikmans M, Nagtzaam NM, Datema G, Swings GM, et al. Human decidual tissue contains differentiated CD8+ effector-memory T cells with unique properties. J Immunol. 2010;185(7):4470-7.
61. Powell RM, Lissauer D, Tamblyn J, Beggs A, Cox P, Moss P, et al. Decidual T cells exhibit a highly differentiated phenotype and demonstrate potential fetal specificity and a strong transcriptional response to interferon. J Immunol. 2017;199(10):3406-17.
62. Mjösberg J, Berg G, Jenmalm MC, Ernerudh J. FOXP3+ regulatory T cells and T helper 1, T helper 2, and T helper 17 cells in human early pregnancy decidua. Biol Reprod. 2010;82(4):698-705.
63. Feyaerts D, Benner M, van Cranenbroek B, van der Heijden OWH, Joosten I, van der Molen RG. Human uterine lymphocytes acquire a more experienced and tolerogenic phenotype during pregnancy. Sci Rep. 2017;7(1):2884.
64. Graham JJ, Longhi MS, Heneghan MA. T helper cell immunity in pregnancy and influence on autoimmune disease progression. J Autoimmun. 2021;121:102651.
65. Wang W, Sung N, Gilman-Sachs A, Kwak-Kim J. T Helper (Th) Cell Profiles in Pregnancy and Recurrent Pregnancy Losses: Th1/Th2/Th9/Th17/Th22/Tfh Cells. Front Immunol. 2020;11:2025.
66. Gomez-Lopez N, Vega-Sanchez R, Castillo-Castrejon M, Romero R, Cubeiro-Arreola K, Vadillo-Ortega F. Evidence for a role for the adaptive immune response in human term parturition. Am J Reprod Immunol. 2013;69(3):212-30.
67. Scaife PJ, Bulmer JN, Robson SC, Innes BA, Searle RF. Effector activity of decidual CD8+ T lymphocytes in early human pregnancy. Biol Reprod. 2006;75(4):562-7.
68. Tilburgs T, Scherjon SA, Roelen DL, Claas FH. Decidual CD8+CD28- T cells express CD103 but not perforin. Hum Immunol. 2009;70(2):96-100.
69. van Egmond A, van der Keur C, Swings GM, Scherjon SA, Claas FH. The possible role of virus-specific CD8(+) memory T cells in decidual tissue. J Reprod Immunol. 2016;113:1-8.
70. van der Zwan A, van der Meer-Prins EMW, van Miert P, van den Heuvel H, Anholts JDH, Roelen DL, et al. Cross-Reactivity of Virus-Specific CD8+ T Cells Against Allogeneic HLA-C: Possible Implications for Pregnancy Outcome. Front Immunol. 2018;9:2880.
71. Tilburgs T, Roelen DL, van der Mast BJ, de Groot-Swings GM, Kleijburg C, Scherjon SA, et al. Evidence for a selective migration of fetus-specific CD4+CD25bright regulatory T cells from the peripheral blood to the decidua in human pregnancy. J Immunol. 2008;180(8):5737-45.
72. Shima T, Inada K, Nakashima A, Ushijima A, Ito M, Yoshino O, et al. Paternal antigen-specific proliferating regulatory T cells are increased in uterine-draining lymph nodes just

before implantation and in pregnant uterus just after implantation by seminal plasma-priming in allogeneic mouse pregnancy. J Reprod Immunol. 2015;108:72-82.
73. Tsuda S, Nakashima A, Shima T, Saito S. New Paradigm in the Role of Regulatory T Cells During Pregnancy. Front Immunol. 2019;10:573.
74. Salvany-Celades M, van der Zwan A, Benner M, Setrajcic-Dragos V, Bougleux Gomes HA, Iyer V, et al. Three Types of Functional Regulatory T Cells Control T Cell Responses at the Human Maternal-Fetal Interface. Cell Rep. 2019;27(9):2537-47 e5.
75. Tsuda S, Sameshima A, Sekine M, Kawaguchi H, Fujita D, Makino S, et al. Pre-conception status, obstetric outcome and use of medications during pregnancy of systemic lupus erythematosus (SLE), rheumatoid arthritis (RA) and inflammatory bowel disease (IBD) in Japan: Multi-center retrospective descriptive study. Mod Rheumatol. 2020;30(5):852-61.
76. Engelhardt H, Croy BA, King GJ. Conceptus influences the distribution of uterine leukocytes during early porcine pregnancy. Biol Reprod. 2002;66(6):1875-80.
77. Engelhardt H, Croy BA, King GJ. Evaluation of natural killer cell recruitment to embryonic attachment sites during early porcine pregnancy. Biol Reprod. 2002;66(4):1185-92.
78. Dimova T, Mihaylova A, Spassova P, Georgieva R. Superficial implantation in pigs is associated with decreased numbers and redistribution of endometrial NK-cell populations. Am J Reprod Immunol. 2008;59(4):359-69.
79. Yu Z, Croy BA, Chapeau C, King GJ. Elevated endometrial natural killer cell activity during early porcine pregnancy is conceptus-mediated. J Reprod Immunol. 1993;24(2):153-64.
80. Yu Z, Croy BA, King GJ. Lysis of porcine trophoblast cells by endometrial natural killer-like effector cells in vitro does not require interleukin-2. Biol Reprod. 1994;51(6):1279-84.
81. Dimova T, Mihaylova A, Spassova P, Georgieva R. Establishment of the porcine epitheliochorial placenta is associated with endometrial T-cell recruitment. Am J Reprod Immunol. 2007;57(4):250-61.
82. Murphy SP, Tayade C, Ashkar AA, Hatta K, Zhang J, Croy BA. Interferon gamma in successful pregnancies. Biol Reprod. 2009;80(5):848-59.
83. Johns DN, Lucas CG, Pfeiffer CA, Chen PR, Meyer AE, Perry SD, et al. Conceptus interferon gamma is essential for establishment of pregnancy in the pig. Biol Reprod. 2021;105(6):1577-90.
84. Kim M, Seo H, Choi Y, Shim J, Bazer FW, Ka H. Swine leukocyte antigen-DQ expression and its regulation by interferon-gamma at the maternal-fetal interface in pigs. Biol Reprod. 2012;86(2):43.
85. Wessels JM, Linton NF, van den Heuvel MJ, Cnossen SA, Edwards AK, Croy BA, et al. Expression of chemokine decoy receptors and their ligands at the porcine maternal-fetal interface. Immunol Cell Biol. 2011;89(2):304-13.

86. Yoo I, Kye YC, Han J, Kim M, Lee S, Jung W, et al. Uterine epithelial expression of the tumor necrosis factor superfamily: a strategy for immune privilege during pregnancy in a true epitheliochorial placentation species. Biol Reprod. 2020;102(4):828-42.
87. Lunney JK, Fang Y, Ladinig A, Chen N, Li Y, Rowland B, et al. Porcine Reproductive and Respiratory Syndrome Virus (PRRSV): Pathogenesis and Interaction with the Immune System. Annu Rev Anim Biosci. 2016;4:129-54.
88. Nieuwenhuis N, Duinhof TF, van Nes A. Economic analysis of outbreaks of porcine reproductive and respiratory syndrome virus in nine sow herds. Vet Rec. 2012;170(9):225.
89. Holtkamp DJ, Kliebenstein JB, Neumann EJ, Zimmerman JJ, Rotto HF, Yoder TK, et al. Assessment of the economic impact of porcine reproductive and respiratory syndrome virus on United States pork producers. JSHAP. 2013;21(2):72-84.
90. Christianson WT, Joo HS. Porcine reproductive and respiratory syndrome: A review. . JASHAP. 1994;2(2):10-28.
91. Adams MJ, Lefkowitz EJ, King AM, Harrach B, Harrison RL, Knowles NJ, et al. Ratification vote on taxonomic proposals to the International Committee on Taxonomy of Viruses (2016). Arch Virol. 2016;161(10):2921-49.
92. Kuhn JH, Lauck M, Bailey AL, Shchetinin AM, Vishnevskaya TV, Bao Y, et al. Reorganization and expansion of the nidoviral family Arteriviridae. Arch Virol. 2016;161(3):755-68.
93. Brinton MA, Gulyaeva AA, Balasuriya UBR, Dunowska M, Faaberg KS, Goldberg T, et al. ICTV Virus Taxonomy Profile: Arteriviridae 2021. Journal of General Virology. 2021;102(8).
94. Balka G, Podgórska K, Brar MS, Bálint A, Cadar D, Celer V, et al. Genetic diversity of PRRSV 1 in Central Eastern Europe in 1994-2014: origin and evolution of the virus in the region. Sci Rep. 2018;8(1):7811.
95. Paploski IAD, Corzo C, Rovira A, Murtaugh MP, Sanhueza JM, Vilalta C, et al. Temporal Dynamics of Co-circulating Lineages of Porcine Reproductive and Respiratory Syndrome Virus. Front Microbiol. 2019;10:2486.
96. Stadejek T, Stankevicius A, Murtaugh MP, Oleksiewicz MB. Molecular evolution of PRRSV in Europe: current state of play. Vet Microbiol. 2013;165(1-2):21-8.
97. de Abin MF, Spronk G, Wagner M, Fitzsimmons M, Abrahante JE, Murtaugh MP. Comparative infection efficiency of Porcine reproductive and respiratory syndrome virus field isolates on MA104 cells and porcine alveolar macrophages. Can J Vet Res. 2009;73(3):200-4.
98. Martínez-Lobo FJ, Díez-Fuertes F, Segalés J, García-Artiga C, Simarro I, Castro JM, et al. Comparative pathogenicity of type 1 and type 2 isolates of porcine reproductive and respiratory syndrome virus (PRRSV) in a young pig infection model. Vet Microbiol. 2011;154(1-2):58-68.
99. Halbur PG, Paul PS, Meng XJ, Lum MA, Andrews JJ, Rathje JA. Comparative pathogenicity of nine US porcine reproductive and respiratory syndrome virus (PRRSV)

isolates in a five-week-old cesarean-derived, colostrum-deprived pig model. J Vet Diagn Invest. 1996;8(1):11-20.
100. Duan X, Nauwynck HJ, Pensaert MB. Effects of origin and state of differentiation and activation of monocytes/macrophages on their susceptibility to porcine reproductive and respiratory syndrome virus (PRRSV). Arch Virol. 1997;142(12):2483-97.
101. Duan X, Nauwynck HJ, Pensaert MB. Virus quantification and identification of cellular targets in the lungs and lymphoid tissues of pigs at different time intervals after inoculation with porcine reproductive and respiratory syndrome virus (PRRSV). Vet Microbiol. 1997;56(1-2):9-19.
102. Karniychuk UU, Nauwynck HJ. Quantitative changes of sialoadhesin and CD163 positive macrophages in the implantation sites and organs of porcine embryos/fetuses during gestation. Placenta. 2009;30(6):497-500.
103. Bordet E, Maisonnasse P, Renson P, Bouguyon E, Crisci E, Tiret M, et al. Porcine Alveolar Macrophage-like cells are pro-inflammatory Pulmonary Intravascular Macrophages that produce large titers of Porcine Reproductive and Respiratory Syndrome Virus. Sci Rep. 2018;8(1):10172.
104. Frydas IS, Verbeeck M, Cao J, Nauwynck HJ. Replication characteristics of porcine reproductive and respiratory syndrome virus (PRRSV) European subtype 1 (Lelystad) and subtype 3 (Lena) strains in nasal mucosa and cells of the monocytic lineage: indications for the use of new receptors of PRRSV (Lena). Vet Res. 2013;44:73.
105. Loving CL, Brockmeier SL, Sacco RE. Differential type I interferon activation and susceptibility of dendritic cell populations to porcine arterivirus. Immunology. 2007;120(2):217-29.
106. Frydas IS, Nauwynck HJ. Replication characteristics of eight virulent and two attenuated genotype 1 and 2 porcine reproductive and respiratory syndrome virus (PRRSV) strains in nasal mucosa explants. Vet Microbiol. 2016;182:156-62.
107. Xie J, Vereecke N, Theuns S, Oh D, Vanderheijden N, Trus I, et al. Comparison of Primary Virus Isolation in Pulmonary Alveolar Macrophages and Four Different Continuous Cell Lines for Type 1 and Type 2 Porcine Reproductive and Respiratory Syndrome Virus. Vaccines (Basel). 2021;9(6).
108. Suleman M, Malgarin CM, Detmer SE, Harding JCS, MacPhee DJ. The porcine trophoblast cell line PTr2 is susceptible to porcine reproductive and respiratory syndrome virus-2 infection. Placenta. 2019;88:44-51.
109. Van Breedam W, Delputte PL, Van Gorp H, Misinzo G, Vanderheijden N, Duan X, et al. Porcine reproductive and respiratory syndrome virus entry into the porcine macrophage. J Gen Virol. 2010;91(Pt 7):1659-67.
110. Whitworth KM, Rowland RR, Ewen CL, Trible BR, Kerrigan MA, Cino-Ozuna AG, et al. Gene-edited pigs are protected from porcine reproductive and respiratory syndrome virus. Nat Biotechnol. 2016;34(1):20-2.

111. Xie J, Christiaens I, Yang B, Trus I, Devriendt B, Cui T, et al. Preferential use of Siglec-1 or Siglec-10 by type 1 and type 2 PRRSV strains to infect PK15(S1-CD163) and PK15(S10-CD163) cells. Vet Res. 2018;49(1):67.
112. Zimmerman JJ, Dee SA, Holtkamp DJ, Murtaugh MP, Stadejek T, Stevenson GW, et al. Porcine Reproductive and Respiratory Syndrome Viruses (Porcine Arteriviruses). In: Zimmerman JJ, Karriker LA, Ramirez A, Schwartz KJ, Stevenson GW, Zhang J, et al., editors. Diseases of Swine. 11th ed: John Wiley & Sons, Inc., Hoboken; 2019. p. 685-708.
113. Terpstra C, Wensvoort G, Pol JM. Experimental reproduction of porcine epidemic abortion and respiratory syndrome (mystery swine disease) by infection with Lelystad virus: Koch's postulates fulfilled. Vet Q. 1991;13(3):131-6.
114. Mengeling WL, Lager KM, Vorwald AC. Temporal characterization of transplacental infection of porcine fetuses with porcine reproductive and respiratory syndrome virus. Am J Vet Res. 1994;55(10):1391-8.
115. Cheon DS, Chae C. Distribution of porcine reproductive and respiratory syndrome virus in stillborn and liveborn piglets from experimentally infected sows. J Comp Pathol. 2001;124(4):231-7.
116. Karniychuk UU, De Spiegelaere W, Nauwynck HJ. Porcine reproductive and respiratory syndrome virus infection is associated with an increased number of Sn-positive and CD8-positive cells in the maternal-fetal interface. Virus Res. 2013;176(1-2):285-91.
117. Karniychuk UU, Saha D, Geldhof M, Vanhee M, Cornillie P, Van den Broeck W, et al. Porcine reproductive and respiratory syndrome virus (PRRSV) causes apoptosis during its replication in fetal implantation sites. Microb Pathog. 2011;51(3):194-202.
118. Novakovic P, Harding JC, Al-Dissi AN, Detmer SE. Type 2 porcine reproductive and respiratory syndrome virus infection increases apoptosis at the maternal-fetal interface in late gestation pregnant gilts. PLoS One. 2017;12(3):e0173360.
119. Guidoni PB, Pasternak JA, Hamonic G, MacPhee DJ, Harding JCS. Effect of porcine reproductive and respiratory syndrome virus 2 on tight junction gene expression at the maternal-fetal interface. Theriogenology. 2022;184:162-70.
120. Guidoni PB, Pasternak JA, Hamonic G, MacPhee DJ, Harding JCS. Decreased tight junction protein intensity in the placenta of porcine reproductive and respiratory syndrome virus-2 infected fetuses. Placenta. 2021;112:153-61.
121. Novakovic P, Harding JC, Ladinig A, Al-Dissi AN, MacPhee DJ, Detmer SE. Relationships of CD163 and CD169 positive cell numbers in the endometrium and fetal placenta with type 2 PRRSV RNA concentration in fetal thymus. Vet Res. 2016;47(1):76.
122. Suleman M, Novakovic P, Malgarin CM, Detmer SE, Harding JCS, MacPhee DJ. Spatiotemporal immunofluorescent evaluation of porcine reproductive and respiratory syndrome virus transmission across the maternal-fetal interface. Pathog Dis. 2018;76(5):fty060.

123. Barrera-Zarate J, Detmer SE, Pasternak JA, Hamonic G, MacPhee DJ, Harding JCS. Detection of PRRSV-2 alone and co-localized with CD163 positive macrophages in porcine placental areolae. Vet Immunol Immunopathol. 2022;250:110457.
124. Blanes MS, Tsoi SC, Dyck MK. Accurate and Phenol Free DNA Sexing of Day 30 Porcine Embryos by PCR. J Vis Exp. 2016(108):53301.
125. Milburn JV, Hoog AM, Winkler S, van Dongen KA, Leitner J, Patzl M, et al. Expression of CD9 on porcine lymphocytes and its relation to T cell differentiation and cytokine production. Dev Comp Immunol. 2021;121:104080.
126. Hayashi Y, Okutani M, Ogawa S, Tsukahara T, Inoue R. Generation of anti-porcine CD69 monoclonal antibodies and their usefulness to evaluate early activation of cellular immunity by flow cytometric analysis. Anim Sci J. 2018;89(5):825-32.
127. Monteiro C, Kasahara TM, Castro JR, Sacramento PM, Hygino J, Centuriao N, et al. Pregnancy favors the expansion of circulating functional follicular helper T Cells. J Reprod Immunol. 2017;121:1-10.
128. Zeng W, Liu Z, Zhang S, Ren J, Ma X, Qin C, et al. Characterization of T follicular helper cells in allogeneic normal pregnancy and PDL1 blockage-induced abortion. Sci Rep. 2016;6:36560.
129. Hoog A, Villanueva-Hernandez S, Razavi MA, van Dongen K, Eder T, Piney L, et al. Identification of CD4(+) T cells with T follicular helper cell characteristics in the pig. Dev Comp Immunol. 2022;134:104462.
130. Ruedas-Torres I, Rodriguez-Gomez IM, Sanchez-Carvajal JM, Guil-Luna S, Larenas-Munoz F, Pallares FJ, et al. Up-Regulation of Immune Checkpoints in the Thymus of PRRSV-1-Infected Piglets in a Virulence-Dependent Fashion. Front Immunol. 2021;12:671743.
131. Kumar BV, Ma W, Miron M, Granot T, Guyer RS, Carpenter DJ, et al. Human Tissue-Resident Memory T Cells Are Defined by Core Transcriptional and Functional Signatures in Lymphoid and Mucosal Sites. Cell Rep. 2017;20(12):2921-34.
132. Schenkel JM, Masopust D. Tissue-resident memory T cells. Immunity. 2014;41(6):886-97.
133. Benner M, Ferwerda G, Joosten I, van der Molen RG. How uterine microbiota might be responsible for a receptive, fertile endometrium. Hum Reprod Update. 2018;24(4):393-415.
134. Heil BA, Paccamonti DL, Sones JL. Role for the mammalian female reproductive tract microbiome in pregnancy outcomes. Physiol Genomics. 2019;51(8):390-9.
135. Altmae S, Franasiak JM, Mandar R. The seminal microbiome in health and disease. Nat Rev Urol. 2019;16(12):703-21.
136. Segales J, Allan GM, Domingo M. Circoviruses. In: Zimmerman JJ, Karriker LA, Ramirez A, Schwartz KJ, Stevenson GW, Zhang J, et al., editors. Diseases of Swine. 11th ed: John Wiley & Sons, Inc., Hoboken; 2019. p. 473-87.

137. Truyen U, Streck AF. Parvoviruses. In: Zimmerman JJ, Karriker LA, Ramirez A, Schwartz KJ, Stevenson GW, Zhang J, et al., editors. Diseases of Swine. 11th edition ed: John Wiley & Sons, Inc., Hoboken; 2019. p. 611-21.
138. Opriessnig T, Coutinho TA. Erysipelas. In: Zimmerman JJ, Karriker LA, Ramirez A, Schwartz KJ, Stevenson GW, Zhang J, et al., editors. Diseases of Swine. 11th ed: John Wiley & Sons, Inc., Hoboken; 2019. p. 835-43.
139. Petroff MG, Nguyen SL, Ahn SH. Fetal-placental antigens and the maternal immune system: Reproductive immunology comes of age. Immunol Rev. 2022;308(1):25-39.
140. Lissauer D, Piper K, Goodyear O, Kilby MD, Moss PA. Fetal-specific CD8+ cytotoxic T cell responses develop during normal human pregnancy and exhibit broad functional capacity. J Immunol. 2012;189(2):1072-80.
141. Tilburgs T, Scherjon SA, van der Mast BJ, Haasnoot GW, Versteeg VDV-MM, Roelen DL, et al. Fetal-maternal HLA-C mismatch is associated with decidual T cell activation and induction of functional T regulatory cells. J Reprod Immunol. 2009;82(2):148-57.
142. Wang S, Chen C, Li M, Qian J, Sun F, Li Y, et al. Blockade of CTLA-4 and Tim-3 pathways induces fetal loss with altered cytokine profiles by decidual CD4(+)T cells. Cell Death Dis. 2019;10(1):15.
143. Wang S, Sun F, Li M, Qian J, Chen C, Wang M, et al. The appropriate frequency and function of decidual Tim-3(+)CTLA-4(+)CD8(+) T cells are important in maintaining normal pregnancy. Cell Death Dis. 2019;10(6):407.
144. Garrels W, Holler S, Taylor U, Herrmann D, Niemann H, Ivics Z, et al. Assessment of fetal cell chimerism in transgenic pig lines generated by Sleeping Beauty transposition. PLoS One. 2014;9(5):e96673.
145. Karniychuk UU, Van Breedam W, Van Roy N, Rogel-Gaillard C, Nauwynck HJ. Demonstration of microchimerism in pregnant sows and effects of congenital PRRSV infection. Vet Res. 2012;43:19.
146. Stinson LF, Boyce MC, Payne MS, Keelan JA. The Not-so-Sterile Womb: Evidence That the Human Fetus Is Exposed to Bacteria Prior to Birth. Front Microbiol. 2019;10:1124.
147. Li N, van Unen V, Guo N, Abdelaal T, Somarakis A, Eggermont J, et al. Early-Life Compartmentalization of Immune Cells in Human Fetal Tissues Revealed by High-Dimensional Mass Cytometry. Front Immunol. 2019;10:1932.
148. Khalaj K, Miller JE, Lingegowda H, Fazleabas AT, Young SL, Lessey BA, et al. Extracellular vesicles from endometriosis patients are characterized by a unique miRNA-lncRNA signature. JCI Insight. 2019;4(18).
149. Chae C. Commercial PRRS Modified-Live Virus Vaccines. Vaccines (Basel). 2021;9(2):185.
150. Pileri E, Mateu E. Review on the transmission porcine reproductive and respiratory syndrome virus between pigs and farms and impact on vaccination. Vet Res. 2016;47(1):108.

151. European Medicines Agency. Modified live porcine respiratory and reproductive syndrome (PRRS) virus vaccines 2021 [Available from: https://www.ema.europa.eu/en/medicines/veterinary/referrals/modified-live-porcine-respiratory-reproductive-syndrome-prrs-virus-vaccines.
152. Loving CL, Osorio FA, Murtaugh MP, Zuckermann FA. Innate and adaptive immunity against Porcine Reproductive and Respiratory Syndrome Virus. Vet Immunol Immunopathol. 2015;167(1-2):1-14.
153. Kreutzmann H, Stadler J, Knecht C, Sassu EL, Ruczizka U, Zablotski Y, et al. Phenotypic Characterization of a Virulent PRRSV-1 Isolate in a Reproductive Model With and Without Prior Heterologous Modified Live PRRSV-1 Vaccination. Front Vet Sci. 2022;9:820233.
154. Dürlinger S, Knecht C, Sawyer S, Balka G, Zaruba M, Rümenapf T, et al. Efficacy of a Modified Live Porcine Reproductive and Respiratory Syndrome Virus 1 (PRRSV-1) Vaccine against Experimental Infection with PRRSV AUT15-33 in Weaned Piglets. Vaccines (Basel). 2022;10(6).
155. Osorio FA, Galeota JA, Nelson E, Brodersen B, Doster A, Wills R, et al. Passive transfer of virus-specific antibodies confers protection against reproductive failure induced by a virulent strain of porcine reproductive and respiratory syndrome virus and establishes sterilizing immunity. Virology. 2002;302(1):9-20.
156. Martínez-Lobo FJ, Díez-Fuertes F, Simarro I, Castro JM, Prieto C. The Ability of Porcine Reproductive and Respiratory Syndrome Virus Isolates to Induce Broadly Reactive Neutralizing Antibodies Correlates With In Vivo Protection. Front Immunol. 2021;12:691145.
157. Robinson SR, Li J, Nelson EA, Murtaugh MP. Broadly neutralizing antibodies against the rapidly evolving porcine reproductive and respiratory syndrome virus. Virus Res. 2015;203:56-65.
158. Kreutzmann H, Dürlinger S, Knecht C, Koch M, Cabana M, Torrent G, et al. Efficacy of a Modified Live Virus Vaccine against Porcine Reproductive and Respiratory Syndrome Virus 1 (PRRSV-1) Administered to 1-Day-Old Piglets in Front of Heterologous PRRSV-1 Challenge. Pathogens. 2021;10(10):1342.
159. Martelli P, Gozio S, Ferrari L, Rosina S, De Angelis E, Quintavalla C, et al. Efficacy of a modified live porcine reproductive and respiratory syndrome virus (PRRSV) vaccine in pigs naturally exposed to a heterologous European (Italian cluster) field strain: Clinical protection and cell-mediated immunity. Vaccine. 2009;27(28):3788-99.
160. Nazki S, Khatun A, Jeong CG, Mattoo SUS, Gu S, Lee SI, et al. Evaluation of local and systemic immune responses in pigs experimentally challenged with porcine reproductive and respiratory syndrome virus. Vet Res. 2020;51(1):66.
161. Bautista EM, Molitor TW. IFN gamma inhibits porcine reproductive and respiratory syndrome virus replication in macrophages. Arch Virol. 1999;144(6):1191-200.

162. Motz M, Stas MR, Hammer SE, Duckova T, Fontaine F, Kiesler A, et al. Identification of MHC-I-Presented Porcine Respiratory and Reproductive Syndrome Virus (PRRSV) Peptides Reveals Immunogenic Epitopes within Several Non-Structural Proteins Recognized by CD8(+) T Cells. Viruses. 2022;14(9).
163. Mokhtar H, Pedrera M, Frossard JP, Biffar L, Hammer SE, Kvisgaard LK, et al. The Non-structural Protein 5 and Matrix Protein Are Antigenic Targets of T Cell Immunity to Genotype 1 Porcine Reproductive and Respiratory Syndrome Viruses. Front Immunol. 2016;7:40.
164. Megli CJ, Coyne CB. Infections at the maternal-fetal interface: an overview of pathogenesis and defence. Nat Rev Microbiol. 2022;20(2):67-82.
165. Crespo AC, van der Zwan A, Ramalho-Santos J, Strominger JL, Tilburgs T. Cytotoxic potential of decidual NK cells and CD8+ T cells awakened by infections. J Reprod Immunol. 2017;119:85-90.
166. Chaturvedi V, Ertelt JM, Jiang TT, Kinder JM, Xin L, Owens KJ, et al. CXCR3 blockade protects against Listeria monocytogenes infection-induced fetal wastage. J Clin Invest. 2015;125(4):1713-25.
167. Centers for Disease Control and Prevention. Congenital CMV Infection [updated 28.04.2020. Available from: https://www.cdc.gov/cmv/clinical/congenital-cmv.html.
168. Njue A, Coyne C, Margulis AV, Wang D, Marks MA, Russell K, et al. The Role of Congenital Cytomegalovirus Infection in Adverse Birth Outcomes: A Review of the Potential Mechanisms. Viruses. 2020;13(1).
169. Knight FC, Wilson JT. Engineering Vaccines for Tissue-Resident Memory T Cells. Adv Ther (Weinh). 2021;4(4).
170. Kang SM, Compans RW. Host responses from innate to adaptive immunity after vaccination: molecular and cellular events. Mol Cells. 2009;27(1):5-14.
171. Masopust D, Soerens AG. Tissue-Resident T Cells and Other Resident Leukocytes. Annu Rev Immunol. 2019;37:521-46.
172. Kok L, Masopust D, Schumacher TN. The precursors of CD8(+) tissue resident memory T cells: from lymphoid organs to infected tissues. Nat Rev Immunol. 2022;22(5):283-93.
173. Costers S, Lefebvre DJ, Goddeeris B, Delputte PL, Nauwynck HJ. Functional impairment of PRRSV-specific peripheral CD3+CD8high cells. Vet Res. 2009;40(5):46.
174. Cao J, Grauwet K, Vermeulen B, Devriendt B, Jiang P, Favoreel H, et al. Suppression of NK cell-mediated cytotoxicity against PRRSV-infected porcine alveolar macrophages in vitro. Vet Microbiol. 2013;164(3-4):261-9.
175. Seder RA, Darrah PA, Roederer M. T-cell quality in memory and protection: implications for vaccine design. Nat Rev Immunol. 2008;8(4):247-58.
176. Kim TS, Shin EC. The activation of bystander CD8(+) T cells and their roles in viral infection. Exp Mol Med. 2019;51(12):1-9.

177. Ge C, Monk IR, Pizzolla A, Wang N, Bedford JG, Stinear TP, et al. Bystander Activation of Pulmonary Trm Cells Attenuates the Severity of Bacterial Pneumonia by Enhancing Neutrophil Recruitment. Cell Rep. 2019;29(13):4236-44 e3.